THE THERMAL CONDUCTIVITY OF URANIUM DIOXIDE

by

I.C. HOBSON M.Sc.

A Thesis presented for the degree of

DOCTOR OF PHILOSOPHY

in the

VICTORIA UNIVERSITY OF MANCHESTER

May 1972

Department of Metallurgy
Faculty of Technology
University of Manchester

ProQuest LLC.
789 East Eisenhower Parkway
P.O. Box 1346
Ann Arbor, MI 48106 – 1346

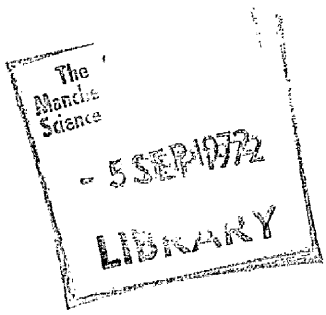
The
Manchester
Science
- 5 SEP 1972
LIBRARY

ABSTRACT

This work is the final part of a three year project to investigate the thermal conductivity of uranium dioxide. The first part contained in a previous thesis (1) covered the initial specimen preparation and characterisation.

Thermal conductivity values have been obtained for the temperature range 500 - 2500°K using the laser - flash technique and specimen discs 1.016 cm. in diameter by 0.0686 cm. thick. Results are quoted for stoichiometric specimens with densities in the range 90 - 96% T.D., for non-stoichiometric specimens of densities 95.89% T.D. and 93.16% T.D. with oxygen/uranium ratios of 2.006, 2.030 and 2.060, and finally for a single crystal of measured density 99.88% T.D. The values show good agreement with published data, normalised and unnormalised, although the values in this work are in most cases slightly higher.

In the process of this investigation a new specific heat curve was obtained using the heat content data of several authors, since the existing published data on the specific heat of UO_2 showed wide discrepancies. Also, owing to the lack of published data, it was necessary to obtain specific heat curves for the hyperstoichiometric specimens by extrapolating from existing data.

The variation of thermal conductivity with pore volume fraction (p) was related using

$$k_m = k_{95} (1 - \beta p)$$

and a value of $\beta = 2.46 - 0.70 \times 10^{-3}$ T was observed. An explanation for this temperature dependence of β is offered.

At high temperatures another heat transfer mechanism (electronic in nature) was found to be operating and the full conductivity equation for 500 - 2500°K was given by

$$k_m = (A + BT)^{-1} + Ce^{-n/T}$$

with $n = (1.8 \pm 0.5) \times 10^4$ (°K).

This mechanism has been discussed in the light of published theories.

From the results, it was also possible to calculate such factors as: the average phonon scattering cross section for excess oxygen ions ($\bar{\sigma}_{O^=}$) and for other impurity atoms ($\bar{\sigma}_L$); a phonon wave length for Umklapp processes (λ_u); and a Debye temperature (θ_D). Where possible, these values have been compared with the results of other workers, and in all cases good agreement was found.

Tabulated experimental results used in this thesis can be obtained from :—

R. Taylor, Metallurgy Department, University of Manchester Institute of Science and Technology, Sackville Street, Manchester, 1.

THE AUTHOR

The author graduated B.Sc. with Honours from the Department of Metallurgy in the University of Manchester Institute of Science and Technology in July 1968. Since graduation, he has carried out research in the Department into the thermal conductivity of uranium dioxide.

As part of the initial work, the author spent six months in the first year at the U.K.A.E.A. establishment in Springfields, where he prepared the necessary specimens. This work together with a literature survey of the published data on the thermal conductivity of UO was submitted for an M.Sc. in October 1969. Since then, the author has been concerned with measuring the thermal diffusivity of these specimens using a laser - flash technique.

During the period of research, the author was a part-time demonstrator in the Department of Metallurgy.

Declaration

Unless stated otherwise, no part of the work described in this thesis has been submitted in support of an application for a higher degree or qualification in this or any other University.

ACKNOWLEDGEMENTS

The author wishes to thank:

Professor K. M. Entwistle for the provision of research facilities and for his helpful comments on the presentation of this thesis.

Mr. R. Taylor M.Sc., for his guidance throughout the period of this work.

The U.K.A.E.A. for the provision of the capital and maintenance grant, and for the use of their facilities at Springfields, where the assistance and advice of Dr. J. B. Ainscough were greatly appreciated.

Mr. I. Brough and Mrs. S. Blain for assistance with electron microscopy.

Mr. D. Wooding for the photography.

Members of the Department of Metallurgy for their assistance and stimulating discussions, especially Dr. T. J. Davies who was extremely helpful.

Finally, his wife, Avril, for typing this thesis and for her constant encouragement.

CONTENTS

INTRODUCTION

The development of nuclear power stations in the United Kingdom has lead to the choice of uranium dioxide as the fuel for the Advanced Gas Cooled Reactor (A.G.R.). This choice of UO_2 was made from considerations of its chemical and physical properties: it possesses a high uranium density; it has a high melting point ($\sim 2800^{\circ}C$); it shows no low temperature phase changes, and it exhibits good high temperature strength. These factors underline its suitability for use in an A.G.R. where the temperatures are of the order of 700 - $1300^{\circ}C$. The one drawback is that UO_2 has a low thermal conductivity, and this can create problems.

Heat is generated in the fuel element by collisions between atoms and slow moving neutrons. This heat of fission is withdrawn from the system by the coolant gas, and by a combination of heat exchangers and turbines electricity is produced. If the fuel has a low thermal conductivity, then this will affect the rate of heat removal from the fuel and thus will reduce the efficiency of the reactor. Another aspect of using a fuel with a low conductivity is that it has the effect of increasing the temperature gradient across the fuel. In some cases the centre of the fuel may reach a temperature of the order of $1450^{\circ}C$, which may cause the fuel to crack and may lead to a build up of the fission product gases krypton and xenon. These gases can exert sufficient pressure on the fuel cladding that the cladding will fail and release radioactive material into the atmosphere. Thus a dangerous situation can arise, which will necessitate the removal of the fuel element at much less than its expected lifetime and the possible shut down of the reactor.

From a knowledge of the thermal conductivity it is possible to simulate in – pile conditions in out – of – pile experiments. This can lead to some improvement in the fuel used in the reactor. Also the rate of grain growth, the creep rate and the melting point can be calculated from a knowledge of the conductivity, and from these factors one can calculate the rate of release of fission gases. Thus it is important to characterise the thermal conductivity in order that one can predict, and therefore anticipate, possible hazards arising out of the use of UO_2 as the fuel.

A large amount of work has been published on the thermal conductivity of UO_2, most of which has already been reviewed (I). The data show a considerable amount of scatter especially at high temperatures. Any correlation of this data is complicated by the lack of characterisation of the various variables that can effect the thermal conductivity. These variables include: pore size, shape and distribution; stoichiometry; grain size; impurity concentration and fabrication route. It was, therefore, felt that an investigation which controlled or characterised these variables would help to resolve some of the discrepancies in the data and perhaps enable a better fuel to be manufactured. Of these variable parameters porosity and stoichiometry appear to have the most effect on the thermal conductivity.

The initial investigation was to consider the effect of porosity on the thermal conductivity of UO_2. To manufacture specimens of varying pore volume fraction, the author prepared, from a single batch of powder, pellets 0.6" long and 0.4" in diameter in which the pore volume fraction varied whilst all other parameters remained constant. The specimens prepared had densities ranging from 90 – 96%of the theoretical density (T.D.). This range was chosen since not only did it include the

values of density most often used in the reactor (~96%T.D.) but also it would enable a comparison with the results of other workers whose densities spanned this range. The lower limit of 90%T.D. was set since few authors had measured conductivity on fuel with densities less than 90%T.D. and since such densities have little technological significance. What scientific interest there may be in producing such fuel is offset by the difficulties of controlling the grain size during fabrication. Also, low density specimens densify on subsequent heating. Therefore, no specimens with densities less than 90%T.D. were manufactured. The actual values of density produced were 95.89%T.D. (nomenclature 96), 93.16%T.D.(93^{I}) and 90.97%T.D.(91^{I}). Since the copper content was above an arbitrarily imposed tolerance level of 100p.p.m. in both the 93^{I} and 91^{I}, new batches were prepared as follows: 94.89%T.D.(94^{II}) and 91.42%T.D.(91^{II}). To complete the investigation into the effect of pore volume fraction, values were to be obtained from two small single crystals. These values for nominally 100%T.D. material could then be compared with those obtained on the prepared specimens.

To investigate the effect of pore distribution specimens with densities close to 93%T.D. and 91%T.D. were produced from some of the 96 specimens. The process involved the redistribution of the pores and the increase in the pore volume fraction of the 96 specimens. These specimens had densities of 94.43%T.D. (nomenclature 9694) and 92.15%T.D.(9691). The effect of pore distribution could thus be investigated by comparing the values for the 9694 and 9691 with those of the 94^{II}, 93^{I}, 91^{II}, 91^{I} and 96. However, an unfortunate side effect of this process of redistribution was that the grain sizes increased three fold, and it was also necessary to hold the specimens for 1 hour at

1600°C in hydrogen to effect some reduction back to stoichiometry. The effect of pore shape on the thermal conductivity could only be investigated by analysis of the results, since there was no method of controlling, and thus varying, the shape of the pores.

Subsequently, the investigation was widened to include the effect of non-stoichiometry on the thermal conductivity. The oxygen/uranium ratios of some of the 96 and 93 were altered to give values of 2.006, 2.030 and 2.060. These values were chosen in an attempt to explain some of the discrepancies in the data and because the value of 2.006 lay close to that observed in the reactor.

The investigation was carried out using a 'flash' technique (2), which measured thermal diffusivity (α) over the temperature range 500 - 2500°K. The heat source was a pulse laser, and induction heating was used to obtain the required specimen temperature. The results were converted into thermal conductivity (k) values using the equation

$$k = \alpha . C . D . \qquad (0.01)$$

where C is the specific heat and D is the density of the specimen. During the course of this investigation it was felt necessary to obtain new specific heat values using the available heat content data of other workers (3), since there were large discrepancies in the published specific heat data. For the hyperstoichiometric specimens, extrapolated specific heat values were obtained using the only available data (4).

This investigation should, therefore, cover the technological aspects of the thermal conductivity of uranium dioxide, since it involves the use of density and stoichiometric values which are most often found in the fuel in a

reactor. From this it is hoped that a new and improved fuel may be manufactured, and that there will be a better control over the conditions in the reactor that may arise from the use of UO_2. The field of investigation has been widened, however, to include those density and stoichiometry values which will make possible a fuller understanding of the important mechanisms governing the transfer of heat in UO_2. It is hoped that this will also resolve some of the discrepancies in the published thermal conductivity results.

CHAPTER I

A. THEORY OF THERMAL CONDUCTION IN SOLID MATERIALS

There are four basic mechanisms by which heat may be transported through a solid material: conduction by phonons (k_p); by electrons (k_{el}); by radiation (k_r); and by excitations (k_{ex}). These contributions to heat transport are additive so the total conductivity is given by:-

$$k_{total} = k_p + k_{el} + k_r + k_{ex} \qquad (1.01)$$

The characteristics of each of these four contributions to the total conductivity will now be summarised. Special emphasis is laid on the variation with temperature of each contribution because this feature can be used to decompose the total measured conductivity into its constituent parts.

1) Phonon or Lattice Conduction (k_p)

When heat is applied to one face of a solid the intensity and amplitude of vibration of the atoms near that face are increased. Since these atoms are in a regular lattice and are bound by strong interatomic forces, some of this extra energy is passed on to their neighbours. If the solid were thermally isolated from its surroundings, it should gradually attain a uniform temperature by this transfer of vibrational energy. In initial calculations this transfer of energy was viewed as changes in vibrational energy of the individual atoms (or oscillators). Einstein foundthe average energy (E) of an oscillator of frequency (w) at temperature T to be equated as follows:

$$E = \frac{\hbar w}{\exp \hbar w/kT - 1} \qquad (1.02)$$

where $\hbar = h/2\pi$, h is Planck's constant and k is Boltzmann's constant. The number of quanta (n) each of energy $\hbar w$ is

$$n = E/\hbar w = (\exp \frac{\hbar w}{kT} - 1)^{-1} \qquad (1.03)$$

However, this approach led to theoretical values for specific heat (C_v)

$$\text{where } C_v = \frac{dE}{dT} \qquad (1.04)$$

which did not fit the observed values, especially the rate at which Cv approached zero at $T = 0^{\circ}K$.

It is necessary therefore to view this transfer of energy not as a change in the vibrational energy of the individual atoms but as a collective change in the vibrational energy of the whole assembly of atoms. This means that the forces binding each atom to its neighbour would have to be considered if a more sophisticated analysis were to be evolved. In this instance it is sufficient to consider the conduction of heat by these elastically connected oscillators as heat transfer in the form of systematically coupled waves representing the simple harmonic displacement of the individual oscillators. The thermal conduction (k_p) is, therefore, a measure of the propagation of energy through the crystal by these waves, and by analogy with photons in electromagnetism these waves are called phonons - heat being transferred by a phonon 'gas'.

In the ideal case of a simple harmonic oscillator, i.e. a defect free lattice of infinite length, nothing should stop the propagation of this phonon 'gas', and the thermal conductivity would be infinite. That it is not infinite reflects the fact that there exists some mechanism for scattering, which does not depend on the presence of defects. The propagation

of a phonon through the crystal lattice will cause a local periodic elastic strain in the lattice, and this strain will modulate in space and time the local density and elastic constants of the lattice. Peierls (5) suggested that these fluctuations were themselves phonon modes, thus creating a mechanism by which phonon - phonon interactions could occur.

However, the model so far is only simple, and in order to account for these interactions it is necessary to consider higher order (anharmonic) terms. The most important interactions are the three phonon processes, where either one phonon is annihilated to yield two others or two phonons combine to form a third. There are two types of three phonon interactions. The first type is a normal or N - process where the three wave vectors add in a simple manner. For N - processes momentum and energy are conserved, and if all interactions were of this type the conductivity would be infinite. However, Peierls (5) described a second process in which the resultant phonon had its wave vector in the opposite sense to that of the initial two. This he called an Umklapp or U - process, and in this process momentum is not conserved. For the U - process to occur one phonon must have its wavelength shorter than twice the interatomic distance (d). Examples of these two types of process are given in fig. 1.01 (after Ziman (6)). Of the two, only the U - processes contribute directly to the thermal resistivity. However, N - processes contribute indirectly in so far as they are responsible for maintaining an energy distribution over a wide range of frequencies, thus creating short wavelength phonons which may then produce U - processes. At

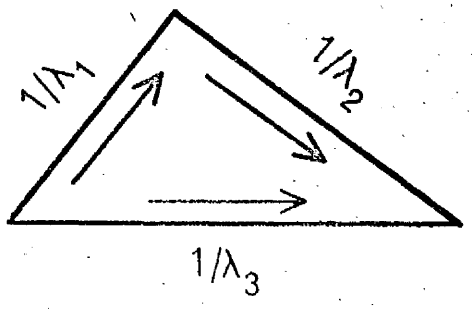

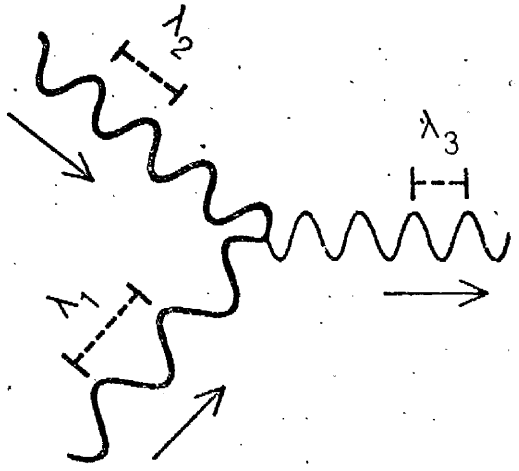

a). N-process.

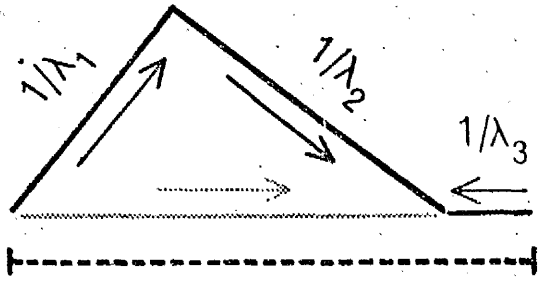

RECIPROCAL OF ATOMIC SPACING

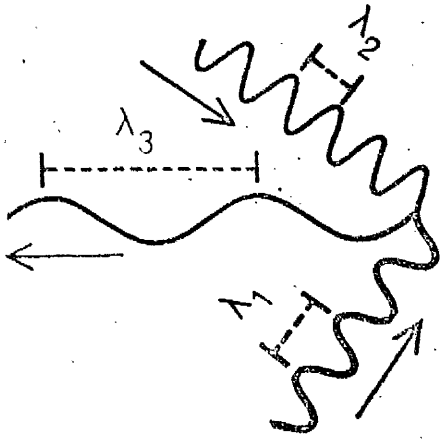

b). U-process.

FIG. 1·01. (after Ziman (6)).

low temperatures the dominant phonon wavelengths are too large for U - processes to occur.

In a perfect crystal lattice the thermal resistance would be accounted for solely by these U - processes, but in a real crystal other mechanism may cause scattering of phonons and hence reduce the conductivity. Any lattice imperfections such as grain boundaries, dislocations, impurities, vacancies and the crystal boundary - all of which affect the periodicity of the lattice by creating local density changes - can scatter phonons. The magnitude of their effect will depend on their concentration, distribution and size. In an electrical conductor phonons will also interact with free electrons. All these processes add to the thermal resistance, and the conductivity will depend on the mean free paths of these scattering processes.

It can be deduced theoretically that the conductivity of a phonon 'gas' can be represented by

$$k_p = \tfrac{1}{3} \int C_v(w).v(w).l_p(w).dw \qquad (1.05)$$

where $C_v(w)$ is the specific heat/unit volume as some function of frequency, $v(w)$ is the velocity as a function of frequency and $l_p(w)$ is the mean free path as a function of frequency. This equation is usually approximated to

$$k_p = \tfrac{1}{3} C_v . \bar{v} . l_p \qquad (1.06)$$

Now each phonon is characterised by three parameters; a) the wave vector $\pm q$ which defines the wavelength (λ)

$$\lambda = \pm 2\pi/q \qquad (1.07)$$

and whose sign defines the propagation direction; b) the angular frequency (w), and c) the polarisation vector ϵ which defines the direction of atom displacement. These give rise

to a spectrum of lattice vibrations which can be very complex for most solids. Since the parameters such as interatomic binding forces are not always accurately known, this makes an accurate solution to such equations as equation 1.05 very difficult. However, the theory of the vibrational spectrum has been simplified by using Debye's theory, in which certain assumptions are made regarding the behaviour of the solid. The solid is assumed to be isotropic and the velocity of wave propagation (v) assumed constant for all frequencies. The energy of the different phonon modes is assumed to be quantised, each having a particular wavelength, wave vector and frequency. The vibrational spectrum is then cut off at some characteristic frequency w_D where

$$\hbar w_{\theta_D} = k\theta_D \qquad (1.08)$$

where θ_D is the Debye temperature of the solid and k is Boltzmann's constant. This equation defines θ_D , and many properties of a solid are expressed in terms of θ_D.

It can be shown that for temperatures above θ_D , that C_v approaches a value of 3Nk (where N is Avogadro's number). This is Dulong and Petit's law. At low temperatures $T \ll \theta_D$, C_v is proportional to T^3, and this is T^3 law of specific heat. Thus this approach gives values for C_v which fit the observed data much more accurately than C_v values obtained at low temperatures from Einstein's analysis.

To discuss the dependence of conductivity on temperature, it is necessary to understand the dependence of phonon mean free path on temperature, since both $C_v(w)$ and $v(w)$ have been well defined in equations (1.05) and (1.06). In fact it is simplified if one considers the frequency dependence of l , and thus arrive at its temperature dependence, since

$$l \propto w_T^{\,n} \qquad (1.09)$$

Equation 1.02

$$E = \frac{\hbar w}{\exp \hbar w/kT - 1}$$

has a maximum at

$$w_{max} = \frac{3kT}{\hbar} \qquad (1.10)$$

If one considers this value of frequency to be the dominant one at temperature T , i.e. $w_T = w_{max}$

then $$w_T \propto T \qquad (1.11)$$

and $$\therefore l \propto T^n \qquad (1.12)$$

This analysis assumes the Debye model such that in the range w to w+dw the number of modes g(w)dw is proportional to w^2dw. Using equation (1.06)

i.e. $$k_p = \tfrac{1}{3} C_v . v . l_p$$

for $T \geqslant \theta_D$, v and C_v are constant

$$\therefore k_p \propto l_p \propto w_T^{\,n} \propto T^n \qquad (1.13)$$

and for $T \ll \theta_D$, v is constant and $C_v \propto T^3$

$$\therefore k_p \propto T^3 . l_p \propto T^{n+3} \qquad (1.14)$$

Thus the conductivity is proportional to T^n for $T > \theta_D$ and to T^{3+n} for $T \ll \theta_D$.

The value of 'n' can be deduced from a study of the thermal resistivity (R_p) where

$$R_p = R_u + R_{pe} + R_{pi} \qquad (1.15)$$

i.e. the total resistivity is expressed as the sum of the resistivity due to U - process (R_u), phonon-electron interactions (R_{pe}) and phonon impurity interactions (R_{pi}). A similar relationship can be given relating the mean free paths due to these scattering processes:

$$\frac{1}{l_p} = \frac{1}{l_u} + \frac{1}{l_{pe}} + \frac{1}{l_{pi}} \qquad (1.16)$$

The relative contribution of the separate resistivity compo-

nents will now be examined for the two temperature ranges $T > \theta_D$ and $T < \theta_D$

a. $T > \theta_D$ where $k_p \propto T^n$

i R_u : the scattering due to U - processes depends on the square of the atomic amplitude (d) , and since $d \propto \sqrt{T}$ then $k_u \propto l_u \propto 1/T$ (1.17)

The full derivation of this equation given by Leibfried/Schlomann (7) is

$$k_u = \frac{24}{10} \quad (4)^{\frac{1}{3}} \quad (\frac{k}{h})^3 \quad \frac{M\delta\theta_D}{\gamma^2 T} \qquad (1.18)$$

where M is the average mass/atom, δ^3 is the average volume/atom, and γ is Grüneisen's constant. Other derivations have been given by different authors (8,9,10,11).

ii R_{pe} : in metals and semiconductors, free electrons scatter phonons, Ziman (12) has related the mathematic expressions for thermal resistivity (R_{pe}) from electron scattering of phonons and electrical resistivity (φ_L) from phonon scattering of electrons as follows

$$\frac{R_{pe} T}{\varphi_L} \leqslant (\frac{e}{k})^2 \quad n_a \quad (\frac{3N_v k}{C_v})^2 \qquad (1.19)$$

where n_a is the number of free electrons/atom, N_v is the number of atoms/volume, e is the electronic charge, and k is Boltzmann's constant. It can be seen from this equation that for $T > \theta_D$, $C_v \rightarrow 3N_v k$ and since $\varphi_L \propto T$ then R_{pe} is constant.

iii R_{pi} : the scattering of phonons by impurity atoms will depend on their concentration. For $T > \theta_D$ the wavelength of the phonons will be predominantly short. Therefore, assuming that

the impurity concentration does not alter with temperature, l_{pi} should be independent of temperature and frequency. It is then to be expected that R_{pi} is essentially independent of temperature.

For $T > \theta_D$., therefore, only R_u is dependent on temperature and the phonon contribution to total conductivity may be expressed as $k_p = (A+BT)^{-1}$ (1.20)

b. $T < \theta_D$ where $k_p \propto T^{3+n}$

i R_u : in general U - processes are scarcer than at $T > \theta_D$ owing to the lack of short wavelength phonons, since U - processes cannot occur of the wavelength is too long (i.e. if the frequency is too low). The number of phonons (n_u) is proportional to $e^{-\theta_D/bT}$, thus as the temperature falls the number of interactions will decrease. If there is a minimum frequency (w_{min}) for U - processes then from equation 1.08

$$n_u = e^{-\theta_D/bT} \qquad (1.21)$$

where $b = w_{min}/ w_{\theta_D}$

The ratio is found to be about 2.

$$\therefore R_u \propto e^{-\theta_D/2T} \qquad (1.22)$$

ii R_{pe} : a temperature dependence for R_{pe} can be obtained by using equation 1.19 and the identities $\varphi_L \propto T^5, C_v \propto T^3$.

This yields $R_{pe} \propto 1/T^2$ (1.23)

Under conditions where the phonon - electron interaction might be important, e.g. in a metal or semiconductor, the number of free electrons/atom (n_a) will be negligible for the semiconductor except where the impurity content is at such a level that impurity bands are formed.

iii R_{pi} : For long wavelengths the scattering cross-section of an impurity is inversely proportional to λ^4, i.e.

$$l_{pi} \propto \lambda^4 \qquad (1.24)$$

Since $w \propto T$ and by invoking the relevant proportionalities, it can be shown that

$$k_{pi} \propto {}^1/_{R_{pi}} \propto l_{pi} \cdot T^3 \propto T^{-1} \qquad (1.25)$$

For $T < \Theta_D$, therefore, the contribution to the total conductivity by phonon conduction is given as:

$$k_p = A'T^{-1} + B'T^{-2} + C'e^{-\Theta_D/2T} \qquad (1.26)$$

where A', B' and C' are constants of proportionality.

These two equations (1.20) and (1.26) are the ones generally used to describe thermal conduction by phonons. In practice the one most frequently used is the former

i.e. $k_p = (A+BT)^{-1}$

since for the majority of metals and ceramics Θ_D is invariably below room temperature.

2) Electronic Conduction(k_{el})

In an electrical conductor thermal energy can also be carried by any charge carriers such as free electrons. This contribution to the observed thermal conductivity is expressed by the modified Wiedemann/Franz law

$$k_{el} = 2({}^k/_e)^2 T \left\{ \sigma + \frac{2\sigma_n \sigma_p}{\sigma} \left(\frac{E_g}{2kT} + 2 \right)^2 \right\} \qquad (1.27)$$

where k = Boltzmann's constant.

e = electrical charge of carrier.

$T = T^{o}K$

σ_n and σ_p = electrical conductivities due to electrons and holes respectively.

$\sigma = \sigma_n + \sigma_p$

E_g = activation energy for exciting an electron into the conduction band.

For metals $\sigma_p \ll \sigma_n$ and this equation reduces to the classical Wiedemann/Franz form of

$$k_{el} = 2(k/e)^2 T \sigma \qquad (1.28)$$

However, the last term of equation 1.27 represents the principle contribution to heat transfer in an intrinsic semiconductor, because each charge carrier carries with it the recombination energy E_g. In this case heat transfer may be by some form of ambipolar mechanism, and this is discussed separately in section 4. For extrinsic semiconductors, the last term again effectively vanishes as $\sigma_p \gg \sigma_n$ for p - type or $\sigma_n \gg \sigma_p$ for n - type.

At high temperatures in metals and semiconductors the free electrons are scattered by phonons, lattice defects or any imperfection which disturbs the potential field. The resulting decrease in the contribution by electrons to the observed thermal conductivity is significant for a semiconductor but is more pronounced for a metal, since the electrons in a semiconductor have larger wavelengths. Christensen (13) says that defects ~1Å will scatter electrons in a metal, whereas the defect has to be ~20Å to scatter them in a semiconductor.

In pure metals $k_{el} \gg k_p$ and the number of free electron

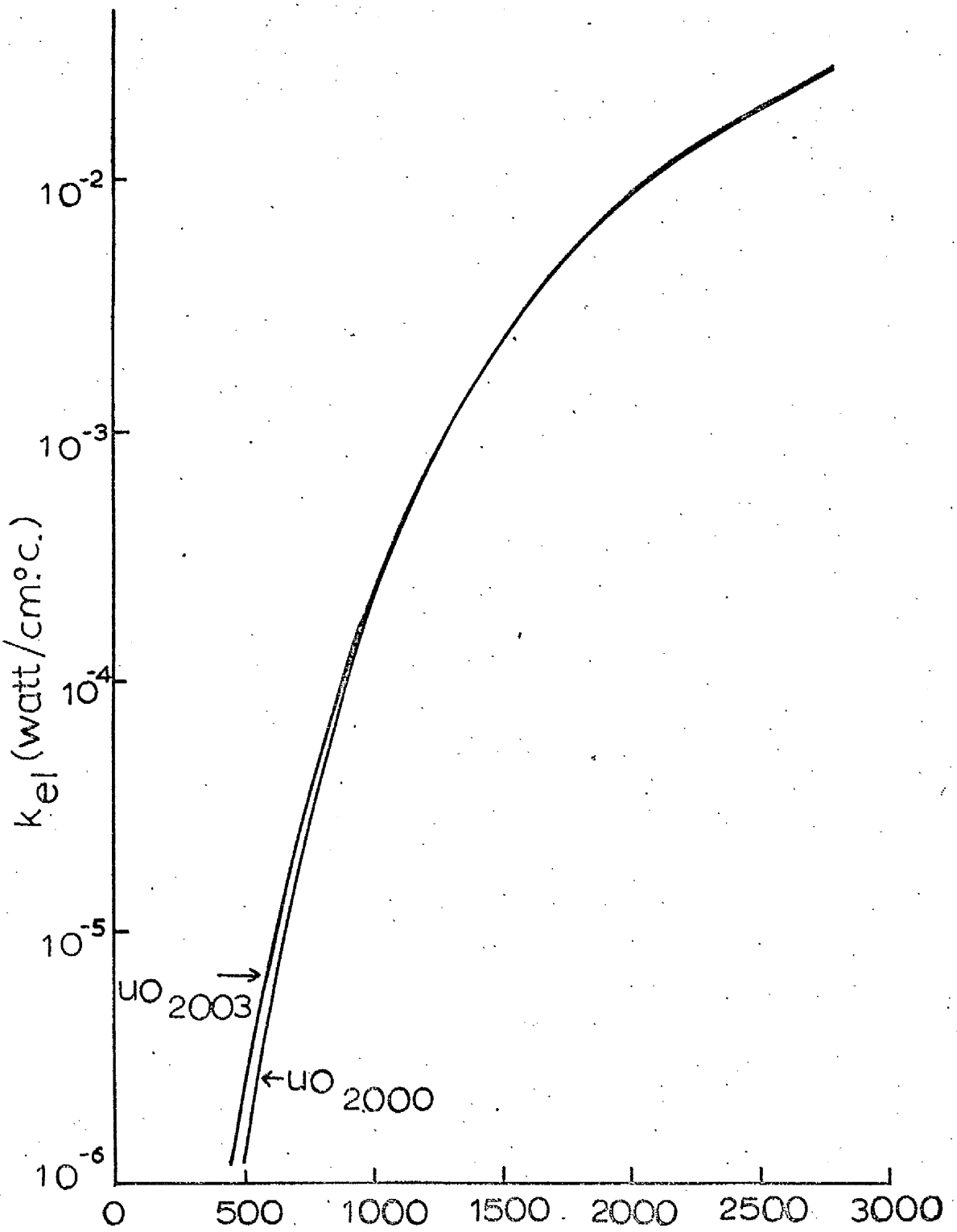

FIG.1·02. K_{el} / T

(after Christensen (13))

carriers increases with temperature. However, in general, the observed thermal conductivity decreases with increasing temperature owing to increased scattering within the metal. In a semiconductor, the improved mobilities of positive holes and electrons tends to make the electrical contribution to k_{total} increase with temperature inspite of the increase in scattering. However, the overall value of this k_{el} remains small compared to k_p except at very high temperatures, i.e. near the melting point, when the band gap may have narrowed quite significantly. Fig. 1.02 (after Christenson (13)) gives the temperature dependence of the electronic contribution to the thermal conductivity for uranium dioxide of several stoichiometries. k_{el} for UO_{2+x} is larger than k_{el} for UO_2 since UO_{2+x} has a larger electrical conductivity. However, k_{total} for UO_{2+x} is less than k_{total} for UO_2 owing to increased phonon and photon scattering by the electrons in UO_{2+x}.

3) Radiation Conduction (k_R)

A small fraction of the energy transferred results from the transmission or absorption and reradiation of electromagnetic energy of high frequency, that is by photons. This is analogous to heat transfer by molecules in a gas except that photons can propagate in a vacuum. The contribution to the total conductivity due to radiant energy transmission through a solid of infinite thickness can be derived from kinetic theory using equation 1.06 $k_R = \frac{1}{3} C_v . v . l_R$.

where $C_v = \frac{16 \sigma T^3 . n^3}{C}$. (1.29)

with $l_R = 1/\alpha$ (1.30a)

and $v = C/n$ (1.30b)

i.e. $k_R = \frac{16}{3} \frac{\sigma n^2 T^3}{\alpha}$ (1.31)

σ is the Stefan - Boltzmann radiation constant; n is the refractive index; T is in ^{o}K; α is the absorption coefficient; l_R is the mean free path of the photons, and C is the velocity of light. It is a convenient way of expressing the process although it does not take into account the dependence of the refractive index (n) and mean free path (l_R) on temperature (T) and wavelength (λ). In general, n can be taken as being independent of λ and T; however l_R varies as a function of λ, T and α. Since heat transport by this mechanism is small compared to that by phonons (K_p), its effect will depend critically on l_R.

There are three possible ranges for l_R:

i If l_R is larger than the sample dimension, then heat transfer will occur without any interaction with the intervening material, and the material will only alter the velocity and hence the rate of heat flow. In transparent and single crystals (where there are no grain boundaries to affect l_R) there will be a significant contribution to the total conductivity (k_T) by k_R at high temperatures.

ii If l_R is $\sim$ sample dimensions then transfer of heat will occur as an exchange between the boundaries and the material, and the rate of energy exchange will be determined by the temperature of the boundaries and the temperature gradient in the material. This mechanism will predominate in some ceramics where $l_R \sim 0.1$ to 100cm.

iii If l_R is smaller than the sample dimension, then transfer will occur by photon processes within the material, and will thus be a material property depending on absorption and scattering usually in the visible or near infrared regions of the spectrum. Absorption is necessary for photon transfer since it is an energy conversion process, and it is intrinsic being the same for polycrystals and single crystals of the same material. However, it does limit the transfer. Scattering, on the other hand, is not necessary but also limits the transfer. There are two mechanisms causing scattering: fluctuation in the density of the material due to sound waves, and structural scattering. The latter is found to be the more predominant, with scattering by pores as its main source - only a few percent can alter the transmission drastically [see fig. 1.03 after Lee/Kingery (14)].

From equation 1.31 it can be seen that for materials with a low absorption coefficient k_R is important at only a few hundred degrees, and that for ones with a high α or substantial scattering, k_R is not significant until very high temperatures. In single crystals and transparent materials, where l_R is of the order of a few centimeters, k_R is appreciable at medium temperatures. l_R increases with increasing temperature owing to higher transmission in wave-lengths $\sim 1-3\mu$, since in general single crystals are transparent in the visible, opaque in the ultraviolet (due to electron excitation) and have absorption bands in the infrared (due to atomic vibrations). In polycrystalline materials l_R is smaller due to scattering, and the total mean free path can be expressed as:

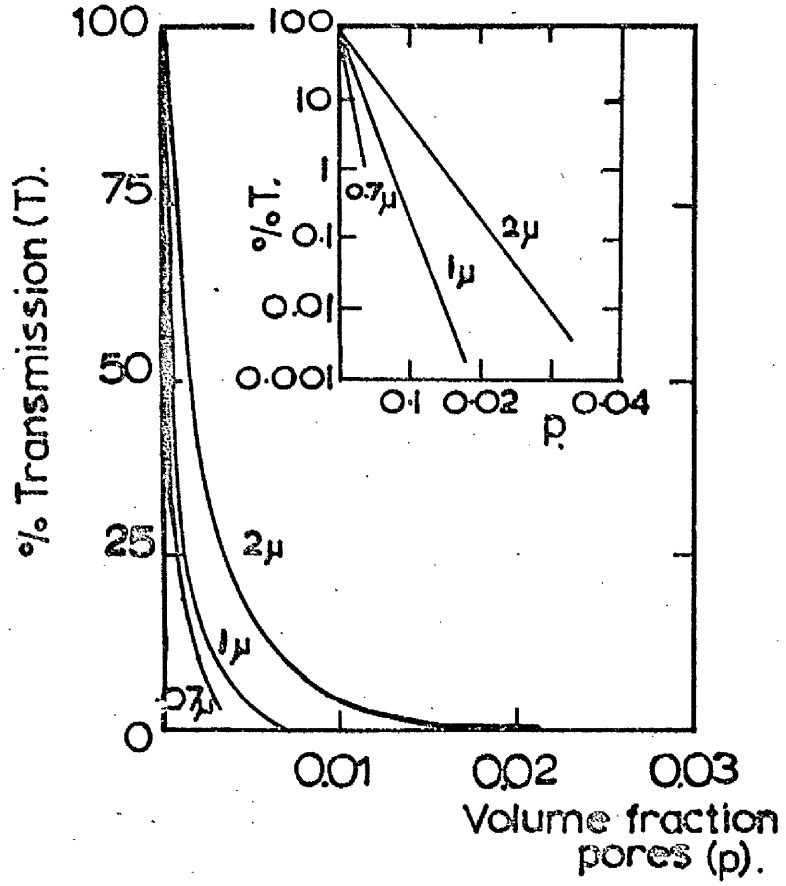

FIG 1.03 After Lee/Kingery (14).

$$\frac{1}{l_T} = \frac{1}{l_{ab}} + \frac{1}{l_s} \qquad (1.32)$$

The mean free path due to absorption (l_{ab}) increases with temperature, whilst that due to scattering (l_s) decreases. l_T should, therefore, pass through a maximum which will occur at higher temperatures for the material with the smallest pore size and volume. Most ceramics are more transparent in the visible and near infrared than at longer wavelengths, therefore k_R will be important only at high temperatures ($\sim 1500^{\circ}C$) when the maximum black body radiation energy will have moved to the lower wavelengths.

When calculating the contribution from radiant heat transfer to the conductivity of UO_2, equation 1.31 is usually used in the following form:

$$k_R = CT^3 \qquad (1.33)$$

where C is a constant of proportionality.

4) Excitation Conduction (k_{ex})

Whereas the thermal conductivities of metals have been adequately described by using k_p, k_{el} and k_r, several anomalies have been observed at high temperatures for several semiconductors. Attempts have been made to account for this anomalous increase in the conductivity by referring to an excitation conduction contribution, and several mechanisms have been postulated including electron-hole pairs (15, 16), internal radiation (17, 18) and other excitation mechanisms (19, 20).

If 'n' is the number of excitation states and E is the energy between the ground state and the 1^{st} excited states of the system and assuming $E/kT \gg 1$, then according to Krumhansl (21)

k_{ex} is given by

$$k_{ex} = k.l.v.\left(\frac{E}{kT}\right)^2 . n^2 . \exp\left(\frac{-E}{kT}\right) \qquad (1.34)$$

where k is Boltzmann's constant, l is the characteristic length for damping out temperature differences, v is the velocity of transport of the excited states. Similar equations have been obtained by Pikus (19) and by Price (16).

If one examines the relationship given by equation 1.27

$$\text{i.e. } k_{el} = 2\left(\frac{k}{e}\right)^2 T \left(\sigma + 2\frac{\sigma_n \sigma_p}{\sigma}\left(\frac{E_g}{2kT} + 2\right)^2\right)$$

one observes that this equation reduces to the classical Wiedemann Franz form $k \propto T\sigma$ for metals ($\sigma_n \gg \sigma_p$) and for extrinsic semiconductors ($\sigma_n \gg \sigma_p$ or $\sigma_p \gg \sigma_n$). However, for intrinsic semiconductors where $\sigma_n = \sigma_p$ there will be a large contribution from the second term in equation 1.27, since both charge carriers (holes and electrons) will carry the recombination energy E_g. These carriers are formed when sufficient energy is absorbed to form an electron and a hole which can then drift down the temperature gradient to the cool region, where they may recombine. Thus heat is transferred by an ambipolar mechanism, and the electron and hole may move independently or together.

Several authors (19, 20, 22, 23) have proposed an excitation conduction in which the electron and hole move together as a stable bound state called an exciton. An exciton (24) is formed when a photon of energy E_g is absorbed by the crystal lattice to create an electron and hole. The attractive Coloumb interaction between the electron and hole enables them to form

a stable bound pair. This pair transports excitation energy but not charge. If the valency band is full, then the energy of the photon required to produce an exciton will be less than the gap energy E_g. Another mechanism suggested for this excitation heat transfer is that of polarons (25 - 28). When an electron in the crystal lattice interacts with the atoms in that lattice, local deformation of the lattice occurs. This deformation can follow the electron and the combination of the electron and its strainfield is called a polaron (24). Thus the electron has a larger effective mass, and in this case both charge and excitation energy are transported. Herring stated (29) that unless exciton transport had a lower activation energy than ambipolar transport then excitons would not make a comparable contribution to that of ambipolar heat transport, since there are a smaller number of momentum states accessible to excitons. Whitmore (22) found this to be the case for TiO_2 where the activation energy for ambipolar transport was much too large, and so he attributed his observed increase to exciton heat transfer.

There has been considerable work done on measuring electrical conductivity and Hall coefficients in an attempt to determine the exact excitation mechanism operating. However, since most measurements of mobilities have been obtained at low temperatures ($T < 1200^{o}K$), the position at high temperatures is still uncertain, and some discrepancies are observed. For example, Devyatkova(17) suggested that exciton transfer was causing the thermal conductivity of lead telluride (Pb Te) to deviate from the form linear form of

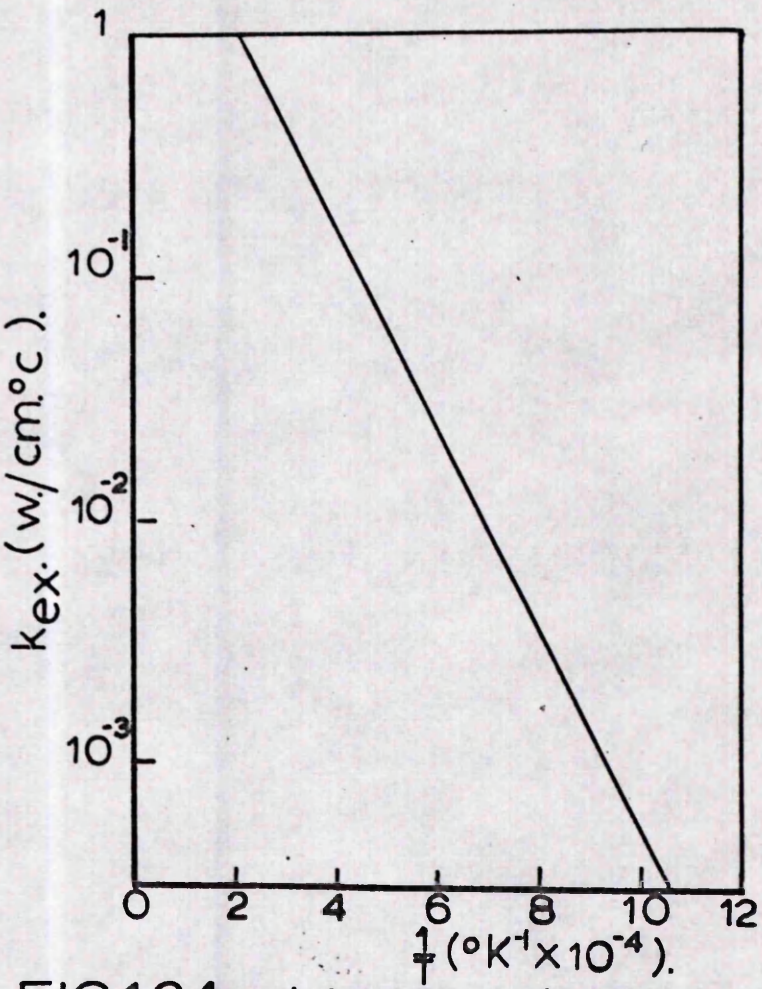

FIG. 1.04. (after Bates (34)).

$k \propto 1/T$. Kanai/Nii (30) found no such deviation. For UO_2 the position is uncertain since some authors (25 - 28) have accounted for the excitation mechanism by polaron transport whilst others (31 - 33) show UO_2 to obey the band theory. Fig. 1.04 shows the contribution by excitation process predicted by Bates (34) for single crystal UO_2 .

From the literature, therefore, it appears that there is an excitation contribution to the thermal conductivity of intrinsic semiconductors. However, discrepancies arise over the mechanism by which this contribution is made, and more work is required in this field.

CHAPTER 1

B. THERMAL CONDUCTIVITY OF UO_2

Most of the published data and theories concerning the thermal conductivity of UO_2 have already been summarised in another thesis (1). The variation in this data has been depicted in fig. 1.05, where the values used apply to specimens with densities 90% T.D. The dotted line represents the values of Nishijima et al (35) for 95% T.D. which differ greatly from any other published data, therefore they have not been included in this analysis. The scatter about a mean k value is of the order of $\pm$ 7% at 200°C rising to $\pm$ 15% at 1200°C. At high temperature the picture is confused since very few measurements have been made and some authors show an enhancement in the conductivity. However, from fig. 1.05 it can be seen that the scatter above 1200°C is still of the order of $\pm$ 20%. Such a scatter in the results will obviously make the design of a reactor more difficult, since some valid judgement regarding the conductivity of the fuel must be made if the actual conditions in the reactor are to be described. The choice of a value on the low side at high temperatures may result in an underestimation of the conductivity by upto 40%. This could lead to there being insufficient coolant flow to remove such heat, with the resultant failure of the fuel. Similarly, the choice of too high a conductivity value will lead to an overestimation of the conductivity with the consequence that the efficiency of the reactor will be reduced.

The scatter in the data can be rationalised if it is realised that the wide variation in the results reflects the wide variation in such parameters as specimen density, stoichio-

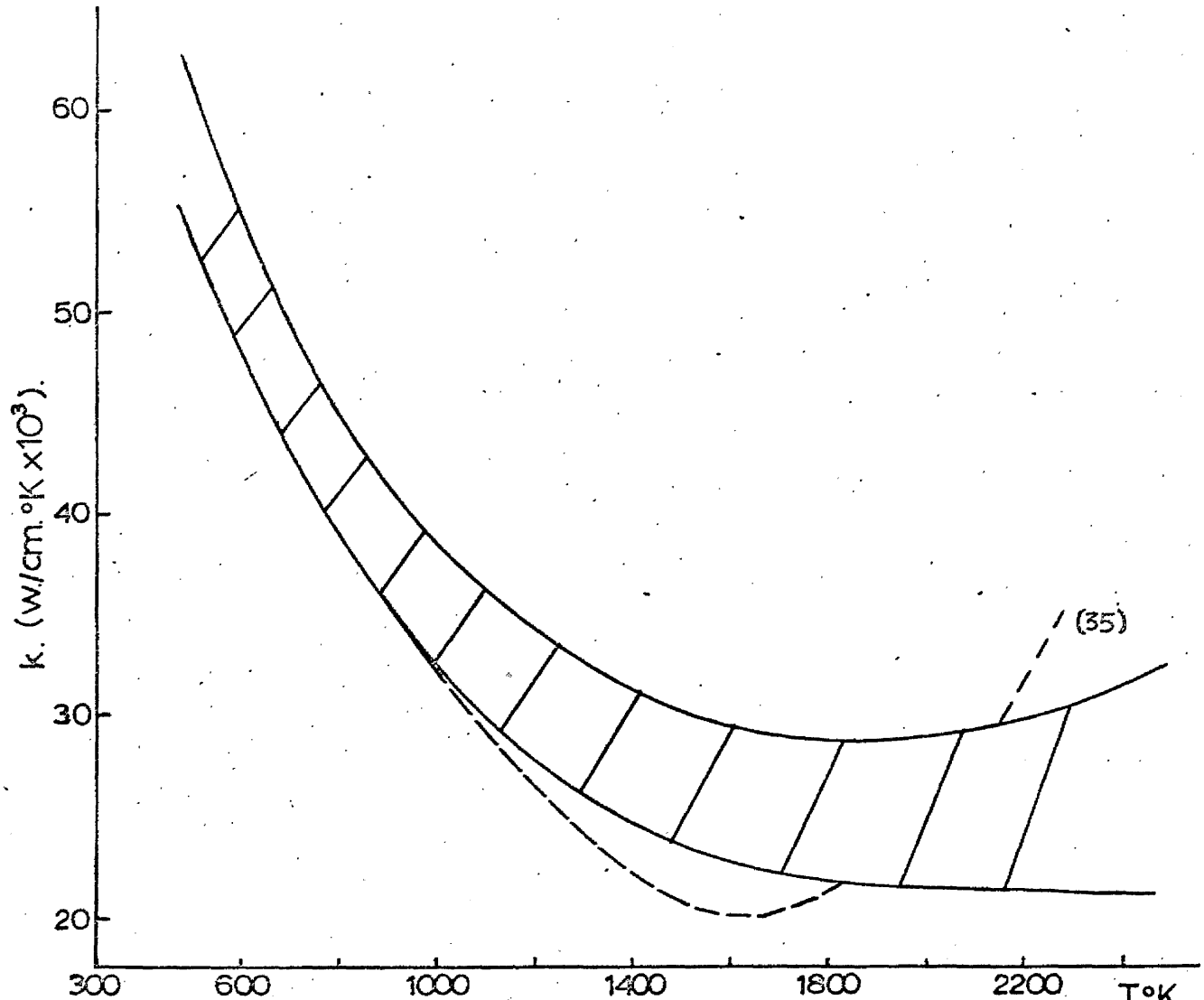

FIG. 1·05. SCATTER IN 'K' DATA OF UO_2.

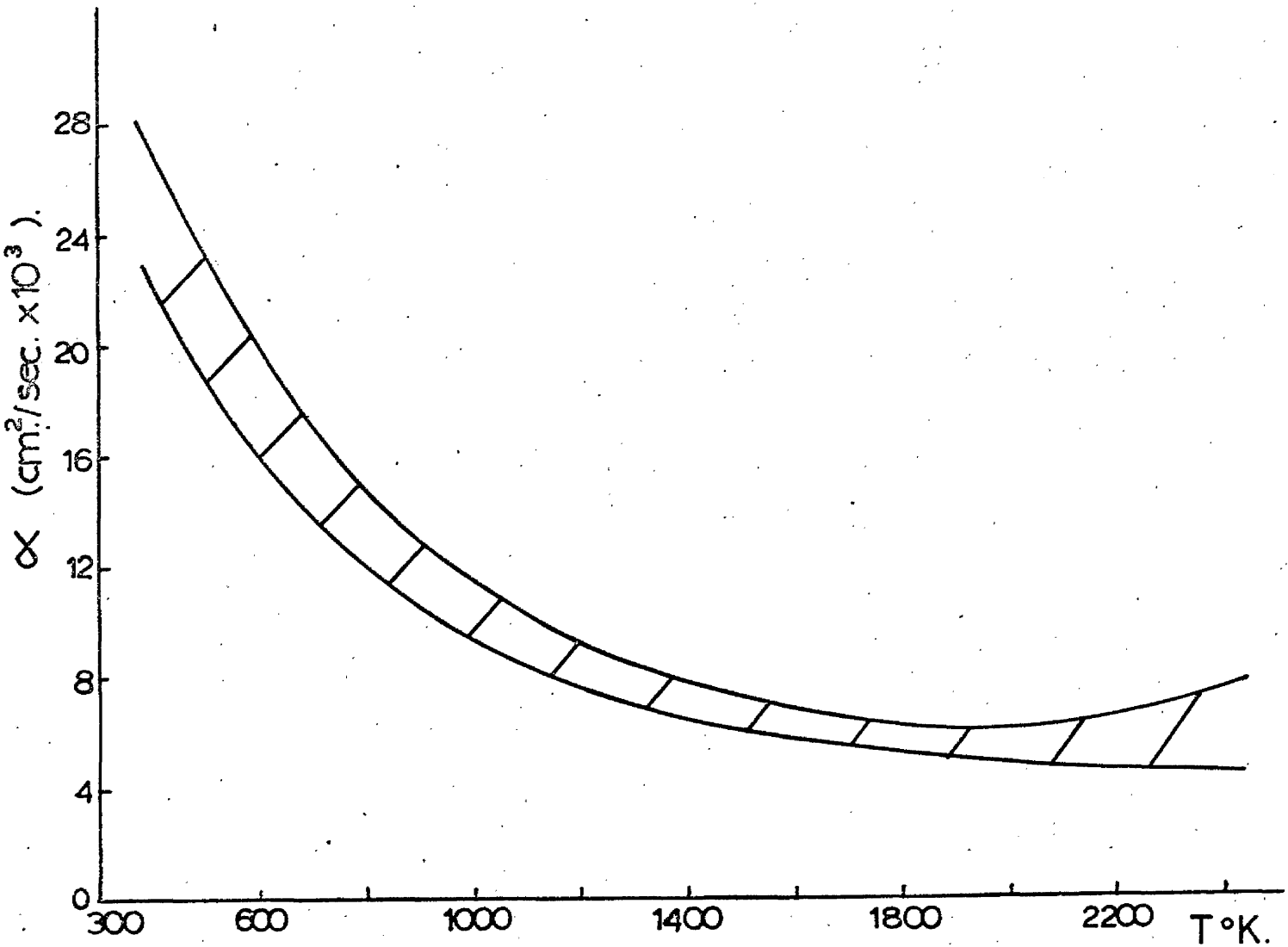

FIG. 1·06. SCATTER IN 'α' DATA OF UO_2.

metry, grain size, impurity content and fabrication route - some of which are discussed later in this chapter. The standardisation of these variables should enable more defined thermal conductivity data to be obtained. Some of the scatter in the data also reflects the uncertainty inherent in the various methods of measurement, each of which will entail certain errors. For example the conductivity values obtained by a thermal diffusivity method will depend on the specific heat values used, and, since there are wide discrepancies in the specific heat values of UO_2 (see Chapter 4b), this will account for some of the scatter in the calculated k values. However the actual published diffusivity values as shown in fig. 1.06 are in good agreement. The scatter about a mean value is $\pm$ 13% over the whole temperature range, and this reflects the differences in the specimen parameters.

In discussing the thermal conductivity of UO_2 it is usual to separate the values into two temperature ranges ($T < 1600^{o}K$ and $T > 1600^{o}K$), since the low temperature values have been well defined.

Low temperature ($400 - 1600^{o}K$)

From fig. 1.05, the scatter in the values at low temperatures is fairly small. In this range, conduction is predominantly by phonons and thus can be described by equation 1.20

$$1/k = A + BT$$

The values of 'A' reflect the contributions to the thermal resistivity from such factors as porosity content, grain size, stoichiometry and impurity concentration, whereas the 'B' values should reflect only that contribution from Umklapp

processes. Most of the published data give values of 'A' lying in the range 3 to 5 $(w/cm^{o}K)^{-1}$ and values of 'B' of 0.020 to 0.024 $(w/cm)^{-1}$.

High temperature ($T > 1600^{o}K$)

At high temperatures the published thermal conductivity data for UO_2 show a deviation from the low temperature linear relationship of $k \propto 1/T$, and some authors have even observed enhancement of the conductivity. There is wide disagreement over the heat transfer mechanism said to be producing the observed deviation, i.e. whether there is a radiation or an electronic contribution. There is even greater disagreement concerning the observation of enhancement of the conductivity although it is widely believed to be a possibility if there is a significant contribution from radiation or electronic heat transfer. Most of the published data has been covered already (1), and therefore the following discussion concerning the possible heat transfer mechanisms will deal mostly with the more recently published data. The following mechanisms have been postulated:

i Radiation heat transfer

Solving equation 1.31

$$k_r = \frac{16}{3\alpha} \sigma . n^2 . T^3$$

depends on the values of 'n' and 'α' chosen. If the values are considered to be independent of temperature, then it is possible to calculate the possible radiation contribution using room temperature data extrapolated to high temperatures. Several authors have done this and found k_r to have a small but significant effect. Bates (34) showed a k_r for single

crystal UO_2 of 4.1×10^{-12} T w/cm.°K. Mogard et al (36) calculated k_r to be 2×10^{-4} w/cm.°C at 500°C rising to 1.5×10^{-3} w/cm.°C at 2750°C using Myers and Gyllander's (37) room temperature value of 'α'. However, since there is no published data relating 'n' or 'α' to temperature at high temperatures, these values can only be rough approximations. It is believed that as temperature increases the number of free charge carriers increases (i.e. the electrical conductivity increases), and these act as scattering centres for photons. Thus the optical absorption increases with increasing temperature, and the contribution by photons to the conductivity is decreased. This absorption will also be large in small grained specimens, impure oxides and in hyperstoichiometric oxides. Even stoichiometric UO_2 is believed to be opaque to infrared radiation at high temperatures owing to the attenuation of photons by free charge carriers (13, 38) - a fact that contradicts the knowledge that most semiconductors are opaque in the visible region and transparent in most of the infrared. Both Christensen (13) and De Halas (39) show a maximum for k_r of 0.016 w/cm.°K around 1000°K thus supporting this theory. Kubota et al (40) postulated that k_r was an important factor causing their conductivity values to level off around 1200°C. However, a lack of high temperature data on the electrical conductivity of UO_2 makes calculations using 'α' suspect.

ii Electronic/Excitation heat transfer

Upto 1100°C UO_2 behaves as an extrinsic semiconductor, and any conduction due to electronic heat transfer (k_{el}) is very small. Above 1200°C UO_2 is intrinsic (13), and since the electrical conductivity is increasing there is ample justifica-

tion for expecting a contribution to the total thermal conductivity from excitation heat transfer. Observing equation 1.27

$$k_{el} = 2(k/e)^2 . T(\sigma + \frac{2\sigma_n \sigma_p}{\sigma} (\frac{E_g}{2kT} + 2)^2) .$$

Most authors take 'E_g' to be constant and assume $\sigma_p = \sigma_n$, i.e. the case for an intrinsic semi-conductor with equal hole and electron mobilities. Both assumptions are unjustified owing to the lack of high temperature data. However, since each charge carrier carries with it a recombination energy E_g (the band gap for intrinsic conduction), the analysis gives a useful pointer to the maximum value of k_{el}. Christensen (13) gave maximum values of $\sim 1 \times 10^{-6}$ w/cm.^{o}C at 500^{o}C rising to $\sim 9 \times 10^{-2}$ w/cm.^{o}C at 2000^{o}C. Godfrey et al (41) gave 0.55×10^{-3} to 2×10^{-3} w/cm.^{o}C between 900 - 1100^{o}C.

There is a need for a much fuller investigation using calculated mobility values for 'σ_n' and 'σ_p', and for more data on the variation of the electrical conductivity upto the melting point. Also, since E_g (the band gap) decreases with increasing temperature, one would expect the possible k_{el} to increase as the temperature increased.

Summary of high temperature mechanisms

The band theory predicts that k_{el} is important at high temperatures and that k_p is insignificant. However, is the band theory applicable to UO_2 , which is not a true semi-conductor (i.e. contains free charge carriers) but is a polar conductor (i.e. polarons: electrons or holes jumping from one cation to a neighbouring cation (38)). Recent high temperature thermal conductivity determinations have not

clarified the situation. Springer et al (42) found no enhancement upto ~ 1800°C, whilst Bates (43) found an upswing in k_{total} around 1800°C. Conway/Flagella (44) got similar if somewhat lower curves to Bates (43), and Van Craeynest et al (45) found enhancement above 1700°C. Stoddard/M^{c} Cormick (46) recently showed k_{el} to be more important than k_r above 2000°C but they felt that both k_{el} and k_r would play significant roles in the thermal conductivity.

Effect of Variables

Most of the variables that affect the thermal conductivity of UO_2 have been discussed in a previous thesis (1). Of these variables, porosity and stoichiometry appear to have possibly the largest effect, and it is felt useful to mention them here together with any data published since 1969.

i Porosity

If a radiation contribution to the total thermal conductivity is important, then pores may well play an important role in the transfer of heat. At low temperatures they will merely act as scattering centres for phonons, thus reducing the conductivity. The amount of reduction will depend on the shape, size, distribution and concentration of the pores. At higher temperatures, enhancement of the conductivity may well occur due to radiation across the pores and to conduction by the media within the pores. The latter may well be significant in low density specimens where the gas volume will be large and the pores may be large and irregular. However, in high density specimens the pores are usually small and spherical, and therefore the gas volume will be very small and any pore

conduction should be negligible.

Several equations for the conductivity of a two phase media containing one discontinuous phase have been obtained.

Eucken (47) and Russell (48) derived expressions using Maxwell's (49) relation for conductors and resistors, and both workers treat isometric (spherical and cubical) pores with equal dimensions in all three axes. Eucken gave

$$k_m = k_c \frac{\left(1 - p + p\left(\frac{3k_d}{2k_c + k_d}\right)\right)}{\left(1 - p + p\left(\frac{3k_c}{2k_c + k_d}\right)\right)} \qquad (1.35)$$

where p is the volume fraction of the discontinuous phase (pores) of conductivity k_d, k_m is the conductivity of the composite, and k_c that of the continuous phase. Russell gave

$$k_m = k_c \left(\frac{p^{2/3} + Q(1 - p^{2/3})}{p^{2/3} - p + Q(1 - p^{2/3} + p)}\right) \qquad (1.36)$$

where Q is the ratio of k_c to the conductivity of the air (k_a) in the pores.

Loeb (50) derived an equation assuming that any pore conduction was due to radiation across the pores. He took into account the distribution of pores, and obtained

$$k_m = k_c \left((1 - p_r) + \frac{p_r}{\frac{p_l k_c}{k_d} + (1 - p_l)}\right) \qquad (1.37)$$

where p_r and p_l are the pore volume fractions in planes that are perpendicular and longitudinal to the direction of heat flow respectively,

$$k_d = 4.\sigma.e.\delta.d.T_m^3 \qquad (1.38)$$

σ is Stefan's radiation constant, e is the emissivity of the

pores, d is the dimension of the pore in the direction of heat flow, γ is a geometrical pore factor, and T_m is the mean absolute temperature.

All of these equations agree well upto 30% porosities according to Francl/Kingery (51), however they preferred to use that of Loeb since it described their results from several ceramics more accurately.

Since the equations of Loeb and Eucken are those most often quoted for correcting the conductivity data of UO_2 , a comparison of them would be useful. By assuming that the pore conduction (k_d) is negligible compared to that of the solid (k_c), the following approximations can be made:

Loeb's equation reduces to

$$k_m = k_c (1 - p) \qquad (1.39)$$

and Eucken's to

$$k_m = \frac{k_c (1 - p)}{(1 + 0.5p)} \qquad (1.40)$$

Expanding equation 1.40 for $p < 0.1$ and ignoring all terms greater than p in the binomial expansion of $(1 + 0.5_p)^{-1}$ then, the follow approximation is obtained

$$k_m = k_c (1 - 1.5_p) \qquad (1.41)$$

Thus there is an obvious discrepancy between the two approximations (eq. 1.39 and eq. 1.41), where Loeb predicts a porosity correction factor of unity whilst Eucken predicts one of 1.5. Both of these values are maximums, and any significant contribution from pore conduction (k_d) will reduce these values. Therefore, in normalising the results, the pore correction factor should be less than or equal to 1.5 and may even be less than unity.

Since the equations given above are approximations, more general forms are usually used. An empirical form of Loeb's equation that is used most often for UO_2 is given as

$$k_m = k_c (1 - \beta p) \qquad (1.42)$$

where β is some material constant depending on the geometry of the porosity, and β is unity for small, spherical pores with $p < 0.1$. The general form of Eucken's equation is

$$k_m = k_c \frac{(1 - p)}{(1 + \alpha p)} \qquad (1.43)$$

where α is a geometrical pore factor equal to $(\beta - 1)$ for $p < 0.1$. Biancheria (52) derived the same equation using an ellipsoidal pore model, and he gave a list of values of β depending on the pore shape. Biancheria suggested that Loeb's equation with $\beta = 1$ was only valid for very small pore concentrations. Instead of using k_c (the conductivity of 100%T.D. material) it is more common to use k_{95} (the conductivity of 95%T.D.) since it usually entails a smaller porosity correction (p) and hence reduces the error in p. In this case

$$p = \frac{\text{density of 95\%T.D.} - \text{density of porous material}}{\text{density of 95\%T.D.}} \qquad (1.44)$$

Of the two equations (1.42 and 1.43), the one that has found preference is that of Loeb's, and values of β ranging from 1 to 4 have been reported for UO_2 by several authors (35, 53-56). The I.A.E.A. panel (38) suggested a β value of 2.5 ± 1.5 to normalise the conductivity values to 95%T.D., but they stated that at high temperatures radiation across the pores would probably affect the value of β. Ross (57) and Mogard et al (36) used a β value of 2, whereas Kjaerheim/

Rolstad (58) gave a higher value of ~3 for 0.96 and 0.98 dense rods. However, Kjaerheim/Rolstad preferred to use the equation

$$k_m = k_{100}(\text{density})^{CD} \qquad (1.45)$$

where CD is an empirical density correction factor. They found this equation gave them more realistic conductivity values for very low density fuel, and this equation was identical to equation 1.42 for high density fuel. Van Craeynest et al (45) used a value of $\beta = 1$ to normalise their results to 100%T.D., and Goldsmith/Douglas (59) found β to be constant and gave a value of 2.8 ± 0.4 for stoichiometric UO_2 and 1.5 ± 0.7 for hyperstoichiometric oxide ($^{O}/_{U} \simeq 2.015$).

Recently several authors have found β to be temperature dependent. Van Craeynest/Stora (60) obtained a temperature dependent β term when measuring the thermal diffusivity of UO_2 from 50 - 1000°C for 72.3 to 100%T.D. They found $\beta = 2.58 - 0.58 \times 10^{-3} t$ (t°C) but offered no explanation for their findings. Earlier, work by Asamoto et al (61) had found that for low density specimens the porosity correction factor decreased with increasing temperature. This they attributed to radiation across and conduction by the pores. However, they said that these factors were self-limiting owing to densification reducing the porosity at high temperatures. Marino (62) has recently studied the variation of β with temperature and pore shape, and he considered both radiation across the pores (k_p^r) and conduction by the gas content of the pores (k_p^c). The variation of β with temperature was found to be too small between 300 - 1900°C to be obtained from plots of $^{1}/_{k}$ against

T for pores containing 20% H_2/ 80% CO. However, from mathematical considerations, it was found that temperature would have an increasing effect on β, and that for disc-shaped porosity this effect would be significant.

There appears to be a wide variation in the values obtained for β, especially over whether it has a constant value or whether it varies with pore volume fraction and/or temperature. Some authors have preferred to use the Eucken's equation 1.43 to normalise their results. Gibby (63) used a value of $\alpha = 0.5$ to normalise their results to 96%T.D., whilst Moore/M^c Elroy (64) used the same value to normalise to 100%T.D. This value of α is of course equivalent to a β value of 1.5 for small pore concentrations ($p < 0.1$). However, Moore/M^c Elroy pointed out that their values could also be fitted by using a β value of 2. Springer et al (42) in 1968 selected α values empirically to normalise their values to 100%T.D. for porosities of 7 to 28%.

It can be seen, therefore, that a difficulty has arisen regarding which normalising equation should be used. Of the two, that of Loeb's

$$\text{i.e.} \quad k_m = k_{95} \ (1 - \beta p)$$

seems to fit the published data with values of $1 < \beta < 4$. Therefore, since this equation has found wide acceptance and since some authors have observed a temperature dependent β value, the results in this investigation will be normalised by the above equation.

ii Stoichiometry

As stated in a previous thesis (1) several authors have established that any alteration in the oxygen/uranium ratio from a value of 2.00 has a considerable effect on the conductivity. The conductivity is seen to decrease with increasing oxygen content, and this effect has been attributed to an increase in phonon and photon scattering by the excess interstial oxygen ions and the strain field associated with them. Also at low temperatures the system will be a two phase one, i.e. $T < 350^{o}C$ and $^{o}/_{u} < 2.25$ the system contains two phases UO_2 and U_4O_{9-y}. Therefore, any low temperature measurements will reflect this change in the composition of the system. This increase in the conductivity with decreasing oxygen content (i.e. $^{o}/_{u} < 2.00$) has been attributed to a significant contribution from photon heat transfer.

Very few authors have related the change in stoichiometry to the measured conductivity in any quantitative way. For the temperature $673^{o}K$ and an $^{o}/_{u}$ ratio change from 2.006 to 2.012, Godfrey et al (41) gave a 5% reduction in the conductivity, whilst Goldsmith/Douglas (59) gave 7%. Obviously more work is required in this field.

CHAPTER 2

A. THEORY OF METHOD

The measurement of thermal diffusivity (α) needs a transient flow method and involves the application of a heat pulse to one face of the specimen and the recording of the time for this pulse to travel through the specimen. To minimize errors the pulse must be uniformly distributed over the front face of a thin, parallel-sided specimen, in a time that is short compared to the rise time of the temperature of the rear face. Under these conditions it is possible to assume that there is one dimensional heat flow within the specimen, and, that if both faces are thermally insulated, that heat losses are negligible.

The equation for heat flow in three dimensions (x,y,z) is the Fourier equation:

$$\frac{\partial T}{\partial t} = \alpha . \nabla^2 T \qquad (2.01)$$

where $$\nabla^2 T = \frac{\partial^2 T}{\partial x^2} + \frac{\partial^2 T}{\partial y^2} + \frac{\partial^2 T}{\partial z^2} \quad , \qquad (2.02)$$

and T is temperature, t is time. This reduces for one dimensional heat flow to

$$\frac{\partial T}{\partial t} = \alpha . \frac{\partial^2 T}{\partial x^2} \qquad (2.03)$$

Assuming no heat losses and an initial temperature distribution of $T(x,o)$, with both ends $x=o$ and $x = L$ thermally insulated, equation (2.03) becomes

$$T(x,t) = \frac{1}{L}\int_o^L T(x,o)dx + \frac{2}{L}\sum_{n=1}^{\infty} e\left(\frac{-n^2\pi^2\alpha t}{L^2}\right) \cos\frac{n\pi x}{L} \int_o^L T(x,o)\cos\frac{n\pi x}{L}dx \qquad (2.04)$$

Parker et al (65) in their analysis assume that a pulse of radiant energy Q is uniformly distributed and instantaneously

absorbed to a small depth "g" at x =o. Then the temperature distribution at $0 < x < g$ is $T(x,o) = \frac{Q}{DCg}$ (2.05)

and at $g < x < L$ is $T(x,o) = 0$ (2.06)

Substitution into equation 2.04 gives

$$T(x,t) = \frac{Q}{DCL}\left[1+2\sum_{n=1}^{\infty}\cos\frac{n\Pi x}{L}\cdot\frac{\sin\frac{n\Pi g}{L}}{\frac{n\Pi g}{L}}\cdot\exp\left(\frac{-n^2\Pi^2\alpha t}{L^2}\right)\right] \quad (2.07)$$

For opaque materials "g" is very small

$$\sin\frac{n\Pi g}{L} \simeq \frac{n\Pi g}{L} \quad (2.08)$$

Then at $x = L$ (the rear face)

$$T(L,t) = \frac{Q}{DCL}\left(1 + 2\sum_{n=1}^{\infty}(-1)^n \exp\left(\frac{-n^2\Pi^2\alpha t}{L^2}\right)\right) \quad (2.09)$$

To solve this equation, Parker et al (65) defined two dimensionless parameters

$$V(L,t) = \frac{T(L,t)}{Tm} \quad (2.10)$$

where Tm is the maximum temperature rise of the rear face

and $$w = \frac{\Pi^2\alpha t}{L^2} \quad (2.11)$$

Equation 2.09 then becomes

$$V(L,t) = 1 + 2\sum_{n=1}^{\infty}(-1)^n e^{-n^2 w} \quad (2.12)$$

This equation is plotted in figure 2.01.

If "w" is known, "α" can, in theory, be obtained from this graph for any value of "V". It can be seen that at V = 0.5, w = 1.37

$$\alpha = \frac{1.37}{\Pi^2} \cdot \frac{L^2}{t_{\frac{1}{2}}} \quad (2.13)$$

where $t_{\frac{1}{2}}$ is the time for the rear face to reach half its maximum temperature rise.

This analysis does not take into account the variation of "α" with temperature, and since the temperature transient

passes through the specimen during measurement, an average diffusivity value (α) over a temperature range is obviously measured. Parker et al (65) defined an effective temperature (T_e) for the specimen,

$$T_e = 1.6T_m \qquad (2.14)$$

However, one generally assumes that measurements are made at ambient temperature, since T_m rarely exceeds 2 - 5°C.

The above analysis requires the enforcement of strict boundary conditions, namely that

i the energy pulse is uniformly distributed over the front face

ii the measurement time is long compared with the heat dissipation time, but short enough to enable heat losses to be neglected

iii the temperature of the specimen is independent of heat loss for a time comparable to the transient time (66)

iv heat losses are sufficiently small so that energy transfer is axially directed

Under certain circumstances these conditions may not be met. At low temperatures, thermal diffusivity increases, thus one may be measuring a $t_{\frac{1}{2}}$ that is so small as to be comparable to the heat pulse duration, and one must consider the use of longer specimens.

At temperatures above 2000°C radiation heat losses are likely to occur even in thin specimens. Heat will flow laterally through the sides of the specimen and, depending on the geometry of the specimen/specimen holder system used, one may get heat losses through conduction at the points of contact.

Detailed analysis has been carried out of the effect of heat losses (67 - 71), both Parker/Jenkins (67) and Cowan (68) have obtained curves for differing degrees of heat loss, and an example of such a curve is given in fig. 2.01. Parker/Jenkins (67) studied the effect of heat loss from one face of the specimen, and Cowan (68) extended this analysis to consider radiation losses from two faces.

According to Cutler/Cheney (69) the solution of Parker/Jenkins (67) can only be applied accurately at low temperatures where radiation losses are almost zero. Cowan (68) considered the case of radiation losses from two faces of a thin disc, where heat losses through the sides of the specimen are negligible compared to those from both faces. Then if heat losses are only from thermal radiation, Cowan defines two heat loss parameters:

$$r = (T_L / T_o)^3 \qquad (2.15)$$

where T_L is the rear face temperature and T_o the ambient temperature in ^oK

and $$a = 2.3 \times 10^5 \, (T/1000)^3 \, (1 + \frac{1}{r}) \, \frac{Le}{k} \qquad (2.16)$$

where L is the length (cm), e is the emissivity and k is the thermal conductivity (ergs/sec. cm ^oK). As previously mentioned, one can assume that $T_L = T_o$, thus for most practical purposes $r = 1$. Cowan suggests the use of two experimental ratios $T(10\, t_{\frac{1}{2}})/ T(t_{\frac{1}{2}})$ and $T(5t_{\frac{1}{2}})/ T(t_{\frac{1}{2}})$, both of which should equal 2 in the ideal case, i.e. no heat losses. Cowan's curves of W/Π^2 plotted against these ratios are given in fig. 2.02.

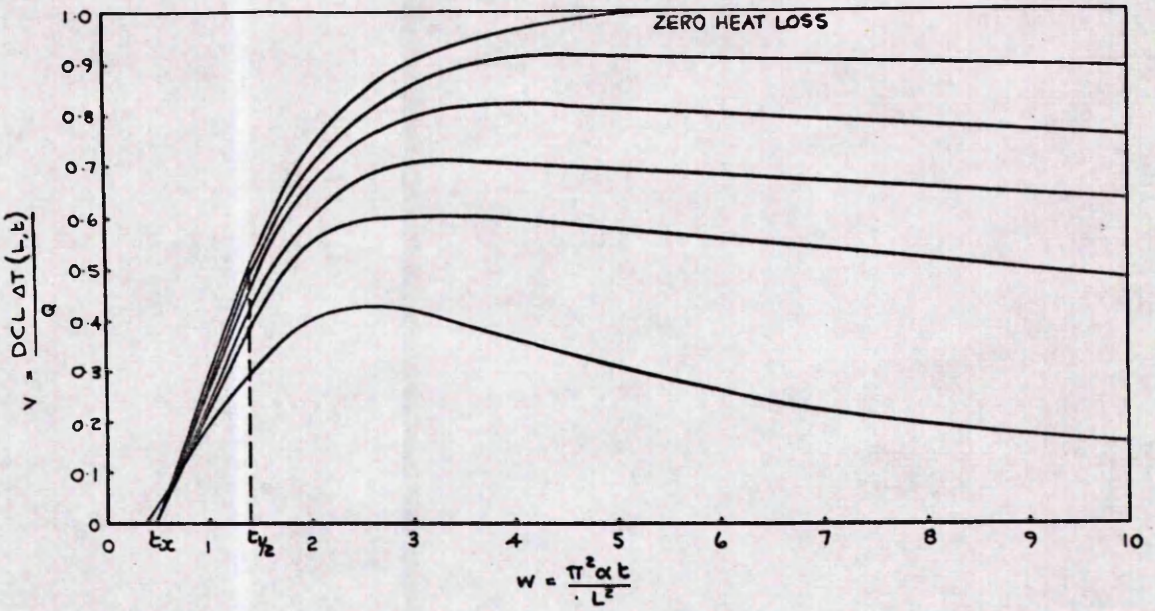

FIG.2·01 EFFECT OF INCREASING HEAT LOSSES ON THE REAR FACE TEMPERATURE HISTORY.

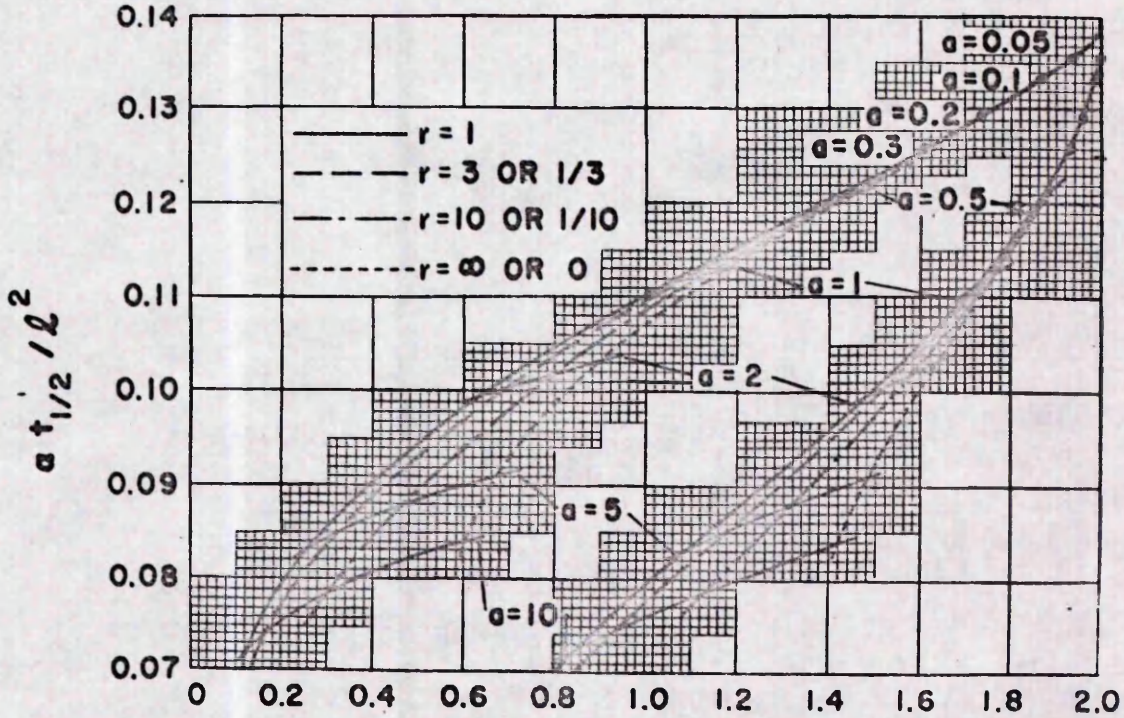

FIG.2·02 $\theta(10\,t_{1/2})/\theta(t_{1/2})$ OR $\theta(5\,t_{1/2})/\theta(t_{1/2})$
(after Cowan(68))

Cape and Lehman (70) and Watt (71) have published more detailed analyses, giving more complete general solutions. Whereas Watt gives only solutions for various step heating functions, Cape and Lehman give detailed numerical solutions. They define a heat loss parameter Y as follows:

$$Y = Y_x + (L/r)^2 \cdot Y_r \qquad (2.17)$$

and $$Y_x = 4\sigma . e_L . T_o^3 . k^{-1} . L \, . \qquad (2.18)$$

$$Y_r = 4\sigma . e_r . T_o^3 . k^{-1} . r \, . \qquad (2.19)$$

where σ is the Steffan - Boltzmann constant, e_r and e_L are emissivities, and Y_x and Y_r are axial and radial parameters respectively. T_o is the temperature of measurement. By determining an initial value for "α" using w = 1.37, and using this value of "α" to calculate Y, one can obtain a correct value of "w" from fig. 2.01. From this one can recalculate a true value for "α".

Watt obtained analytical solutions for different shaped heat pulses, such as for a square pulse (corresponding to a laser pulse) of duration τ:

$$V(L,t) = \left\{ 1 + 2 \sum_{n=1}^{\infty} (-1)^n \exp\left(\frac{-n^2 t}{t_c}\right)\left(\exp\left(\frac{n^2 \tau}{t_c}\right)-1\right) \frac{t_c}{n^2 \tau} \right\} \qquad (2.20)$$

where $$t_c = \frac{L^2}{\pi^2 \alpha} = t/w \qquad (2.21)$$

Taylor and Cape (72) give an equation similiar to equation 2.21. They have also evaluated the change in " w " with the ratio τ/t_c.

In calculating the results included in this thesis, the author has made use of Cowan's curves (as shown in fig. 2.02). Of the two curves shown, preference has been given to

the $T(10t_{\frac{1}{2}})/T(t_{\frac{1}{2}})$ and r = 1 curve. This can be seen to give a more accurate value than the $T(5t_{\frac{1}{2}})/T(t_{\frac{1}{2}})$ curve simply from the nature of the two curves. The former is flatter and thus allows a wider error in $T(10t_{\frac{1}{2}})/T(t_{\frac{1}{2}})$ without affecting the value of W/Π^2 too much:- by careful measurement one can measure $t_{\frac{1}{2}}$ to $\pm$ 0.25 mm. therefore, for $T(10t_{\frac{1}{2}})$ of 48.00 mm. to 48.50 mm., and $T(t_{\frac{1}{2}})$ of 27.00 mm., the ratio is 1.78 to 1.80. This gives an error in W/Π^2 of less than $\frac{1}{2}$%. On the same figure 2.02, if $T(5t_{\frac{1}{2}})$ lies between 53.00 mm. and 53.50 mm., with a $T(t_{\frac{1}{2}})$ of 27.00 mm., the ratio is 1.96 to 1.98. This gives an error in W/Π^2 of 2%.

In recent years there has been a movement towards the measurement of thermal conductivity by thermal diffusivity methods, such as the Angstrom, laser - flash and electron beam methods, rather than by direct measurement especially for high temperatures. Whereas in the direct method one is measuring the quantity of heat flowing, in the diffusivity method one is measuring the rate of heat flow. Thus the former requires the accurate measurement of temperatures at several points, whereas the latter requires the measurement of the duration of the heat flow. Therefore, at high temperatures, measurement errors can be large for direct methods, and such errors are increased when one considers heat losses. Heat loss by radiation is proportional to $(T^4 - T_o^4)$, where T and T_o are the temperatures (^oK) of the body and its enviroment. This factor may be larger for the direct measurement method, than for the diffusivity method since the measurement time of the latter can be extremely small. Jain/Goel (73) found large

errors in some published conductivity data obtained using direct methods. These errors were attributed to underestimations of the heat losses.

Though the measurement of thermal conductivity at high temperatures by the measurement of thermal diffusivity appears to be preferable to direct measurement, the former requires an accurate knowledge of the specific heat of the body if accurate conductivity values are to be calculated. This can be seen from the equation 0.01.

$$k = C.\alpha.D.$$

Most solid materials have their specific heat and its variation with temperature well documented, and thus the values of specific heat in the above equation have been well characterised. However, there is a wide variation in the available specific heat data for a few materials including uranium dioxide (see Chapter 4b), and this detracts from the advantages of using a diffusivity method. These advantages are highlighted in Chapter 5 which deals with the errors involved in the laser - flash method used by the author.

CHAPTER 2

B. EXPERIMENTAL TECHNIQUE

Description of the Equipment

A detailed description of the construction of the equipment and its use for measurements on graphite form part of another Ph.D. thesis (2), and will, therefore, only be briefly described here. The equipment has been designed to permit measurements over the temperature range 20 - 3000°C using either vacuum or an inert gas atmosphere. The heat pulse source is a ruby laser, and the specimen is raised to the measurement temperature by induction heating. The transient is recorded by either a thermocouple (at 20°C) or lead sulphide or indium antimonide radiation detectors. A schematic diagram is given in fig. 2.03 and a picture in fig. 2.04. Details of the equipment will be outlined under the following headings:

i Heating system.

ii Detection and measuring system.

iii Vacuum/Pressure chamber.

and the contributions made by the author will be mentioned under the section 'Comments'.

i Heating system

This consisted of essentially two things: a heat source providing the temperature transient and induction heating the sample to the desired temperature of measurement.

a) heat source:-

A $\frac{5}{8}$" diameter, solid state ruby laser (Bradley type 351) supplied power in the range 5 - 100 Joules in a pulse of dissipation time 8×10^{-4} sec. Temperature rises in the specimen

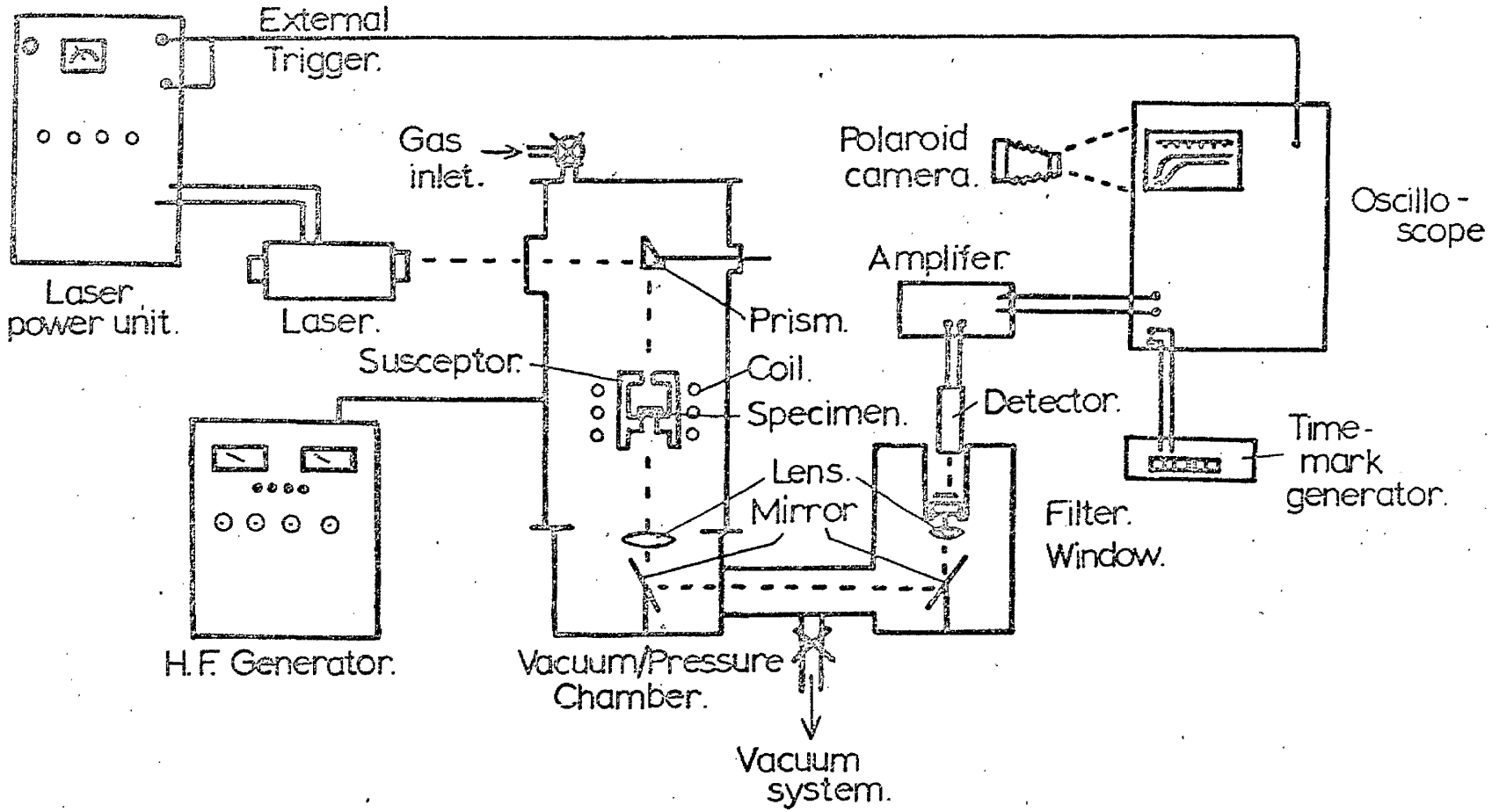

FIG. 2·03. Schematic Diagram of Apparatus.

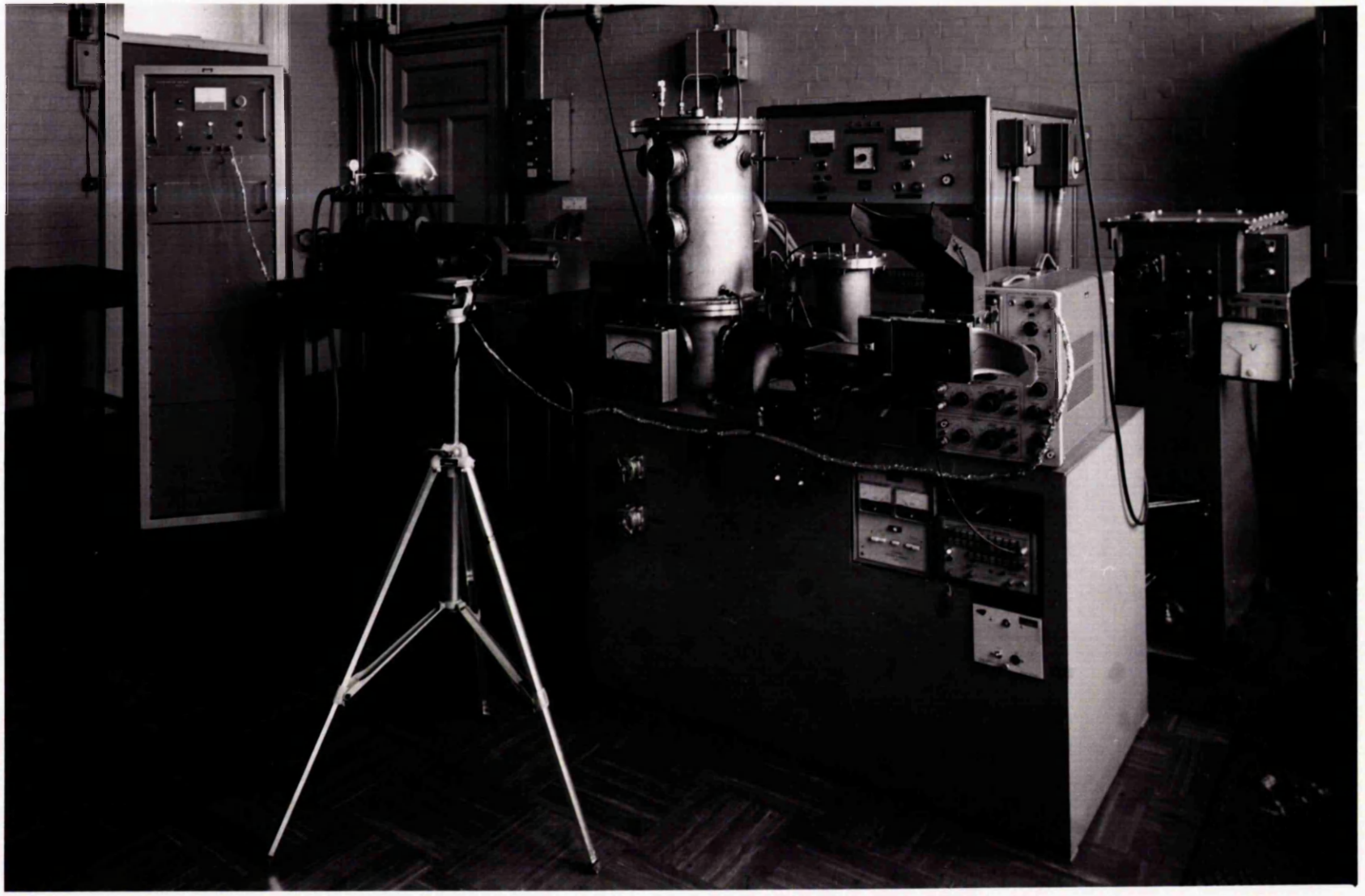

FIG. 2·04.

of approximately 3°C were observed for 1 - 16 J heat inputs.

b) induction heating:-

The power to the induction heating system was supplied by a low impedance valve operated generator (Stanelco - Thermatron Type 20L). It was capable of delivering 25 kw. In order to achieve close coupling for high temperatures and to avoid containment problems, the heating coil was placed inside the vacuum/pressure chamber.

ii Detection and measurement system

Since no one detector was capable of measuring temperature transients over the whole range to be investigated, three different detectors were used.

a) For room temperature measurements a thermocouple was used with a modified holder (see section 4 'Comments') and a Fenlow AD103S operational amplifier to amplify its signal. This arrangement has the inherent difficulty that it introduces heat losses by conduction from the rear face, and it requires good electrical contact between the specimen and the thermocouple. It was, therefore, necessary to coat the rear faces of the specimens with a graphite pencil, as suggested by R. Taylor (74) and Iacobelli and Moretti (75). The problems encountered in the use of this method are discussed in section 4 'Comments'.

b) An indium antimonide photoconductive detector (Mullard ORP13) was used in the range 60° - 400°C. It must be cooled by liquid nitrogen and was supplied mounted in a Dewar. Because it had to be mounted vertically, it did affect the design of the vacuum/pressure chamber. It had a maximum sensitivity to radiation at wavelengths of 3$\mu$to 5μ, so it had to be used in

conjunction with special calcium aluminate lenses and a window which transmit radiation of these wavelengths. The detector had a dark cell resistance of 2kΩ and was used in a simple bridge circuit biased with a 9V supply. The outputs from this bridge were in the range 500μV to 2mV and were fed directly into the oscilloscope.

c) A lead sulphide photoconductive detector (Mullard 62SV) was used for the range 270° - 2300°C. It had optimum sensitivity to radiation of wavelength 3μ, and so could be used in conjunction with the quartz lenses and window. The detector had a dark cell resistance of 2MΩ and was used in a bridge circuit biased with a 60V supply. However, since outputs from this bridge were only 100mV -3mV depending on the temperature of measurement , a small amplifier circuit was incorporated into the system (see fig. 2.05). This had switched gains of X6,X12, X18 and X30. It was found necessary to reduce the amount of radiation falling on the detector by defocussing, i.e. raising the detector. Stray laser light was prevented from reaching the detector and thus possibly damaging it by the use of a silicon filter placed on top of the right hand window in the optical system (fig. 2.04). This filter cuts out all radiation below 1μ at temperatures above 1000°C. At even higher temperatures (~ 1600°C) a neutral density filter was added to reduce the radiation intensity to 10%. In this way it was possible to prevent the detector's resistance from falling so low and hence its current from rising to too high a level that the trace became sensitive to vibration and electrical interference.

The signals from these three sensors were displayed on one beam of a Tektronix 502A dual beam oscilloscope; the other

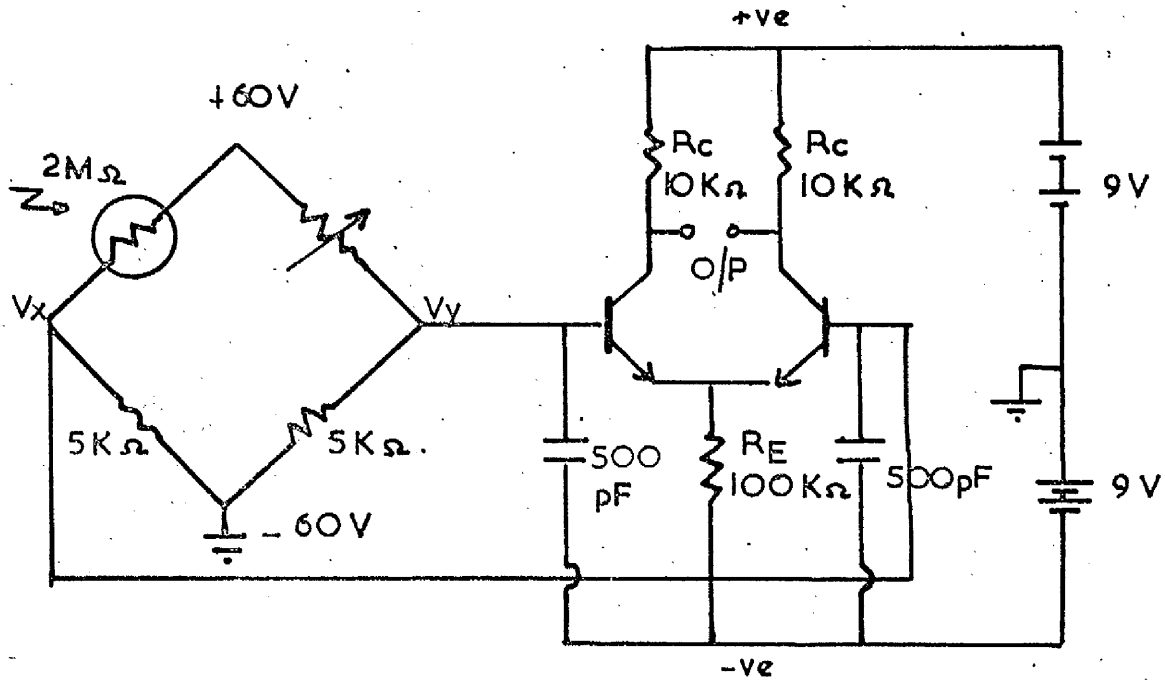

FIG. 2·05 PbS bridge and amplifier circuit.

beam receiving time pulses from a Tektronix type 184 time mark generator. From the first beam $t_{\frac{1}{2}}$ could be measured, whilst the second beam was used to calibrate the first. The oscilloscope was triggered from the laser unit, and a Polaroid land camera was used to photograph the two beams. An example of a typical photograph is given later in fig. 2.10.

iii Vacuum/Pressure chamber

Construction of the system was to a large extent governed by the use at low temperatures of an indium antimonide detector, which had to be mounted vertically. The radiation from the rear face of the specimen had to be bent through two right angles, so the system was constructed in the form of an 'H' with the left hand vertical arm, (the heating chamber) being larger than the other.

The left hand arm was 12" internal diameter and 30" high, comprising of a top vessel 21" high which could be used for maintenance and access purposes. This vessel together with the top flange and the induction flange at the rear were all water cooled. It contained three 1" diameter portholes: one on the l.h.s. for the entrance of the laser beam which was deflected down onto the specimen via a 45^{o} glass prism attached to a fixed shaft seal mounted diametrically opposite; one front porthole to enable the temperature of the susceptor containing the specimen to be measured through the work coil using an optical pyrometer; and one spare porthole above at 90^{o} to the first for use should alternative measuring arrangements be required. The internal flange on the base vessel was only 7" internal diameter to enable the susceptor to be supported

within the induction coil on a simple tripod arrangement, and to enable a ring support to be attached for the 8" focal length quartz or calcium aluminate lenses (see fig. 2.06).

Several systems were tried (see 'comments') before the final design of susceptor and support was evolved. The graphite suceptor was $1\frac{3}{4}$" diameter by 2" long, and it contained the specimen holder, which was initially $\frac{1}{8}$" thick pyrolytic graphite disc with a central hole (recessed $^{1}/_{32}$") some 0.020" smaller than the specimen diameter. A similar holder was made from tungsten for use at high temperatures to eliminate the risk of contamination of the specimen by the graphite holder. A graphite plug placed in the top of the susceptor cut off the excess laser beam. The susceptor was supported inside the induction coil on a graphite cylinder which was in turn mounted on a 4" diameter base. This whole system of susceptor and base was supported on a tripod arrangement, which itself was supported on the internal flange. The arrangement is shown in fig.2.06.

In the base of the l.h. vessel a $4\frac{1}{2}$" by 3" elliptical, front aluminised, silicon monoxide - coated mirror was mounted at 45^{o}. It was supported on four adjustable levelling screws, and light collected from the specimen rear face was deflected through a right angle via an iris diaphragm along the horizontal tube to the r.h. chamber. Here the light was deflected through a further right angle by a similar mirror, and a quartz lens (focal point $1\frac{1}{2}$") brought it to a focus.

The induction coil was led into the rear of the l.h. chamber via a 6" diameter port. The coil was $^{3}/_{16}$" nominal bore copper tubing, and vacuum tight seals were made between the copper tubing and the port using either a cast araldite plug

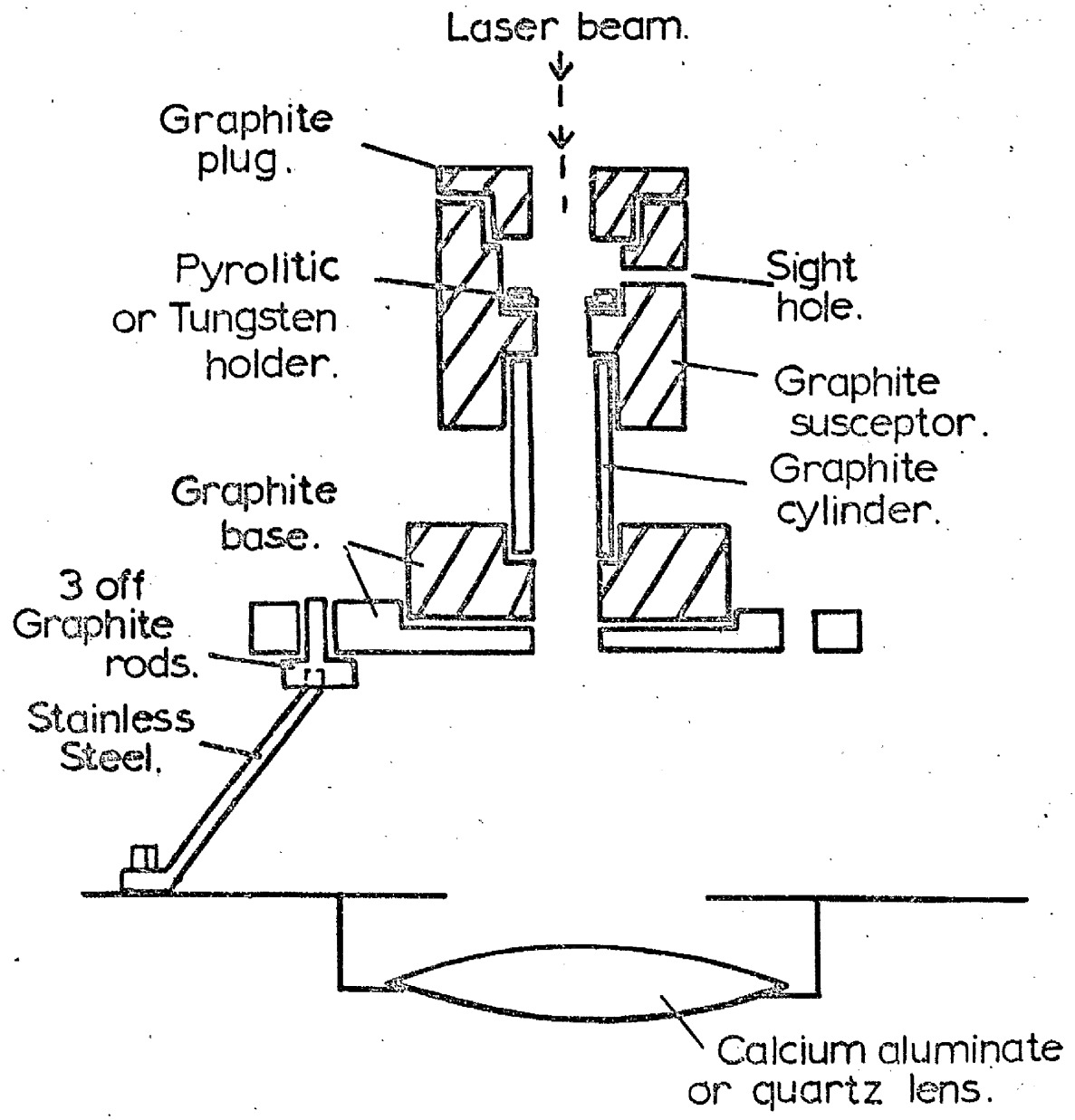

FIG. 2·06 Susceptor and Support.

or polytetrafluoroethylene (P.T.F.E.). In both the coil was rigidly supported.

The temperature of the susceptor was measured using an optical pyrometer sighted via the second quartz window above onto a $\frac{1}{8}$" diameter hole in the susceptor. The measured values (T_B) were corrected for emissivity (e) and transmission through the window (t_r) using $e = 0.95$ for carbon and $t_r = 0.91$ for quartz. Fig.2.07 shows the temperature correction factor for each measured temperature (T_B). For temperatures less than 800°C a chromel-alumel thermocouple was used, the leads for which left the apparatus via a proprietory coaxial four-pin lead through-mounted on a small flange at the front and base of the l.h. chamber.

An outlet in the horizontal arm was connected through a baffle valve and liquid nitrogen trap to the vacuum system. This consisted of an Edwards E04 diffusion pump backed by an E.S.150 rotary pump. The horizontal arm also supported Pirani and Penning guages. An air admission valve in the top flange of the l.h. chamber was used as the gas inlet when the system was to be used under an inert atmosphere. The Penning guage was then replaced by a pressure guage. The whole assembly was pressure tested to 10 atmospheres of internal pressure.

Comments on use of equipment

The original high frequency set did not provide a sufficient temperature range, and initial measurements could only be made in two stages: a) 800-1200°C using two phases and b) 1200-1600°C using three phases. To achieve a wider range of temperatures an autotransformer was obtained so that, when it

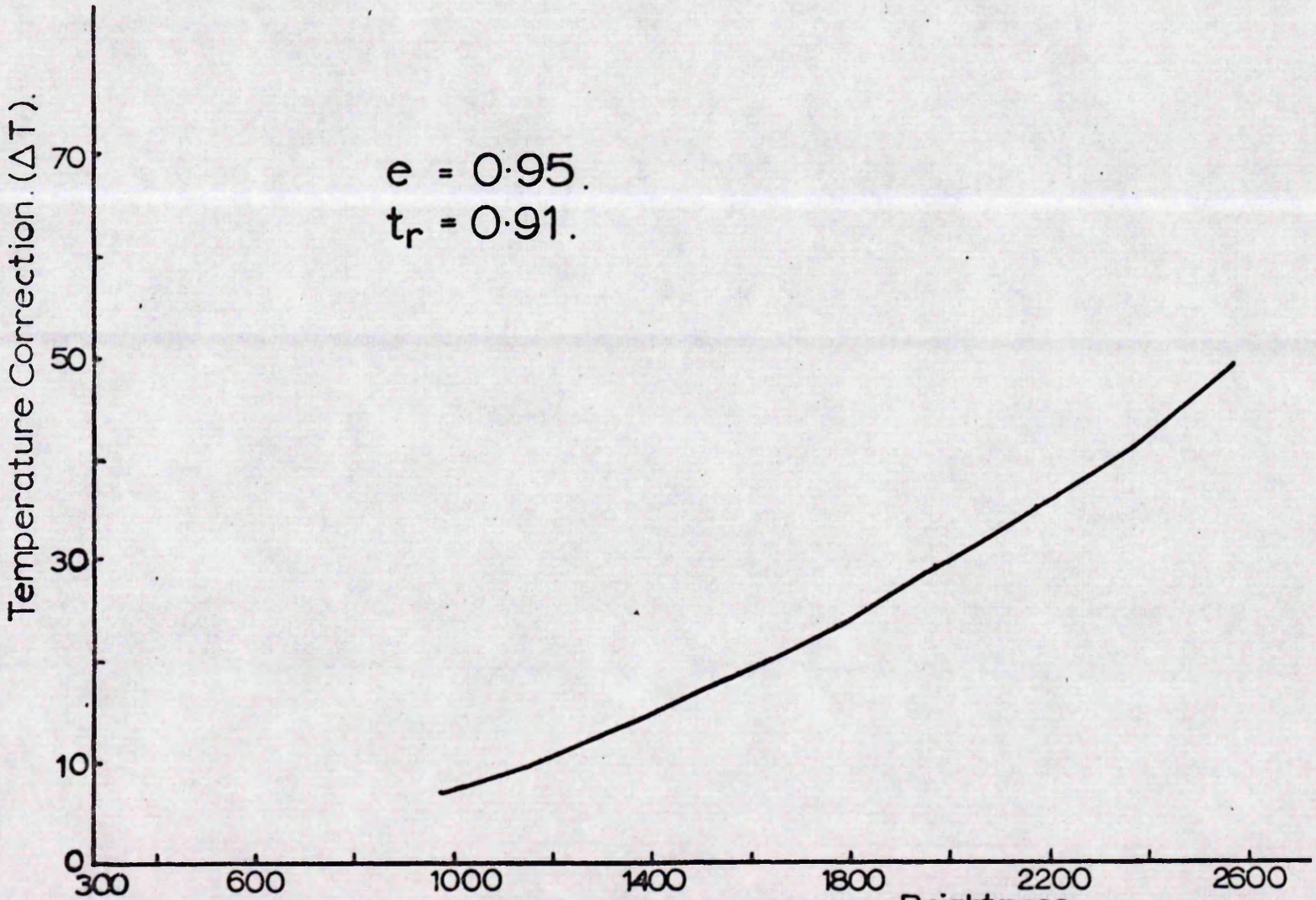

FIG. 2·07. Temperature Correction for Optical Pyrometer.

was coupled to the input side of the H.F. set, the input voltage to the set could be varied from 0-440V. It was then possible to obtain temperatures from 50° to 2300°C in one operation, although in practice the range had to be covered in two stages since above 800-900°C the thermocouple that had been used to read the temperature of the specimen had to be removed.

It was hoped to obtain measurements at room temperature with the use of thermocouples and a special graphite or steel specimen holder(74). The thermocouple was screwed tightly up against the rear face of the specimen, and when the holder was inverted and placed in position the specimen was solely supported by the thermocouple. Since it was also important to place the thermocouple near the centre of the specimen's rear face, the difficulties in obtaining good electrical contact (between the specimen and the thermocouple) were considerable. However, the use of a graphite pencil to cover the rear face of the specimen did improve the electrical contact. Several specimens were broken owing to the thermocouple being screwed too tightly in an attempt to improve this contact and to hold the specimen firmly. It was, therefore, decided not to pursue measurements at room temperature. A lower limit for measurements was instead set by the specific heat curve to be used (lowest temperature $\sim$ 500°K see chapter 4b).

As mentioned previously an autotransformer had been purchased in an attempt to obtain temperatures in excess of 2000°K. However, the geometry of the system (i.e. susceptor and support design and coil size) being used enabled only temperatures of the order of 2000°K to be reached. In order

to get higher temperatures radiation heat shields were tried, using molybdenum or pyrolytic graphite foil. However, these shields tended to couple with the coil and thus prevented the outer layer of the susceptor from coupling. Hence the shields became incandescent, whilst the susceptor and specimen remained relatively cool. Consequently, slots were cut in the shields to prevent them from coupling, even so no significant increase in the maximum temperature was observed. Different susceptor/support/coil geometries were tried until the final arrangement (shown previously in fig.2.06) was evolved.

During this attempt to obtain higher temperatures, problems arose due to the use of a vacuum. It was found necessary to hold the vacuum at values below $\sim 10^{-4}$ Torr in order to prevent sparking, and it was difficult to maintain such low pressures since the susceptors evolved occluded gases and since at high temperatures the vapour pressure of UO_2 is of the order of 10^{-4} Torr (see fig.2.08 after Ackermann et al (76)). The first difficulty was overcome by purging the susceptors by several heating runs prior to measurement; the second (UO_2 vapour pressure) proved more difficult and it was decided to use an argon atmosphere instead of a vacuum at high temperatures. However, this proved unsuitable since above 1800°K sparking occurred between the coil and the susceptor (the design of which had not yet been finalised). The alteration of the geometry of the susceptor system reduced the incidence of sparking, but it was then found that at high temperatures the oscilloscope trace fluctuated irregularly. Alteration of the pressure of argon did not affect this observation, which was

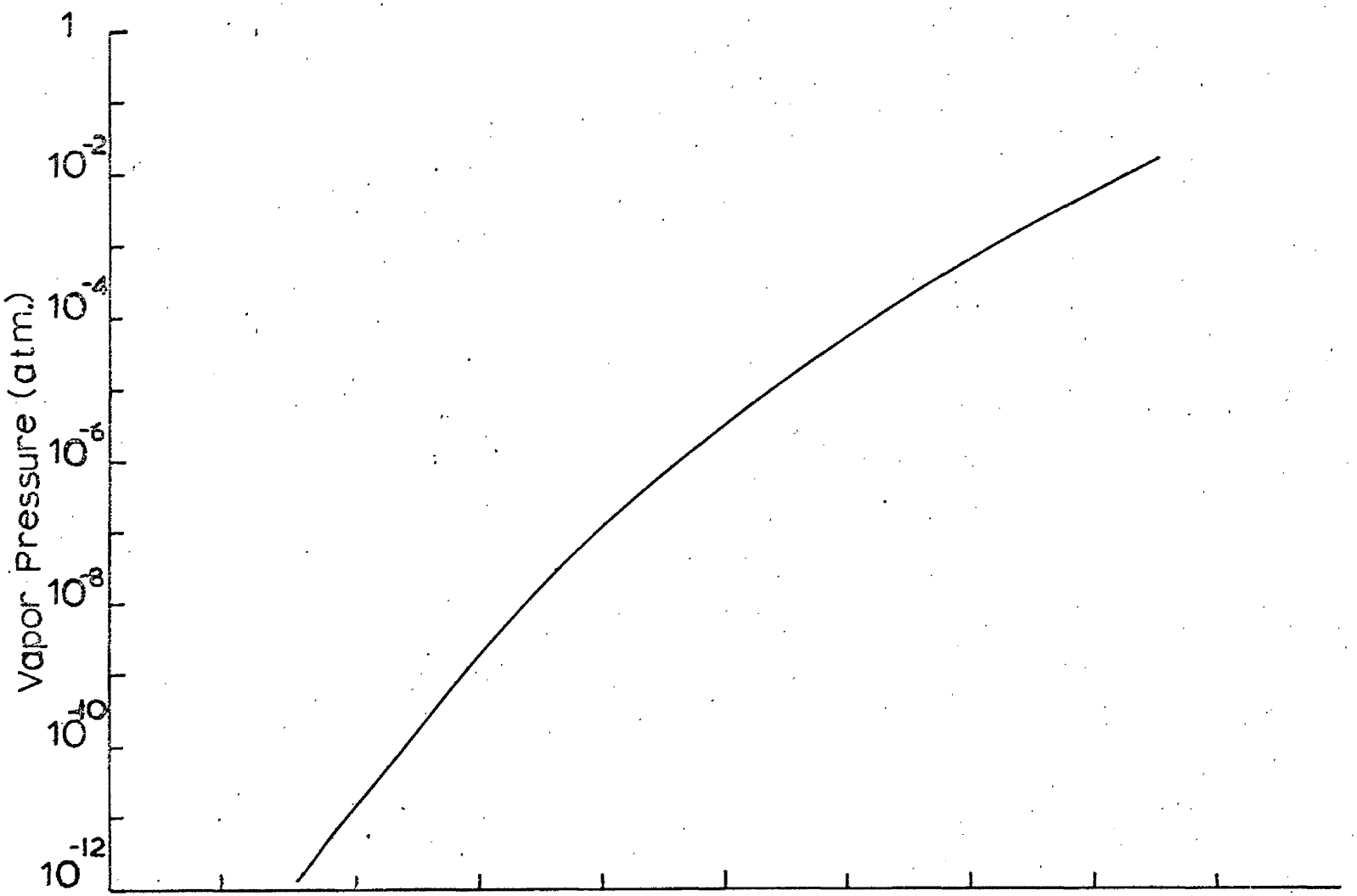

FIG.2·08. UO_2 Vapor Pressure.(76).

attributed to convection currents which were causing a slight temperature difference between the top and lower faces of the specimen in the susceptor. Thus there was assumed to be a small temperature gradient across the specimen with the rear face being at the higher temperature. It was, therefore, decided to alter the geometry of the furnace for high temperature measurements.

A new furnace was designed such that the coil could be wound around it and thus reduce the possibility of sparking since the gas atmosphere would not be in contact with the coil. It was necessary to have this furnace held horizontally in order to eliminate the 'convection' problem. This arrangement would also make alignment easier between the heat pulse source at the front and the detection system at the rear. It was intended to use the existing susceptor ($\sim$ 2" diameter) and graphite felt as the insulating material. Since it was necessary to get good coupling between the coil and the susceptor, they were to be as close together as possible therefore the smallest possible tubing was to be used. An alumina tube 2" diameter was obtained and water cooled brass flanges were designed to fit this tube at either end. A schematic diagram is given in fig.2.09. No arrangement for holding the specimen vertically had been finalised at this time.

While this furnace was being made, the problems of sparking, fluctuating trace and high temperatures were solved when a helium atmosphere and the new susceptor design were tried. Helium has a higher electrical strength than all other gases, as can be seen from the Paschen curves given by Guseva (77).

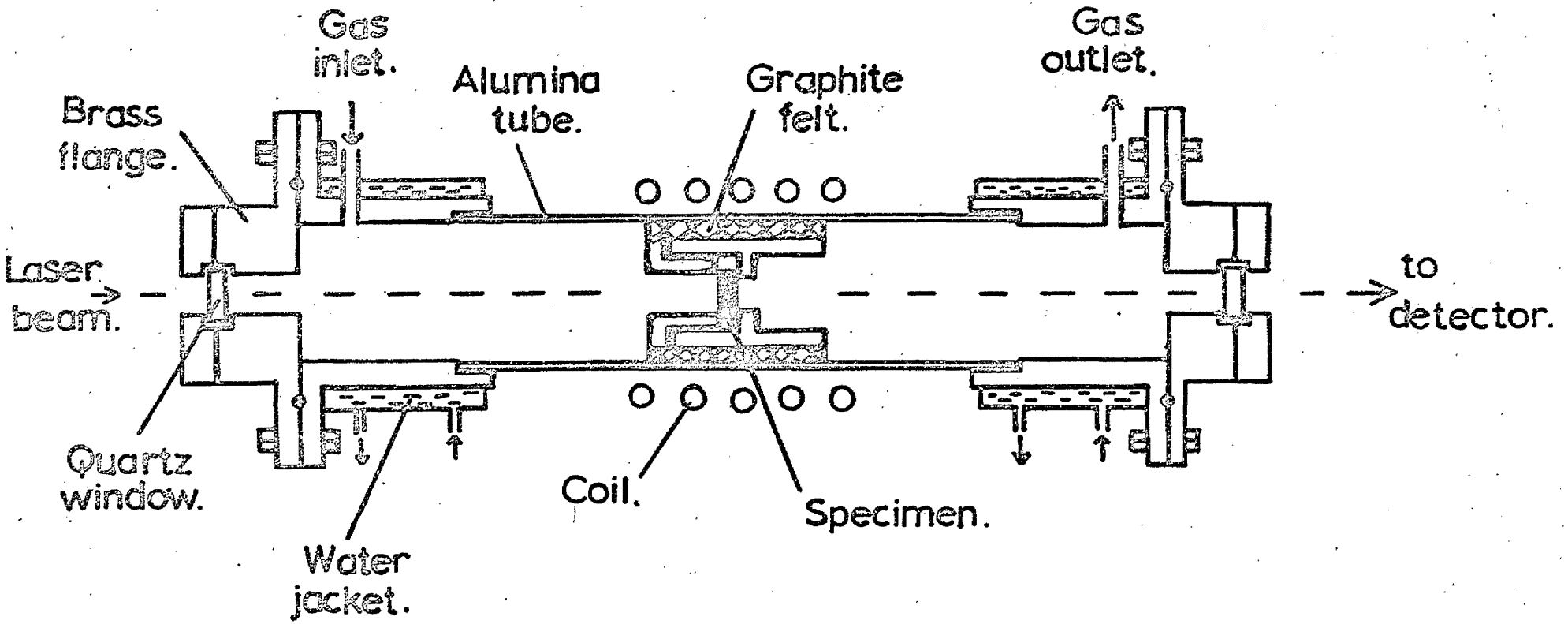

FIG. 209 High Temperature Furnace.

Also helium has one of the largest thermal conductivities of the inert gases, second only to hydrogen, and it has a value X9 that of argon. This should reduce the effect from convection since no large temperature difference should occur in the helium in contact with the specimen. The addition of a central tap from the H.F. set coil to the furnace chamber reduced the voltage above earth of the work coil inside the chamber, i.e. instead of having a voltage between the work coil and the surroundings (susceptor) of V volts, one had a voltage of $\pm V/2$. This reduction in the voltage difference minimised still further the possibility of sparking. It therefore made future measurements under vacuum or argon possible. All high temperature measurements on UO_2 were made using an atmosphere of 21-24 p.s.i. of high purity helium.

At all temperatures Cowan's correction for heat loss had to be applied (see Chapter 2A). This heat loss correction sometimes rose as high as 40-50% at very high temperatures. The results with this correction greater than 40% were not used in this investigation. To evaluate the correction required and to conserve Polaroid film, two traces at different sweep rates were taken on the same photograph. From one trace $t_{\frac{1}{2}}$ was measured and from the other the ratio of $T(10t_{\frac{1}{2}})$ to $T(t_{\frac{1}{2}})$ was measured. The photograph was mounted on the rear of a printed card, which also contained the relevent information for the calculation of the thermal conductivity. An example of a typical trace and card is given in fig.2.10. These cards could then be stored for future reference.

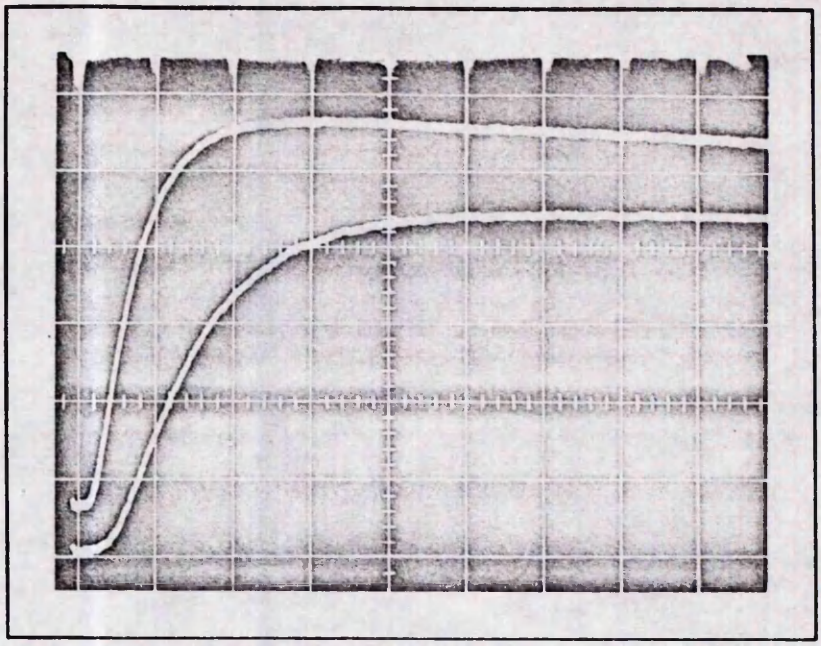

MEASUREMENTS No.

Material				Date	
Sensor	T/C		O/P	Lenses	Quartz / Ca Al.
Detector	T/C	InSb	PbS	Laser Output	(kV)
Temp.			(°C)	Corrected Temp.	(°C)
Heating Details					
Time base			(Sec/cm)	Sensitivity	(V/cm.)
$t_{\frac{1}{2}}$			(sec)	Specimen Length	(cm.)
$\Delta T\ (10t_{\frac{1}{2}})/\Delta T(t_{\frac{1}{2}})$				w/π^2	
Spec.Heat (Cp)			(watts/gm/°C)	Density(D)	(gms/cm^3)
Thermal Diff.(α)			(cm^2/sec)	Therm.Con.(K)	(W/cm/°K)

FIG. 2·10 TYPICAL TRACE AND CARD

CHAPTER 3

SPECIMEN PREPARATION

For the purpose of this investigation it was necessary to prepare specimens with varying pore volume fractions and with varying stoichiometries. The values of porosity and oxygen to uranium ratio were chosen such that they not only encompassed those values found within the reactor fuel but also enabled suitable comparisons to be made with other authors. In order to satisfy the last requirement the ranges had to be widened to include values seldom found in the reactor, i.e. oxygen to uranium ratios greater than 2.005 and porosities below 95-97% T.D.

A. Initial Material

The initial investigation was to examine the effect of porosity on the thermal conductivity, and considerable attention has been devoted to the preparation of the specimens in a previous thesis (1). However, a review of this work may be appropriate here.

To investigate the effect of pore volume fraction, specimens were to be prepared with densities in the range 90-96% T.D. A lower limit of around 90% T.D. was set since below this value there is a tendency for exaggerated grain growth to occur (78). A further drawback arises from the tendency for low density specimens to densify on subsequent heat treatment (78). From one batch of powder the specimens were prepared by pressing and sintering, and the following densities were obtained: 95.89% T.D. (nomenclature 96), 93.16% T.D. (93^{x}), 90.97% T.D. (91^{x}). These specimens had randomly distributed pores and their grain sizes lay in the range 4 to 6μ.

Unfortunately, the specimens of 93^{I} and 91^{I} had too high an impurity content of copper, for which an arbitrary tolerance level of 100 p.p.m. (parts per million) had been set by the U.K.A.E.A. (78). It was necessary, therefore, to prepare new batches in order that the effect of impurities could be disregarded. Specimens were prepared having densities of 94.89% T.D. (94^{II}) and 91.42% T.D. (91^{II}), and they had grain sizes around 8 μ.

To investigate the effect of effect of pore redistribution on the thermal conductivity, specimens were prepared having densities nominally 93% T.D. and 91% T.D. from the 96 (95.89% T.D.) by holding some of the specimens of 96 at 1600°C in a mixture of 90 vol.% carbon dioxide and 10 vol.% hydrogen. The CO_2 acts as an oxidiser with respect to the hydrogen, and thus oxygen diffuses into the UO_2 lattice. This oxygen reacts with the carbon left from the binder used during pressing, and forms CO/CO_2 bubbles. On cooling these bubbles form isometric pores, and, since the carbon is finely dispersed along the grain boundaries, the pores form on grain boundaries and at triple points. Also existing pores grow at the expense of smaller ones thus intergranular pores tend to disappear. The net effect is a reduction in the density of the original 96 material and a redistribution of the pores. By varying the duration of the process, any amount of reduction can be effected. After 26 hours a density of 94.43% T.D. (nomenclature 9694) was obtained; after 90 hours 92.15% T.D. (nomenclature 9691). A side effect of this process was that the grain sizes increased by a factor of three to $\sim 17 - 30$ μ. It was also

necessary to hold the specimens in hydrogen at 1600°C for one hour, and then at 1300°C for 2 - 6 hours in order to effect some reduction back to stoichiometry.

All the above sample batches were made in the form of pellets 1.016cm. diameter 1.27cm. long. Initially specimens 0.1524cm. thick were sectioned from these discs and used for thermal diffusivity determinations. At high temperatures $t_{\frac{1}{2}}$ for these samples was about 0.5 seconds. With this value of $t_{\frac{1}{2}}$ inordinately large heat losses occurred, necessitating a heat correction of the order of 50% in the value of the constant w/π^2. Moreover, the total sweep time was of the order of 5 seconds compared to a more desirable time of <1 second, and this meant that one had to wait longer for equilibrium conditions, i.e. for when the trace would be stable enough for a measurement to be taken. Therefore, to give more practicable $t_{\frac{1}{2}}$ values ($\sim 0.05 - 0.10$ seconds), further specimens 0.0686cm. long by 1.016cm. diameter were sectioned from the pellets. Considerations of the optical arrangement of the system showed that only radiation from the centre of the sample was collected and focussed on the detector. Since the total heat loss from the sample may include heat conducted into the sample holder, this should have a proportionately greater effect on the conductivity measured using a sample of smaller diameter. (This is of special interest to the single crystal specimen, see next section). Accordingly samples 0.6604cm. diameter by 0.0686cm. long were prepared, and this represented a 40% reduction in the cross sectional area. Details of the specimens and the sizes which were finally measured are given in tables 3I and 3II.

Nomenclature	Density (g/cm^3)	o/u ratio	Grain Size (μ)	Impurity Content (ppm.)								
				Fe	Si	Cr	Ni	Mg	Ca	Cu	C	N
96	10.51	2.001	4.6	60	15	7	2	15	17	11	20	30
93^{I}	10.21	2.001	5.7	65	25	7	2	15	45	275*	20	30
91^{I}	9.97	2.001	6	60	25	7	2	15	18	155*	20	20
94^{II}	10.40	2.001	8 9	75	10	5	3	15	19	35	20	20
91^{II}	10.02	2.001	8	80	35	5	2	15	18	90	20	20
9694	10.35	-	17									
9691	10.10	-	30									

* above tolerance level of 100 ppm.

TABLE 3.I.

SPECIMEN SIZES

Type A - 1.016 cm. diameter by 0.1524 cm. thick

Type B - 1.016 cm. diameter by 0.0686 cm. thick

Type C - 0.6604cm. diameter by 0.0686 cm. thick

Name	Type Tested
96	A,B,C
94^{II}	B
93^{I}	A,B,C
91^{II}	B
91^{I}	A,B,C
9694	A,B,C
9691	A,B,C

96	2006	B
	2030	
	2060	

93^{I}	2006	B
	2030	
	2060	

TABLE 3. II

B. Single Crystal

Two single crystals had been supplied (78), and it was intended to cut suitable specimens for use in the laser - flash apparatus. The thermal conductivity values obtained from these specimens would be of scientific interest since very little work has been performed on single crystal UO_2. However, more relevant to this investigation, the values would provide a reference against which the polycrystals could be compared, i.e. the single crystal will have no resistivity contribution from grain boundaries and porosity. An attempt was made to cut a parallel-sided piece from one of the crystals using a diamond cutting wheel. This was not successful, the crystal breaking. It was decided, therefore, to use a microslice annular saw which was known to be able to cut discs of any thickness from the most brittle of materials. Since this machine was not available, the second single crystal was sent to Metals Research to be cut into 0.0762cm. and 0.1270cm. thick slices on their annular saw. They managed to obtain two discs each of these thicknesses plus one disc 0.0254cm. thick. Owing to the irregular shape of the crystal, the cut discs were of irregular shape but were approximately 0.2cm. square. It was necessary to machine graphite holders for them and graphite lids for the susceptor. Then, using a fine file, final adjustments to the holders were made to ensure a better fit. The discs used in the laser - flash apparatus were orientated before and after measurement, and the results are given in Chapter 6.1. Any effect on the structure caused either during cutting or during measurement would be observed from an exam-

ination of the X-ray patterns.

C. Variation of $^{O}/_{U}$ ratio

Subsequent to the investigation of the effect of porosity, it was decided to prepare specimens of higher oxygen content and to investigate the effect of non-stoichiometry. Pellets of 96 and 93^{I} were sent to Springfields where they were cut into discs 0.0686cm. thick and then held in a furnace at 1800^{O}K for $4\frac{1}{2}$ hours in a carbon dioxide/carbon monoxide atmosphere. By varying the ratio of this gas mixture, the required amount of oxidation was achieved:

a ratio of CO_2/CO = 0.57 gave an $^{O}/_{U}$ ratio of 2.006
" " " = 1.198 " " " " " 2.030
" " " = 8.97 " " " " " 2.060

These values were fairly close to the ones required namely 2.005 - 2.05. This low value $\sim$ 2.005 was chosen since during fission in a reactor the surplus oxygen must be shared between the molybdenum and the uranium dioxide, and one gets $UO_{2.003 \pm 0.001}$ (thus 2.005 is a realistic value). The range 2.005 to 2.05 was chosen in order that the results could be used in a comparison with results by other workers, i.e. one might be able to explain their results and the reason for the divergency between them in terms of non-stoichiometry. It was felt that three discs of each $^{O}/_{U}$ ratio would be sufficient for measurement of diffusivity and for post test $^{O}/_{U}$ ratio, density and grain size determinations. This proved to be a little optimistic since the specimen weight was less than 1gm. (the lower limit for a stoichiometric analysis) and hence two specimens were required for one stoichiometric analysis. This left one specimen

for density and grain size determinations. Thus, providing not too many specimens were broken, and that all broken pieces were collected, it was just possible to obtain all the information required to characterise the specimens after testing. Unfortunately the batch 96 with $^{o}/_{u} = 2.030$ provided no specimen for density or grain size determinations.

D. Tungsten coating

The final stage in the preparation of all the specimens prior to their use in the "flash" apparatus required their being coated in tungsten on both front and rear faces. This was done to ensure that all the heat from the laser was absorbed in the surface layer, and that no heat was transmitted through the specimen without being first absorbed by it. This would cause an incorrect higher diffusivity to be recorded. Other research workers (43, 79) have coated UO_2 specimens in tungsten for this reason, however Bates (43) noticed no difference in his results on coated and uncoated polycrystalline specimens upto 2500°C in argon. It was felt to be more important for the single crystals which would be more transparent by nature than the polycrystals (39).

A schematic diagram is given in fig. 3.01. The specimens were held in a vacuum of the order of 10^{-4} Torr, whilst tungsten was evaporated onto them. By using a glass slide placed over some of the holes in the holder, it was possible to determine whether sufficient tungsten had been evaporated in order to give an opaque coating to the specimens (a layer $\sim$2000Å was required). The method of support left a region around the edge of the discs which was not coated, however, this rim (< 0.1cm.) was of the same order as that of the pyrolytic and tungsten

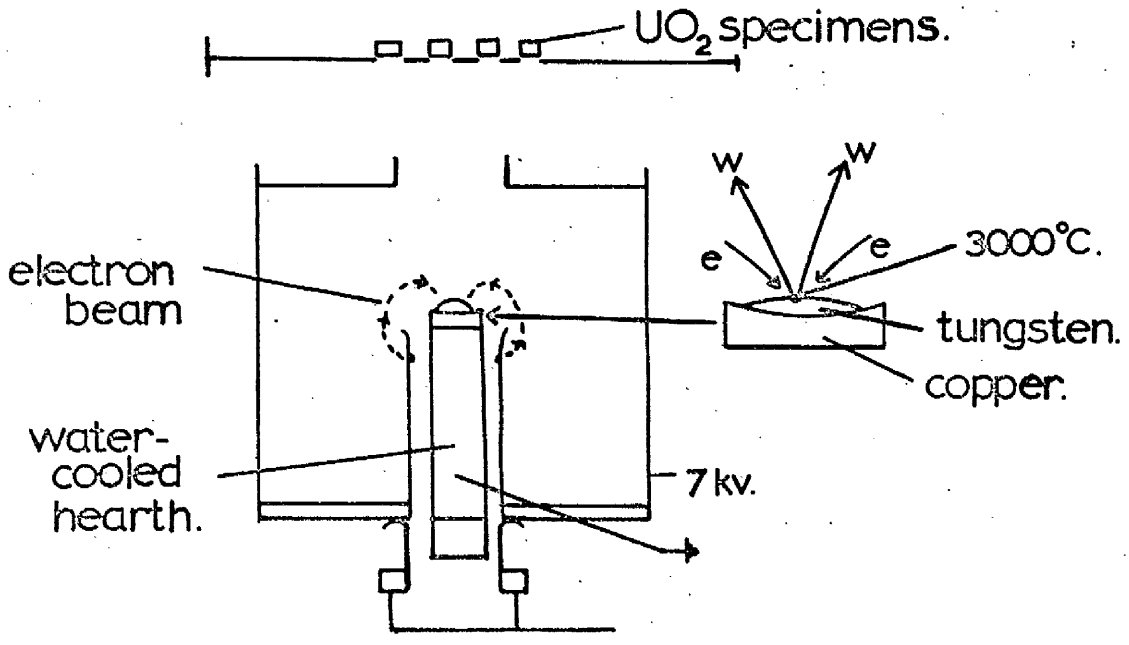

FIG.3.01. Tungsten Coating.

holders in the "flash" apparatus. Using this method of support upto six discs could be coated at any one time. The single crystals were held one at a time in a vice - like holder, which enabled the whole face to be coated, i.e. it left no uncoated region. Initially, some of the high density discs became very hot during the coating operation, reaching about 500°C. Thus the coating had to be performed in short bursts, allowing the discs to cool sufficiently before applying another layer of tungsten. There was a tendency for the tungsten coating to flake off during measurement in the "flash" apparatus. This occurred, however, only amongst the early batches of material to be coated, and no signs of any flaking were found amongst subsequently coated specimens. Since the conditions for coating did not alter, it was felt that the cause of flaking lay in the purity of the tungsten. It may not have been coating as a sufficiently fine vapour owing to impurities such as occluded gases.

E. Metallography

Initial tests showed that the 'A' specimens (see table 3II) had too large a $t_{\frac{1}{2}}$ and this increased the possible errors due to heat losses. The 'C' specimens were too fragile and most of them broke either during measurement or during handling. As a consequence only a few results were obtained on 'C' specimens, and no complete runs were possible. Since the 'B' specimens were producing consistent results and the few results from the 'C' specimens were in very good agreement with these, it was decided to make use of the former and disregard the latter. Also, the few values obtained initially on 'A' specimens were slightly lower than those

from the 'B' type, so these were disregarded as being less accurate. Consequently, post - test examinations were performed only on 'B' specimens.

When the tested specimens were examined under the microscope, some cracking was found in those which had been mounted by hot pressing. Since cracks were not observed in other specimens of the same category which had been cold mounted, it was assumed that the method of mounting had caused the cracking. A few specimens did crack across their diameter whilst being removed from the apparatus after being tested, but no cracks were found in these specimens when the two halves were examined. As a consequence of loss of specimens due to cracking (during handling or in the room temperature holder (see chapter 2B)) and the need to send some away for analysis, there were no specimens of 91^{II} or 96.2030 left for metallography.

The remaining post test specimens were polished on emery paper and then 6μ and 1μ diamond paste. Finally an attack polish was performed using a suspension of alumina in hydrogen peroxide (10% by vol. H_2O_2/90% H_2O) on a selvyt cloth. They were etched in 95% vol. H_2O_2/5% vol. H_2SO_4 at 60^{o}C for approximately 10 to 15 seconds.

Density measurements were performed prior to etching using the quantimet. Since there was good contrast between pores and matrix, consistent results were obtained for each specimen (i.e. within 1% of each other). It was not possible to measure grain sizes using the quantimet, since the instrument relied on being able to differentiate between the

light intensities of the grain boundaries and the grains. In these specimens considerable etch pitting (and some grain tear-out) occurred causing the quantimet to register the pitting as possible grain boundaries. Any attempt to compensate for this intergranular "grass" led to results which could differ by as much as 300% (i.e. 5μ to 15μ). For this reason grain sizes were obtained by counting using a Vickers microscope and a magnification of X300. This technique was used in ref.1.

Specimens were sent to Springfields for stoichiometric analysis, where the U^{6+} ion concentration was measured by a polarographic method. This method had the disadvantage that it could not detect whether the specimens had gone hypo-stoichiometric ($^{O}/_{U} < 2.00$), although it could state the oxygen/uranium ratio to less than 2.001.

Since the single crystals were too few in number and too small, no stoichiometric or impurity content determinations were possible. Therefore, no values have been quoted for these parameters for the single crystals. However, in an attempt to further characterise the crystals, X-ray patterns were taken before and after measurement. Laue's back reflection method was used together with white radiation. The tungsten coating was removed from the single crystals by fine emery paper prior to the post test X-ray analysis. The crystal was then aligned on a goniometer so that one of the two parallel-sided faces was perpendicular to the X-ray beam and 3cm. from the X-ray film. Values of 40kv and 16ma were applied across a tungsten tube in order to produce white radiation, and suitable negatives were obtained after an exposure of approximately 45 minutes. By using a Greninger chart and a

Wulff net, the angles between the spots on the negatives could be measured. The spots could then be orientated using the angle values given by Mirkin (80). It was assumed that the spot coinciding with the centre of the negative, or the spot closest to the centre, was the spot caused by X-rays being reflected from the front face of the crystal. An example of a typical negative and the crystal orientation are given in fig. 6.01 Chapter 6.1.

The results from the stoichiometric and metallographic analyses are given in Chapter 6 Table 6I.

Further to this metallography, photomicrographs were taken at a magnification of X300 using a Reichert microscope and these are given in chapter 6. For micrographs at large magnifications (X1000 to X1500), the electron microscope and secondary carbon replicas were used. The mounted specimens had their surfaces covered in a plastic layer, which on removal was coated in a fine layer of germanium and then in a thicker layer of carbon. The layer of carbon and germanium (i.e. the replica) was separated from the plastic by dissolving the plastic in acetone. The replica was then put onto a grid for use in the electron microscope. Micrographs obtained from these carbon replicas are shown in chapter 6.

CHAPTER 4

VARIABLES

The equations being used to calculate 'α' and 'k' values have already been given as $\alpha = \left(W/\pi^2 / t_{\frac{1}{2}}\right) . L^2$

and $k = \alpha . C . D$

Of the variables within these equations only C and L could not be measured directly in this thesis, every other variable could be measured, (L in this context is not the actual length measured but refers to the coefficient of linear expansion required to correct the measured L at 300°K to L at T°K). These two variables must be obtained from published data, and the choices and factors influencing them are discussed below.

4a) Coefficient of Linear Expansion

$\frac{W}{\pi^2}$ and $t_{\frac{1}{2}}$ are easily obtained by direct measurement of the trace, and they have already been mentioned in Chapters 3A and B. For an accurate determination of the length (L) it is necessary to know the coefficient of linear expansion of UO_2. Values quoted in the literature give values that agree quite well:

Rough/Dickerson	(81)	12.6×10^{-6} / °C	800 - 1250°C
Krikorian	(82)	12.19×10^{-6} / °C	25 - 1200°C
Bradshaw/Mathews	(83)	11.15×10^{-6} / °C	25 - 1750°C
Warde	(84)	11.2×10^{-6} / °C	27 - 1260°C
Baker/Baldock	(85)	9.4×10^{-6} / °C	20 - 2000°C

A comparison of the values given by Conway et al (86), Burdick and Parker (87) and M^c Ewan (88) are given in fig 4.01. This is not a true comparison since each author took their unit length at different temperatures: Conway et al used L at 25°C, Burdick/Parker used L at 27°C, and M^c Ewan used L

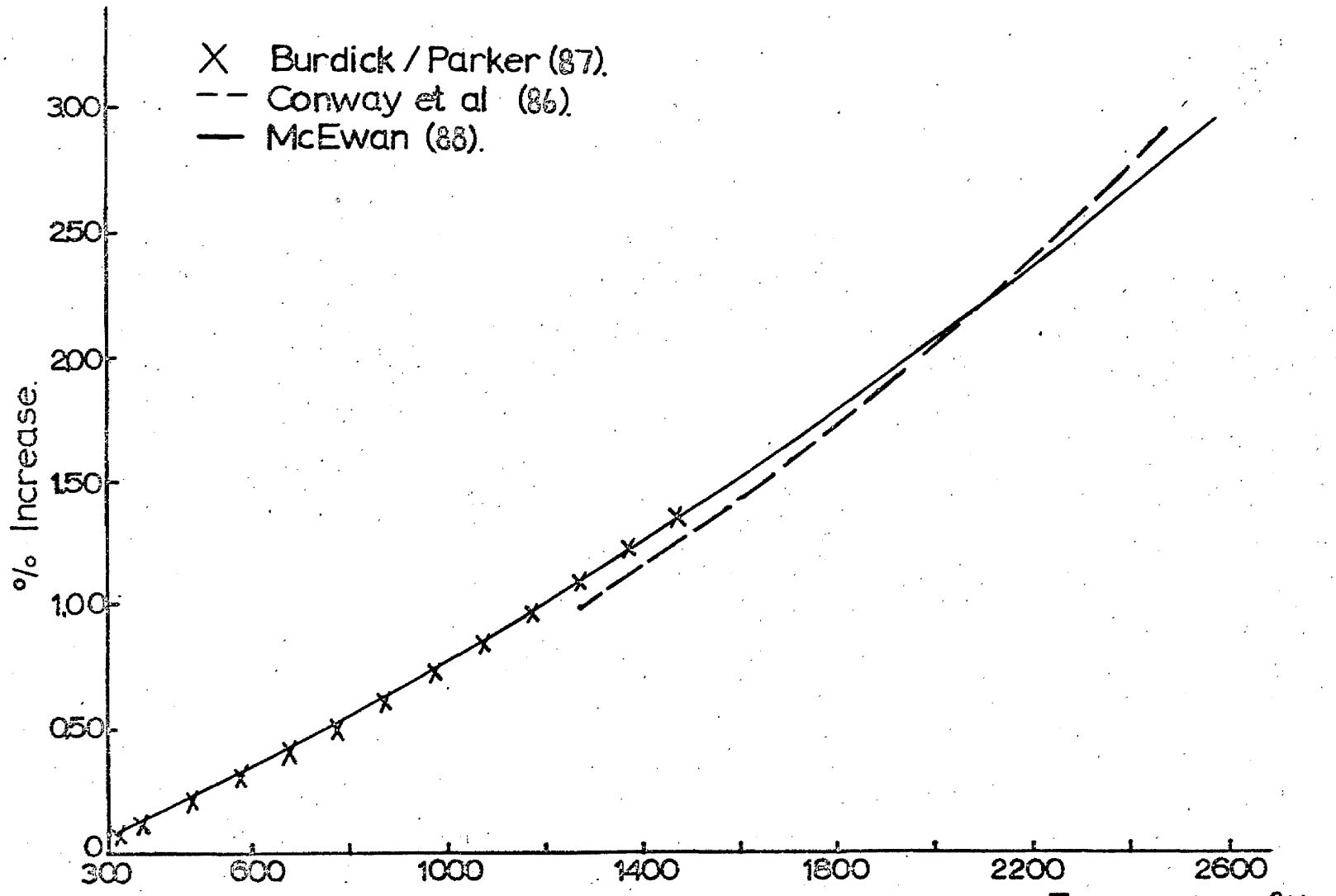

FIG. 4-01. % increase in L with T.

at 20°C. The value chosen for use in this thesis was that of M^{c} Ewan, a choice that was arbitrary.

The coefficient of linear expansion decreases with increasing $^{O}/_{U}$ ratio, Murray/Thackray (89) show the difference in this coefficient between $^{O}/_{U}$'s of 2.00 and 2.13 to be 1% at 500°K rising to 2% at 1200°K. The difference, therefore, is very small, i.e. at the most of the order of 2%, and so the above coefficient was used for the non-stoichiometric specimens as well.

4b) Specific Heat

In order to calculate thermal conductivity (k) from the measured thermal diffusivity values (α), equation 0.01 is used:

i.e. $$k(T) = \alpha(T).C_p(T).D$$

The density (D) is well described and is assumed to be constant with temperature. Therefore, the computed conductivity values will be strongly influenced by the specific heat values (C_p) chosen. A large number of investigations have been carried out to determine the specific heat of uranium dioxide. However, the results tend to show quite a wide variation.

The most quoted data is that of Moore/Kelley (90) who used a drop method and found C_p to increase steadily with temperature. Conway et al (86) also used a drop method, and Conway/Hein (91) analysing the results found a more rapid increase in C_p with temperature than Moore/Kelley. Godfrey et al (92) used published data to obtain an equation for C_p, and this equation fitted the values calculated from the data of Popov et al (93), but was higher than that calculated using Moore and Kelley's data. Ogard/Leary (94) used drop

calorimetry to get C_p UO_2 between 1338 - 2303°K. They applied a least squares analysis to their enthalpy results, and chose the most suitable C_p equation. This equation agreed better with the data of Moore/Kelley than with that of Conway/Hein, so they used the former and their own equation to derive a final enthalpy equation. Hein/Flagella (95) and Hein et al (96) used the drop technique (1200 - 3260°K) plus a least squares analysis. They agreed well with Moore/Kelley and with Conway/Hein but not with Ogard/Leary. More recently Affortit (97); Leibowitz et al (98); Engel (99); Grønvold et al (100); Hach (101); Fredrickson/Chasanov (102) have all tried to define C_p UO_2 . Engel (99) and Affortit (97) both used thermal analysis rather than drop calorimetry, and both, measured heat capacity directly. Engel agrees well with Moore/Kelley. Affortit gives values that differ greatly from those of other workers, being lower over the whole temperature range. The results of Grønvold et al (100) and Fredrickson/Chasanov (102) agree fairly well - the latter making the point that the results of Moore/Kelley (90) and Hein/Flagella (95) were obtained using hypo - and hyperstoichiometric specimens respectively.

Some of the results of the above workers are given in fig. 4.02 along with the values used in this work. It can be seen from this graph that the values show wide variation and different trends and, the scatter is of the order of 8% at 1300°K, rising to 26% at 2300°K. Shaw (103) observed that, though the C_p data of other workers showed wide variation, their heat content measurements were in good agreement. Since specific heat is obtained by differentiating heat content with respect to temperature:

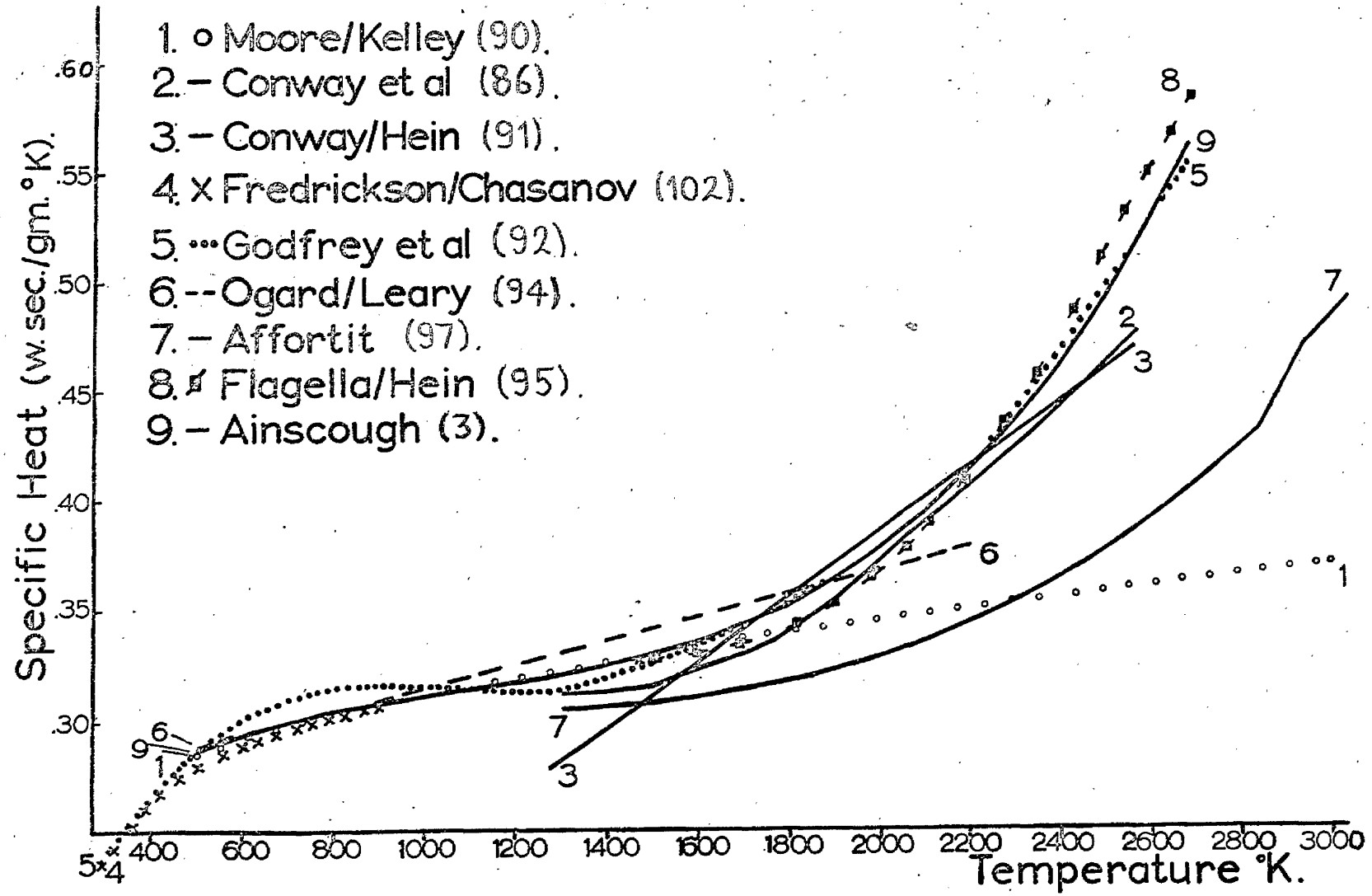

FIG. 4.02. Specific Heat Data for UO_2.

$$\frac{d(H_T - H_{298})}{dT} = C_p(T) \qquad (4.01)$$

(where H_T is the enthalpy at T^oK, H_{298} is the enthalpy at 298^oK), the variation must lie in the form of the mathematical expression chosen to describe the heat content values. It can be seen, therefore, that there is a great need for direct measurement of specific heat, and the IAEA Panel (104) stressed the importance of obtaining high temperature C_p values by adiabatic techniques rather than by enthalpy increment determinations. Several authors have since obtained C_p by direct measurement (4, 97, 99).

Since the wide variation in existing C_p data appears to be occasioned by selection of curve used for enthalpy, it was decided to collate all available data. Accordingly all available enthalpy data for UO_2 was assembled in order to be fitted, using a computer programme, to a polynomial expression from which a new C_p curve could be obtained. A fourth order polynomial was adopted (Ainscough (3)):

$$(H_T - H_{298.2}) = -4802.30 + 14.299T + 6.3679 \times 10^{-3}T^2 - 3.3357 \times 10^{-6}T^3 + 7.6990 \times 10^{-10}T^4 \qquad (4.02)$$

(T^oK)

which on differentiation gave:-

$$C_p = 14.299 + 1.2736 \times 10^{-2}T - 10.0071 \times 10^{-6}T^2 + 3.0776 \times 10^{-9}T^3 \quad cal/mole^oK \qquad (4.03)$$

This expression gave C_p to increase with temperature, whereas the 5^{th} order polynomial gave a slight decrease in C_p of the order of 0.66% between the temperatures 1000 - 1400^oK. There is no theoretical reason for such a decrease in C_p except the choice of the wrong polynomial, therefore the 5^{th}

order or above were not used. Only the 4^{th} order curve is given in fig. 4.02 (it is interesting to note that the curve of Godfrey et al (92) shows a similar drop between 900 - 1300°K).

This C_p curve is in good agreement with the curves of other authors, except those of Conway/Hein (91) below 1700°K; Affortit (97) and Moore/Kelley (90) both of which are much lower at high temperatures. It agrees well with Flagella/Hein (95) and Godfrey et al (92) at high temperatures. Thus it was decided to use this calculated data to convert the diffusivity data into conductivity values, rather than to attempt any direct measurement of specific heat of the test specimens. This would have required the use of a specialised piece of equipment and would have taken the author into an area which, though important, was felt to be outside the range of this investigation. Similarly, since the curve obtained by Ainscough was in good agreement with other workers and since most of the existing heat content data on UO_2 were in good agreement, it was felt unnecessary to use facilities which were available elsewhere. Such facilities may have confused the matter further by producing contrasting specific heat data, and it was felt that Ainscough's curve would describe the specific heat adequately. Obviously if it had been possible, it would have been interesting to obtain direct specific heat measurements on test specimens to see how they compared with those calculated by Ainscough.

Although this curve was thought satisfactory for stoichiometric UO_2 , it can not be considered suitable for use with the hyperstoichiometric samples ($UO_{2.060}$, $UO_{2.030}$ and $UO_{2.006}$),

since it has been shown that the specific heat increases with increasing oxygen/uranium ratio due to an electronic contribution (ref. Hoch (101)). Very little work has been performed to relate $^{O}/_{u}$ ratio to C_p , however Affortit/Marcon (4) and Grønvold et al (100) have supplied some C_p results for selected $^{O}/_{u}$ ratios. Affortit/Marcon used a dynamic method to measure directly the specific heat of several hyperstoichiometric samples between 1600°K and their melting point. Grønvold et al measured the specific heat of $UO_{2.017}$ and $UO_{2.254}$ between 300 - 1000°K using adiabatic calorimetry. Both gave graphs of specific heat against temperature, but as yet no one has equated C_p to $^{O}/_{u}$ ratio. The values of Affortit/Marcon were considered very low (about 12% low at 2500 °K), therefore they could not be used, but as they were the only workers to give concerted data for hyperstoichiometric UO_2 their values have been used for comparison purposes.

It was decided to extrapolate their results to 500°K and to use them to obtain the ratios $\frac{C_p\ UO_{2.060}}{C_p\ UO_{2.00}}$, $\frac{C_p\ UO_{2.030}}{C_p\ UO_{2.00}}$ and $\frac{C_p\ UO_{2.006}}{C_p\ UO_{2.00}}$. These ratios could be used in conjunction with the $C_p\ UO_{2.00}$ values of Ainscough (3) to arrive at the required $C_p\ UO_{2.060}$, $C_p\ UO_{2.030}$ and $C_p\ UO_{2.006}$ values. In order to do this a graph of Affortit/Marcon's values had to be plotted (fig. 4.03a) from which the ratios $C_p\ UO_{2+x}/C_p\ UO_{2.00}$ could be calculated (using five temperature values and their three "x" values, namely 2.10, 2.04 and 2.03). These ratios were plotted as percentages against $^{O}/_{u}$ ratio (fig. 4.03b), and consequently

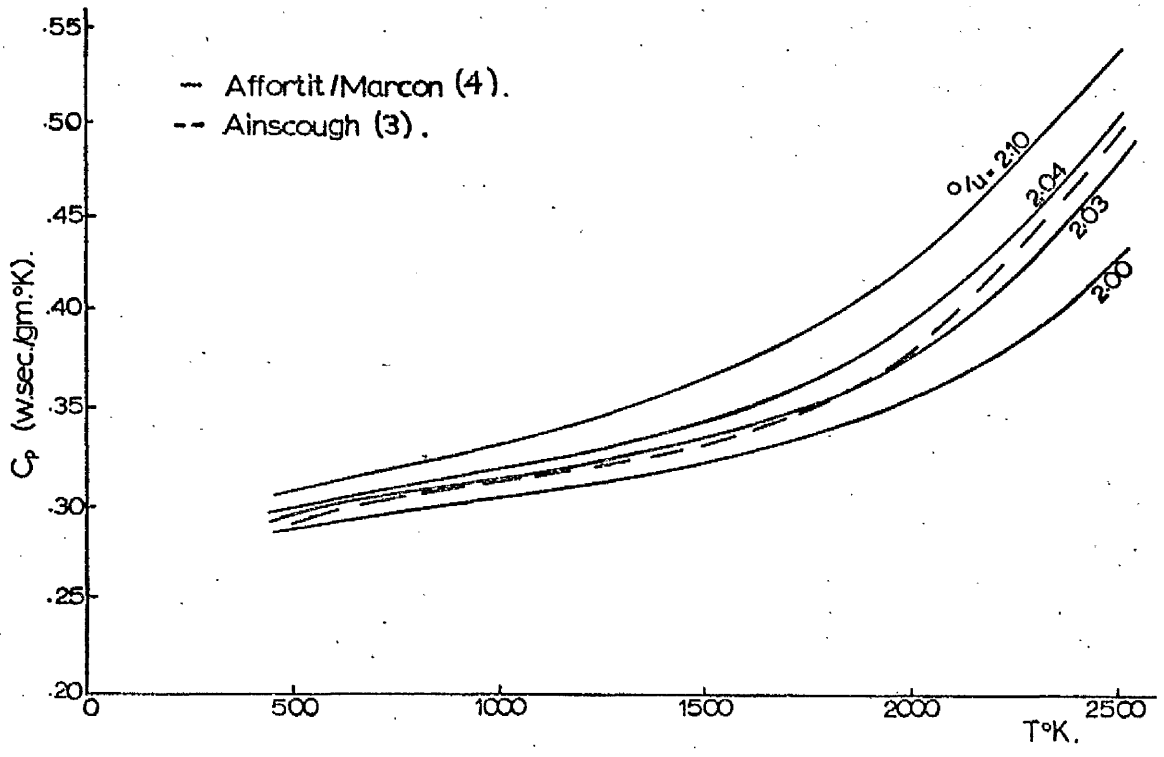

(a).

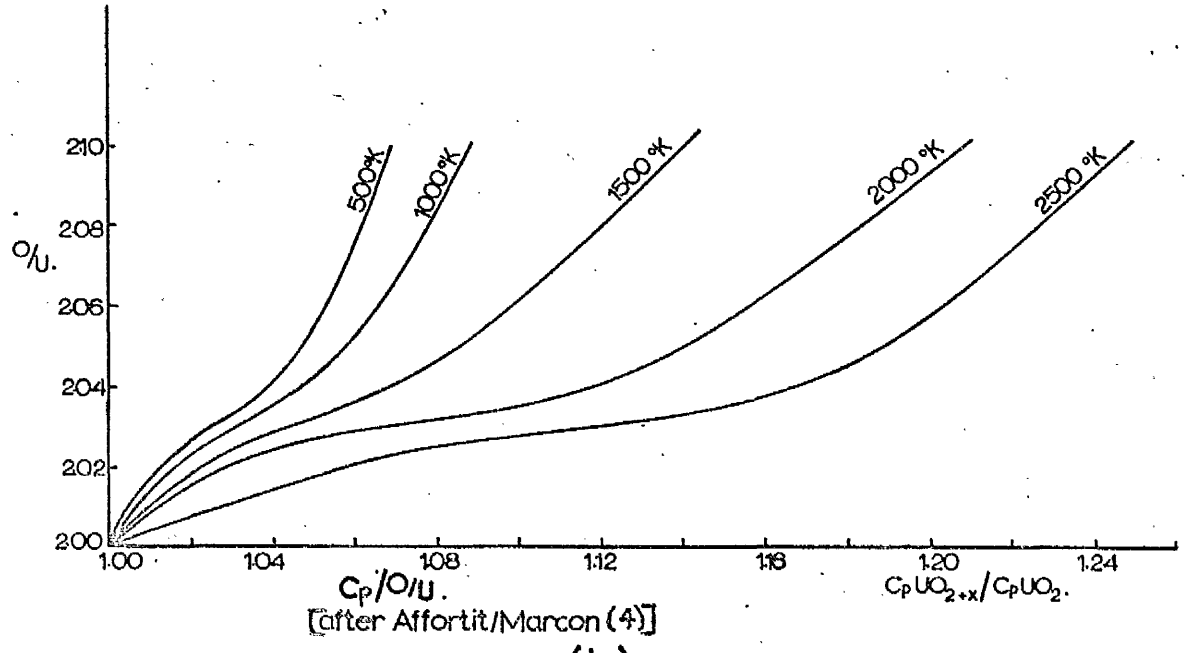

(b).

FIG. 4·03. C_p Data for UO_{2+x}.

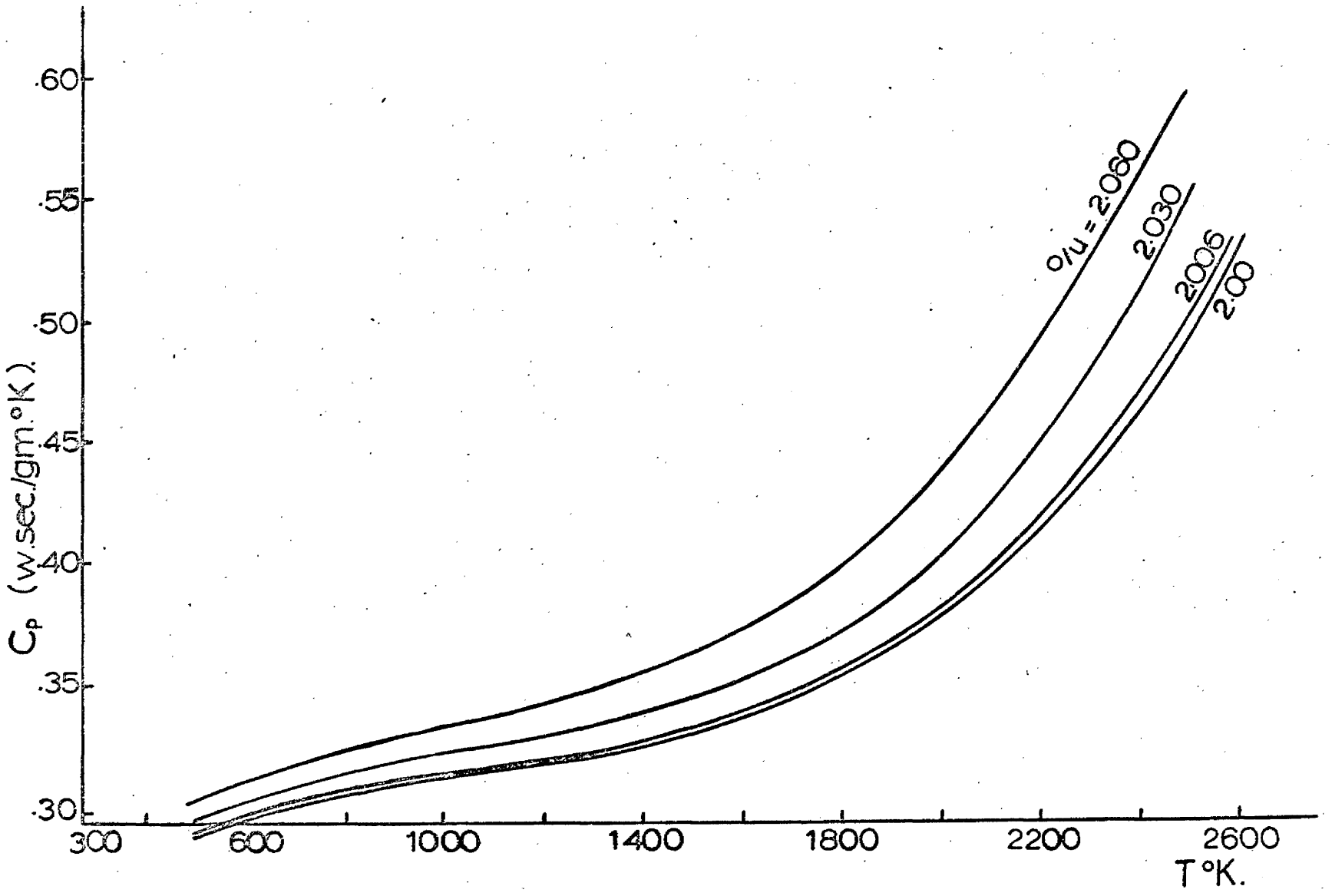

FIG. 4.04. Calculated C_p Curves for UO_{2+X}.

the ratio $C_p\ UO_{2+x}/C_p\ UO_{2.00}$ for x = 2.060, 2.030 and 2.006 could be read off at the five temperatures. These ratios, when multiplied by the corresponding $C_p\ UO_{2.00}$ value of Ainscough at each of the five temperatures, gave the absolute values of $C_p\ UO_{2.060}$, $C_p\ UO_{2.030}$ and $C_p\ UO_{2.006}$. These values are plotted in fig. 4.04. Since the difference between the values of $C_p\ UO_{2.00}$ of Ainscough and the calculated values of $C_p\ UO_{2.006}$ was only of the order of one percent, it was decided to use the values of Ainscough for $C_p\ UO_{2.00}$ when calculating the thermal conductivity of the $UO_{2.006}$ specimens.

CHAPTER 5

ERROR ANALYSIS

In examining the errors in the calculated "α" and "k" values, it is important to separate those errors which are due to direct measurement and those due to the use of unknown variables (such as C_p and L, see chapter 5). It is possible to view these separately under the headings:

i absolute error in measurement of diffusivity

ii error in calculated conductivity

i Error in α

Since the diffusivity is calculated from

$$\alpha = (W/\pi^2) \cdot L^2/t_{\frac{1}{2}} \qquad (5.01)$$

we get

$$\therefore \ln \alpha = \ln W/\pi^2 + 2\ln L - \ln t_{\frac{1}{2}} \qquad (5.02)$$

$$\text{giving } \frac{\partial \alpha}{\alpha} = \frac{\partial (W/\pi^2)}{W/\pi^2} + \frac{2\partial L}{L} - \frac{\partial t_{\frac{1}{2}}}{t_{\frac{1}{2}}} \qquad (5.03)$$

a) $\partial t_{\frac{1}{2}}$:

Measurements carefully taken by different observers show that $t_{\frac{1}{2}}$ can be measured to $\pm$ 0.25 mm. and since $t_{\frac{1}{2}}$ lay in the range 10-20 mm., the error was given as lying between ($\pm$ 1.25 to $\pm$ 2.50)%.

b) ∂L :

The specimen length of 0.70mm. could be measured to $\pm$ 0.005 mm., thus giving an error of $\pm$ 0.7%. This length was corrected for different temperatures using M^{c} Ewan's (88) coefficient of linear expansion (chapter 4 fig. 4.01). The error in reading from this curve is $\ll$ 1%, but the actual error

due to the use of this curve is indeterminate.

c) (W/π^2):

The error in Cowan's correction is more difficult to calculate. It depends on such factors as actual value of $t_{\frac{1}{2}}$ and the rate of heat loss, both of which will affect the magnitude of $\Delta T(10t_{\frac{1}{2}})$, i.e. the larger $t_{\frac{1}{2}}$ and the rate of heat loss; the smaller $\Delta T(10t_{\frac{1}{2}})$ and hence the larger the error in measuring $\Delta T(10t_{\frac{1}{2}})$. Two traces were always measured, one from which $t_{\frac{1}{2}}$ was obtained and another at 0.4 or 0.5 times the sweep rate from which $\Delta T(10t_{\frac{1}{2}})$ was obtained. One feature was that as heat losses increase then $t_{\frac{1}{2}}$ may be larger, remembering that in the ideal case $t(T_{max}) > 5t_{\frac{1}{2}}$ but with increasing heat losses $t(T_{max}) < 5t_{\frac{1}{2}}$. Two cases are illustrated:

case I At a temperature of 1300°K some of the typical values measured were: $t_{\frac{1}{2}} \sim 8$mm. $\pm$ 0.125 ,

$\Delta T_m \sim 42 \pm 0.25$mm. (i.e. $\Delta T(t_{\frac{1}{2}}) \sim 21 \pm 0.125$mm.)

$\Delta T(10t_{\frac{1}{2}}) \sim (37.25 \text{ to } 36.50)$ mm. $\pm$ 0.25 mm.

$\therefore$ Error in $\Delta T(10t_{\frac{1}{2}}) = \pm 0.6\%$

$\therefore$ Error in $\Delta T(t_{\frac{1}{2}}) = \pm 0.5\%$

$\therefore$ Error in $\Delta T(10t_{\frac{1}{2}})/\Delta T(t_{\frac{1}{2}}) = \pm 1.1\%$

Taking this ratio $T_{10}/T = 1.75$

then $1.73 < T_{10}/T < 1.77$

From Cowan's curve this gives

$.1290 < W/\pi^2 < .1300$

i.e. Error in $W/\pi^2 = \pm 0.4\%$

(It can be seen that this justifies the use of T_{10}/T rather than T_5/T, as an error of 1% in T_{10}/T gives an error in W/π^2

of $\pm$ 0.4%, whereas an error of 1% in T_5/T would give an error of $\pm$ 0.8% (taking $T_5/T \sim 1.93$ as a typical value).)

Case II At a temperature of 2000°K some of the typical values measured were : $t_{\frac{1}{2}} \sim 5.25 \pm 0.125$,

$T_{max} \sim 39$mm. $\pm$ 0.25mm. (i.e. $T = 19.5 \pm$ 0.125mm.) and $T_{10} = (15.75$ to $13.50) \pm 0.25$mm.

$\therefore$ Error in $T_{10} = \pm$ 1.9%

$\therefore$ Error in $T = \pm$ 0.6%

$\therefore$ Error in $T_{10}/T = \pm$ 2.3%

Taking $T_{10}/T = 0.75$

$$0.73 < T_{10}/T < 0.77$$

From Cowan's curve this gives

$$.1025 < w/\pi^2 < .1035$$

i.e. Error in $w/\pi^2 = \pm$ 0.5%.

c) Error in Temperature

$\therefore$ Total error in $\alpha = 0.5 + 2(0.7) + (2.5)$ %

$= \pm$ 4.4% (for $t_{\frac{1}{2}} \sim 10$mm.)

This error in α is the error in each measurement, however the actual error in the curve fitting the α values over the whole temperature range will be less than $\pm$ 4%.

ii Error in k

$$k = C_p \cdot \alpha \cdot D$$

a) $\delta(C_p)$:

The error in C_p is difficult to assess since the values quoted by other observers show a wide variation. As stated in chapter 5, the curve chosen used the enthalpy results

of other workers, thus the error is even harder to assess. However, the curve used can be read to $\pm$ 0.0001 w sec./$g^{o}K$, thus giving a reading error of $\sim$ 0.14% at $500^{o}K$ and $<$ 0.14% at $T > 500^{o}K$.

b) (∂D):

The error in the density is of the order of 1% for values between 9.9 to 10.5 g/cm^{3}.

$\therefore$ Error in k = (4 + 0.1 + 1)%

$\simeq \pm$ 5 %.

The error in the best fit curve to all the k values should be less than this value.

CHAPTER 6

RESULTS

As was stated in chapter 3 only the results from the 'B' specimens have been used, since complete sets of results were not obtained using the 'A' or 'C' specimens. Several specimens were tested in each category in order firstly to ensure reproducibility of results and secondly because it was necessary owing to specimens being broken on removal from the apparatus.

The results from post test metallographic and stoichiometric analyses are given in table 6I. The densities were checked using the quantimet and results were obtained which were within 1-2% of the pretest values. For this reason it was assumed that the densities had not altered during testing. The densities for the non-stoichiometric specimens lay within 1-2% of the densities of the parent materials, i.e. 96 and 93^{I}, so the densities of the parent materials were used for each specimen. For the single crystal it was necessary to take the average of several measurements all of which lay within 1% of each other.

The measurement of grain sizes showed that in nearly every case there had been an increase of at least 100% on the pretest values. Since no pretest grain size determinations had been performed for the non-stoichiometric specimens, the values for the parent materials of 4.6μ for 96 and 5.7μ for 93^{I} had been taken as the pretest grain sizes for all non-stoichiometric specimens. The post test grain sizes for the non-stoichiometric specimens showed an increase of 300-400% on these values. However, it was expected that the assumed pretest values would be too small, since the grain sizes of the non-

NAME	DENSITY (g/cm^3)	p+	o/u RATIO		GRAIN SIZE(μ)		TOTAL IMPURITY (ppm.)	No. of specimens tested
			BEFORE	AFTER	BEFORE	AFTER		
96	10.51	-.0094	2.001	<2.001	4.6	9.1	177	2
94^{II}	10.40	.0012	2.001	<2.001	8 9	20.1	202	2
93^{I}	10.21	.0194	2.001	<2.001	5.7	8.9	484	2 + 1 argon
91^{II}	10.02	.0377	2.001	<2.001	8	-	285	1
91^{I}	9.97	.0424	2.001	<2.001	6	10	322	2
9694	10.35		2.001*	<2.001	17	17	177*	2
9691	10.10		2.001*	<2.001	30	30	177*	3
S.X.	10.95		—	—	—	—	—	3
96	10.51*		2.006	<2.001	4.6*	16.9	177*	2
	10.51*		2.030	<2.002	" *	-	"	2
	10.51*		2.060	<2.002	" *	13.2	"	2
93^{I}	10.21*		2.006	<2.001	5.7*	16.0	484*	1
	10.21*		2.030	<2.001	"	16.0		1
	10.21*		2.060	<2.001	"	20.0		2

+ $p = \frac{\varphi_{95} - \varphi_x}{\varphi_{95}}$

* Assumed values taken same as parent material

\- no specimen

TABLE 6.I

stoichiometric specimens would have altered by at least x2 during the 'non-stoichiometric' process. In this process the parent materials of 96 and 93^{I} had been held at 1800°K for $4\frac{1}{2}$ hours in order to obtain $^{O}/_{u}$ ratios of 2.006, 2.030 and 2.060. Thus it can be seen that the real increase in grain size during testing was probably ~100-200%.

Results from the stoichiometric analysis showed that in all cases the $^{O}/_{u}$ ratio of the non-stoichiometric specimens had decreased to values below 2.002. This fact had been indicated during testing since, when selected measurements were made on the cooling cycle for the specimens with $^{O}/_{u}$ = 2.060, higher diffusivity values had been observed.

The measured values of thermal conductivity (k) were fitted where possible by a regression analysis to the equations

$$^{1}/_{k} = A+BT \qquad (6.00a)$$

for $T < 1673^{\circ}K$

and $$k = X(A+BT)^{-1} + CT^{3} \qquad (6.00b)$$

where X is a coefficient ~ 1, for $500^{\circ}K < T < 2500^{\circ}K$.

The first equation applied to that range of the results where it could be assumed that phonon conduction was the predominant conduction mechanism. The range was obtained by observing the curve of $^{1}/_{k}$ against T and selecting the temperature at which the $^{1}/_{k}$ values began to deviate from the linear form $^{1}/_{k} \propto T$. This temperature was found to be $< 1673^{\circ}K$ for the specimens $96, 94^{II}, 93^{I}, 91^{II}, 91^{I}$, 9694 and 9691, but varied for the non-stoichiometric ones. The second equation (6.00b) assumed that the deviation from linearity was due solely to conduction by radiation, and hence the results

were fitted using a CT^3 term. This will be shown to be inappropriate as the calculated curve did not fit the results very well (see chapter 7).

The results are presented under the following headings:

1 Single Crystal

2 Effect of Porosity

3 Effect of non-stoichiometry

6. 1 Single Crystal

To characterise the crystal more fully X-ray patterns were taken before and after testing using Laue's back reflection technique (see chapter 3d). These patterns gave useful information concerning the orientation of the front face and indicated whether any strain had been produced in the crystal during diffusivity measurement. An example of a typical X-ray pattern is given in fig. 6.01a. By indexing the X-ray points it was possible to orientate the crystal (see fig. 6.01b), and the front face is shown to be close to (519). By comparing patterns before and after it could be seen that there had been no change within the crystal during testing.

Two specimens of different thicknesses 030" and 050" were tested, and the results were in complete agreement with each other.

Fig. 6.02a. shows the plot of α against T and includes the values quoted for Montgomery (105).

Fig. 6.02b. shows the plots of k and $^{1}/_{k}$ against T where the broken line represents

$$^{1}/_{k} = -(1.36 \pm 1.20) + (2.26 \pm 0.10) \times 10^{-2} T \ (w/cm^{o}K)^{-1} \qquad (6.01)$$

for $T < 1673^{o}K$

The solid lines represent the k and $^{1}/_{k}$ values given by the full equation for 600 - 2000°K. of:

$$k = {}^{1}/(-1.39 + 2.30 \times 10^{-2} T) + 3.68 \times 10^{-13} T^{3} \ w/cm^{o}K \qquad (6.02)$$

where $1\sigma = 2.258 \times 10^{-3}$ w/cm°K

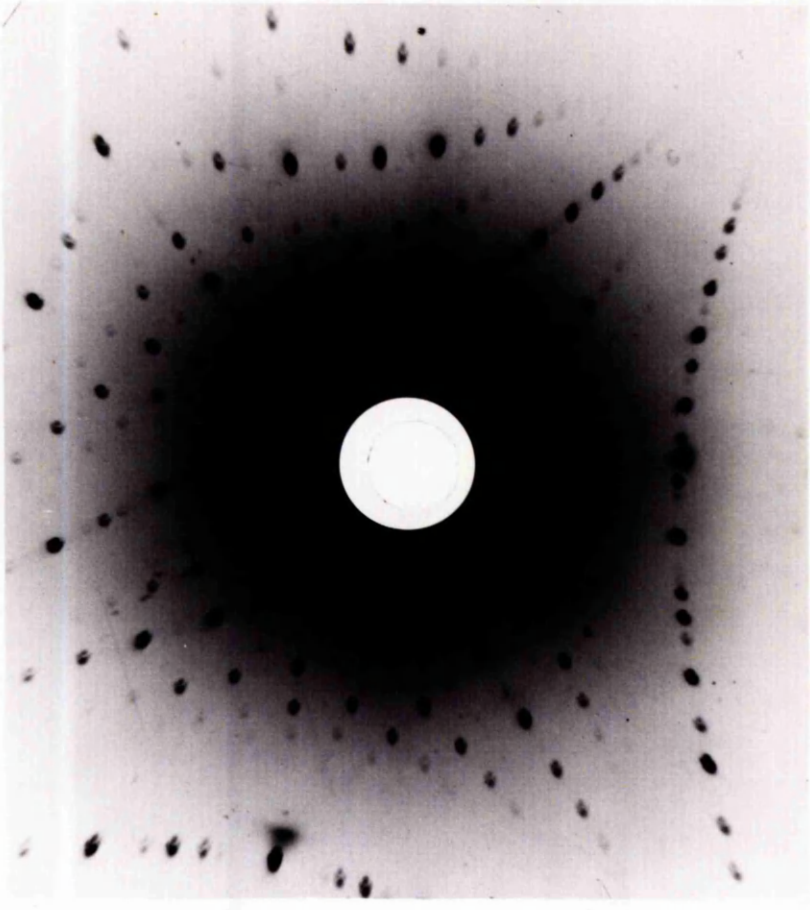

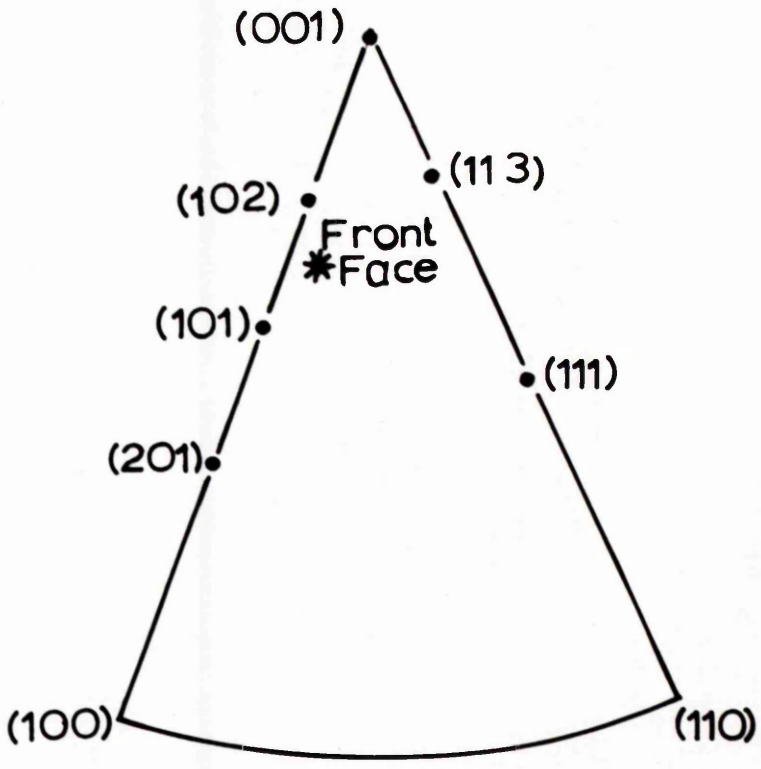

FIG. 6·01, Single Crystal Orientation.

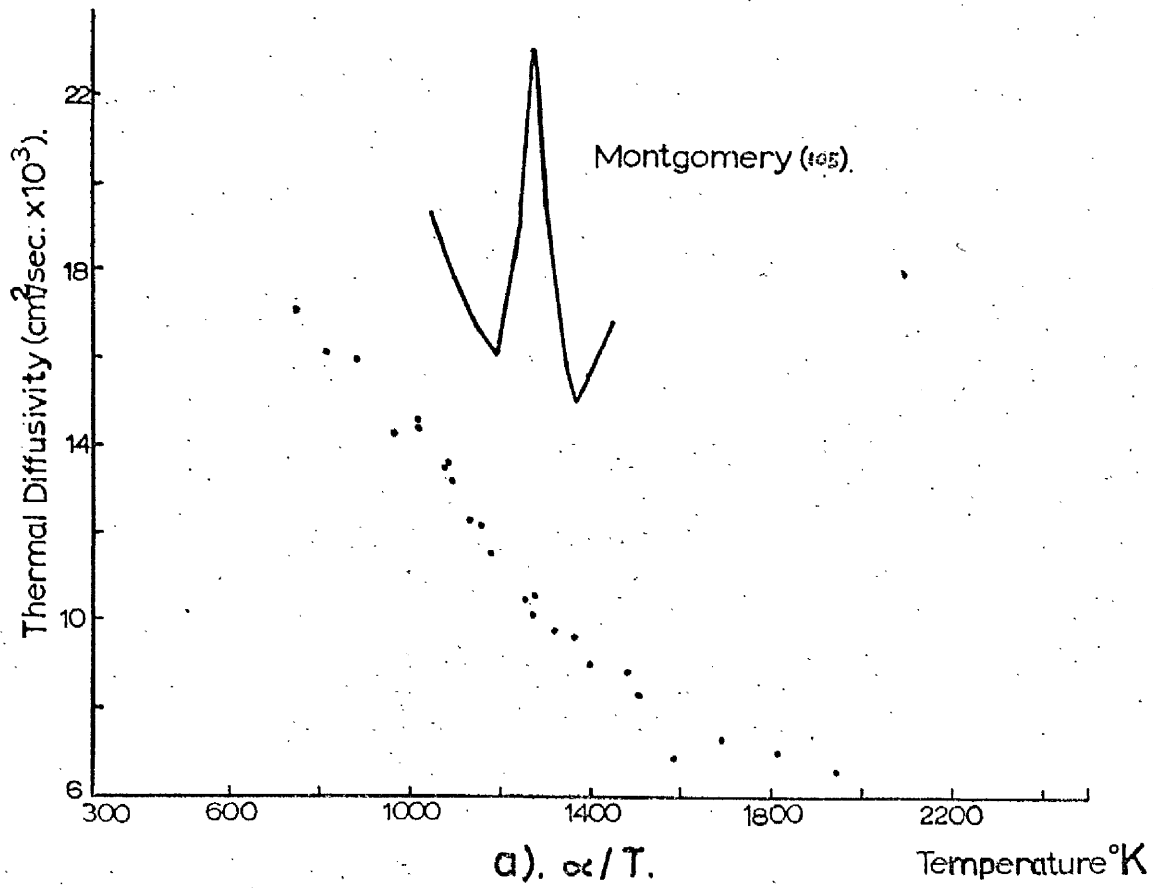

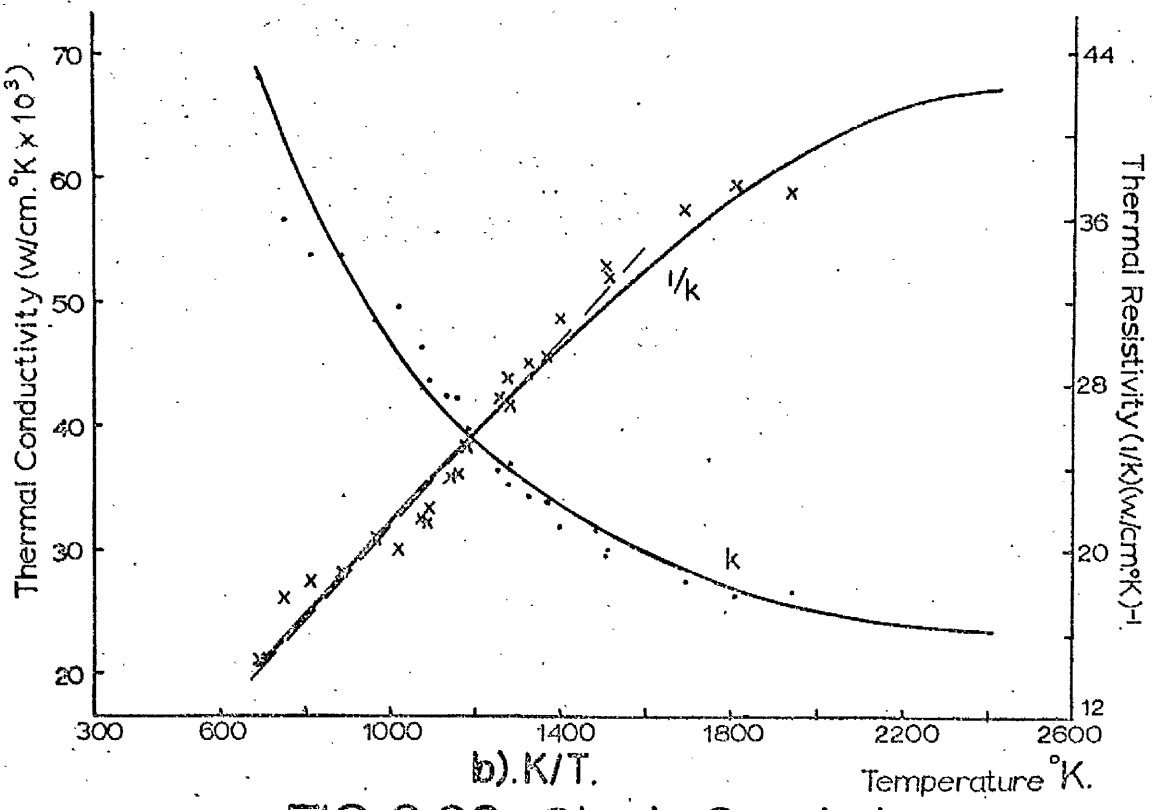

FIG.6·02. Single Crystal.

6. 2 Effect of Porosity

The results are presented in order of decreasing density, and they will consist of a characterisation of the specimen on one page facing photomicrographs on the other. The following page holds both the thermal diffusivity and thermal conductivity curves plotted against temperature. Unfortunately, there were no specimens of 91% for metallography, hence there is no photomicrograph of this density.

a) 96

Density = 10.51 g/cm^3

$^{O}/_{u}$ ratio before = 2.001

" " after = < 2.001

Grain size before = 4.6 μ

" " after = 9.1 μ

Total impurity level = 177ppm

The micrographs in fig. 6.03 shows that the porosity is mostly spherical and very small (< 5 μ in diameter). Fig. 6.03b is a secondary carbon replica.

A regression analysis on the results below 1673^{O}K gave

$$^{1}/_{k} = (5.57 \pm 0.33) + (2.02 \pm 0.03) \times 10^{-2} T \quad (w/cm^{O}K)^{-1} \qquad (6.03)$$

The complete equation for 400 - 2200^{O}K was

$$k = {}^{1}/_{(5.58 + 2.02 \times 10^{-2} T) + 1.97 \times 10^{-13} T^{3}} \quad w/cm^{O}K \qquad (6.04)$$

with $1\sigma = 1.09 \times 10^{-3}$ w/cm^{O}K

Fig. 6.04a shows the plot of α against T, and fig. 6.04b shows the plots of k and $^{1}/_{k}$ against T. The broken line represents equation 6.03, and the solid lines represent the k and $^{1}/_{k}$ values given by equation 6.04.

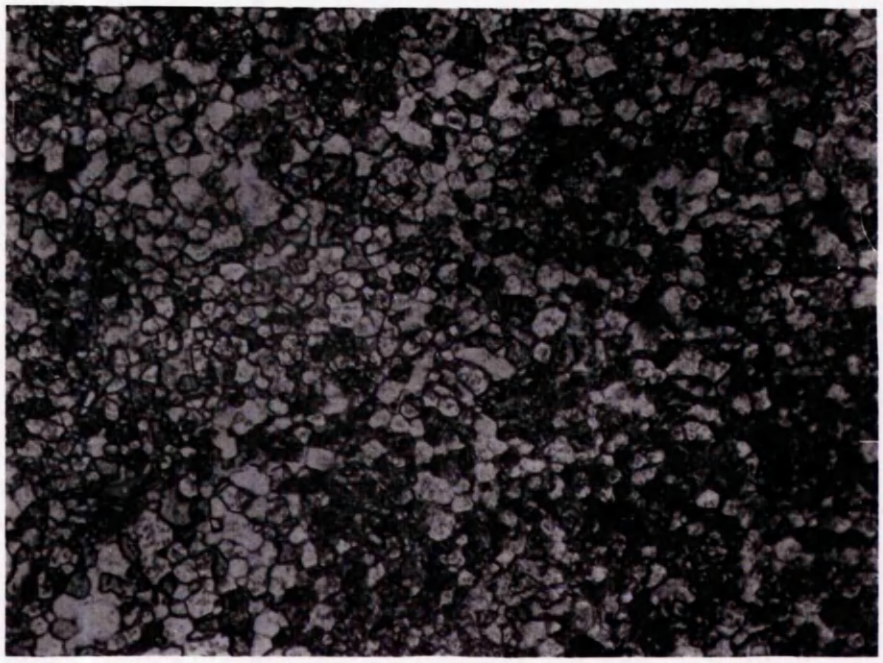

x300.

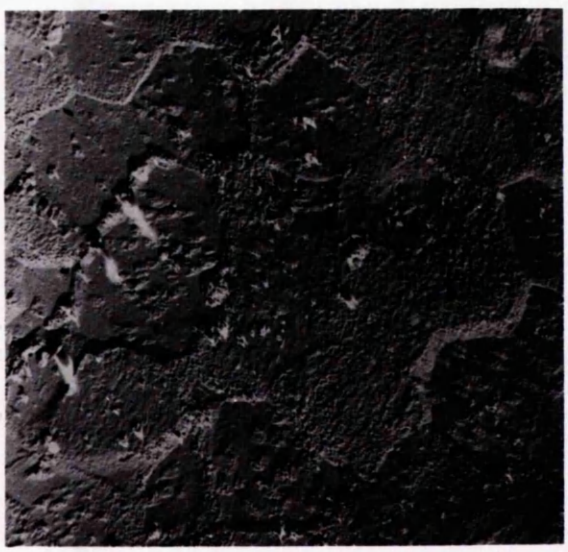

x1500.

FIG. 6·03. 96.

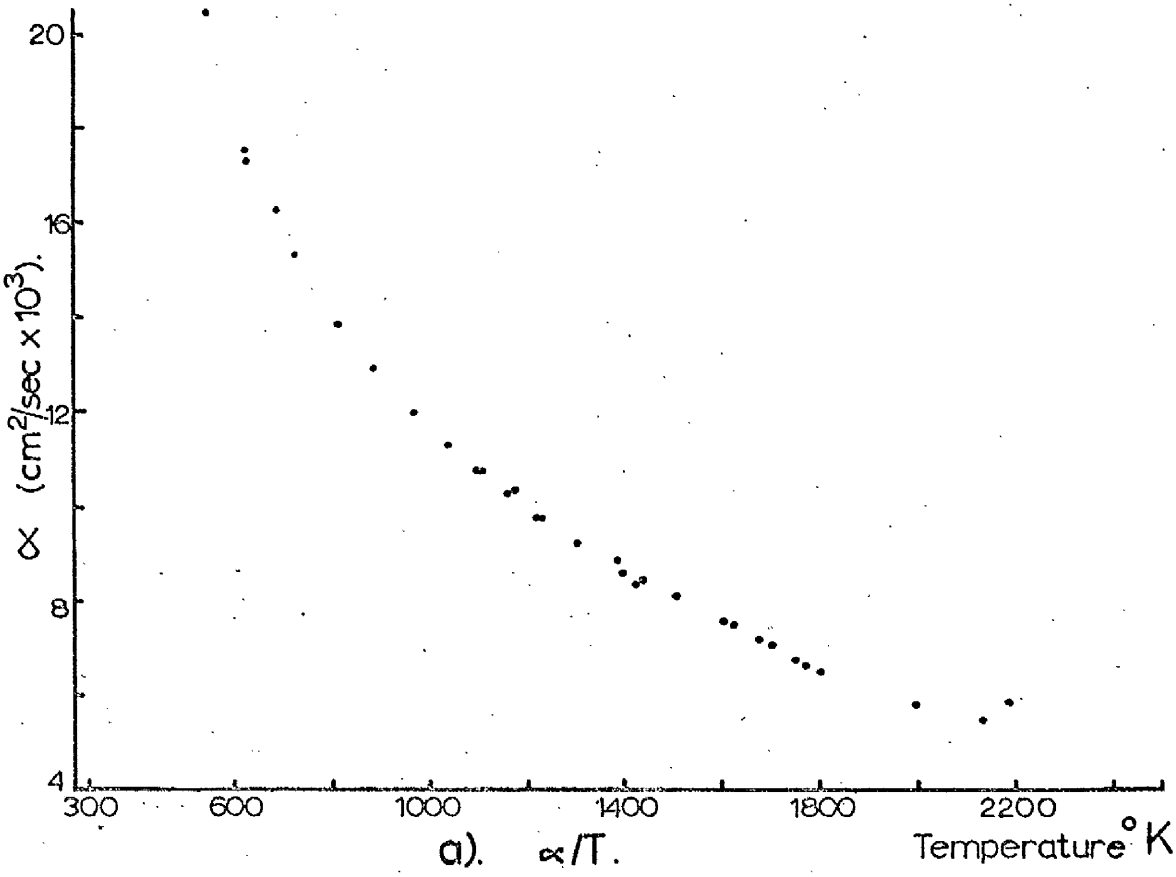
20
16
12
8
4
∝ (cm²/sec x 10³).
300
600
1000
1400
1800
2200
a). ∝/T.
Temperature °K

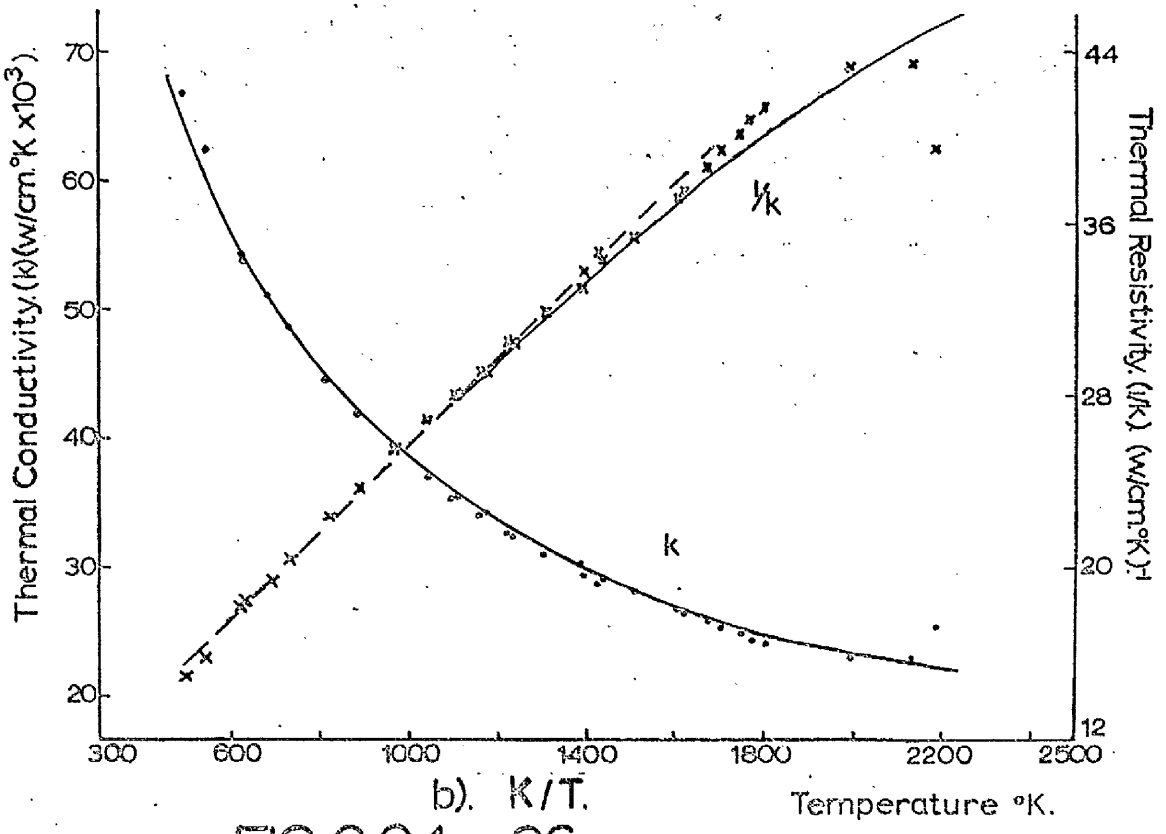
Thermal Conductivity.(k)(w/cm.°K x10³).
70
60
50
40
30
20
1/k
k
44
36
28
20
12
Thermal Resistivity. (1/k). (w/cm.°K).⁻¹
300
600
1000
1400
1800
2200
2500
b). K/T.
Temperature °K.

FIG.6·04. 96.

b) 94^{II}

Density = 10.40 g/cm^3

$^{o}/_{u}$ ratio before = 2.001

" " after = <2.001

Grain size before = 8.9 μ

" " after = 20.4 μ

Total impurity level = 202 ppm.

The micrographs in fig. 6.05 show that the porosity is evenly distributed and mostly spherical (5 - 15 μ in diameter). There is some large porosity which is irregular with diameters of the order of 40 μ. Some of this porosity could be due to grain tear out which may have occurred during polishing.

A regression analysis on the results below 1673^{o}K gave the equation

$$^{1}/_{k} = (6.15 \pm 0.23) + (2.15 \pm 0.02) \times 10^{-2} T \quad (w/cm^{o}K)^{-1} \qquad (6.05)$$

The full equation for 500 - 2200^{o}K was

$$k = {}^{1}/_{(6.24 + 2.19 \times 10^{-2} T) + 3.52 \times 10^{-13} T^{3}} \quad w/cm^{o}K \qquad (6.06)$$

with $1\sigma = 0.73 \times 10^{-3}$ w/cm^{o}K.

Fig. 6.06a shows the plot of 'α' against T. In fig. 6.06b the broken line represents equation 6.05, and the solid lines represent the values of k and $^{1}/_{k}$ given by equation 6.06.

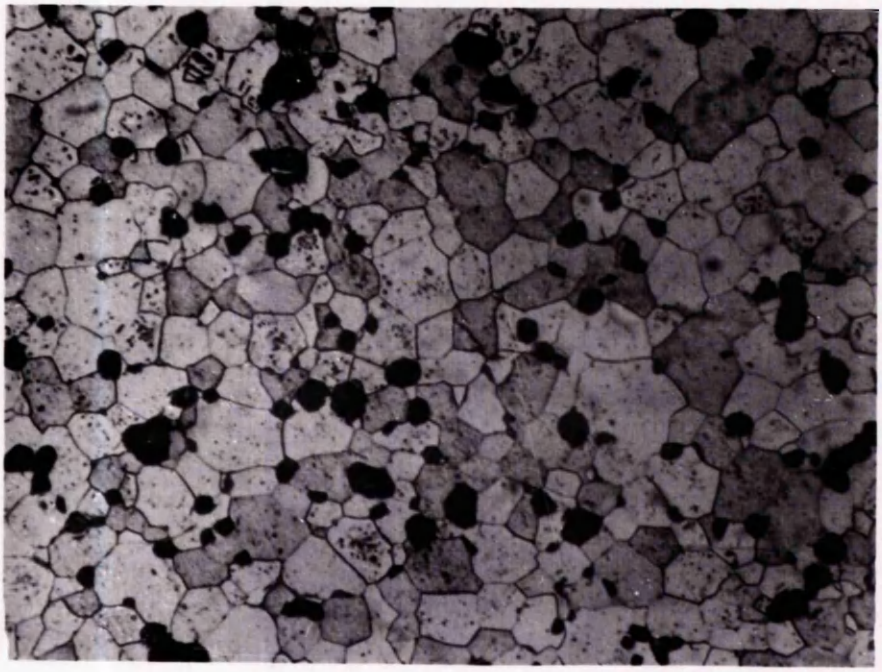

x 300.

x1000.

FIG.6·05. 94[π].

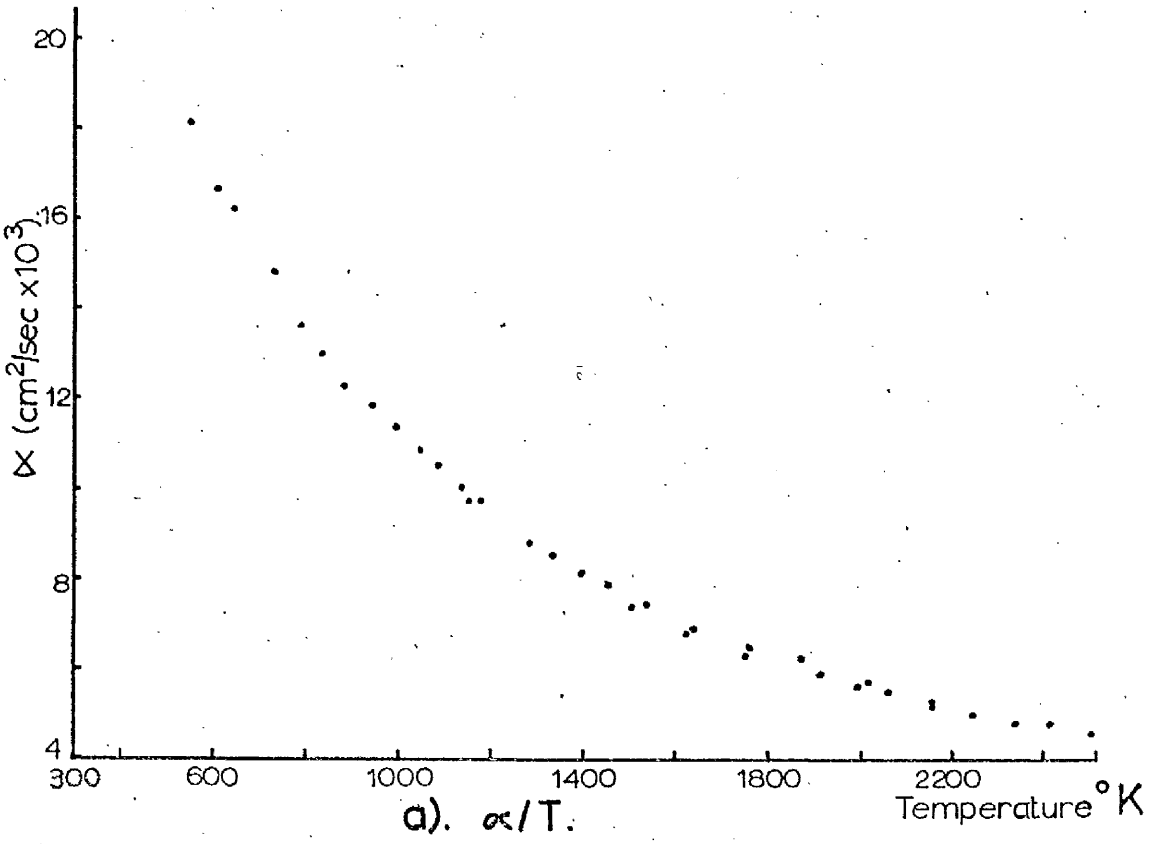

a). α / T.

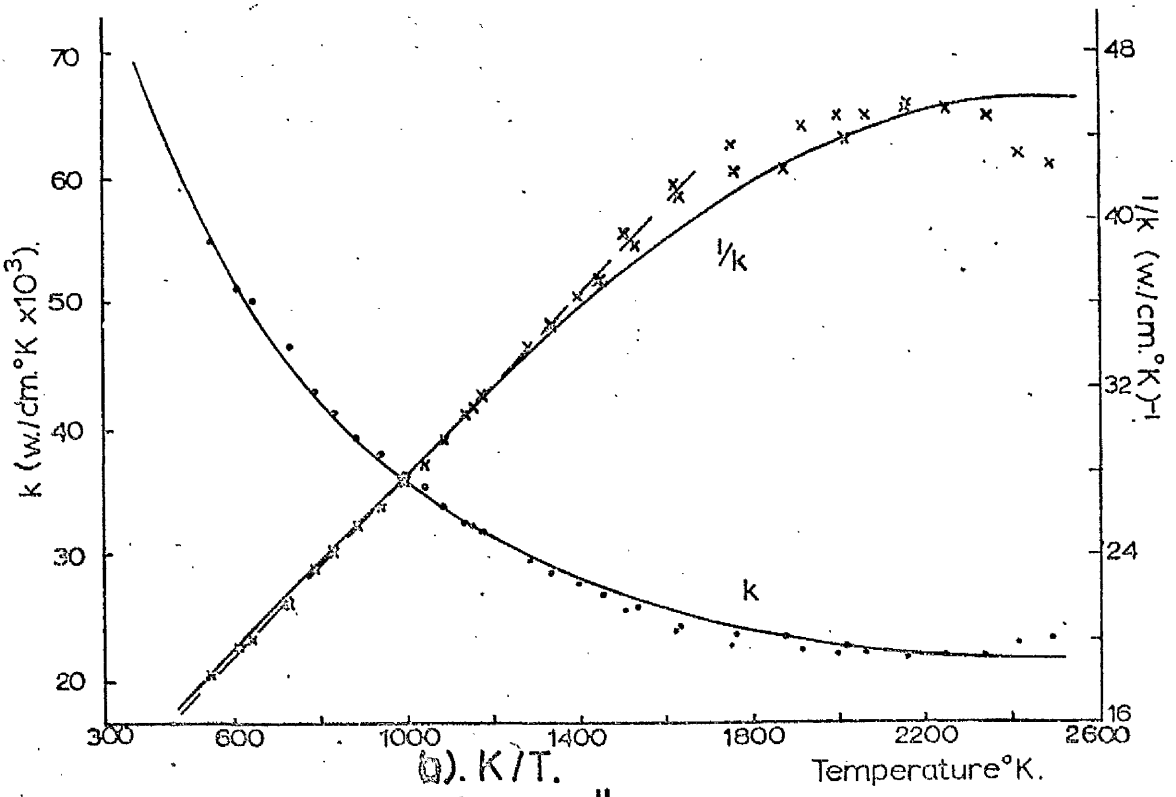

b). K / T.

FIG. 606. 94".

c) 93^{I}

Density = 10.21 g/cm^3

O/U ratio before = 2.001

" " after = < 2.001

Grain size before = 5.7 μ

" " after = 8.9 μ

Total impurity level = 484 ppm*

(* This high impurity level reflects the high copper content (275 ppm)).

The micrographs in fig. 6.07 show that the porosity is spherical and mostly less than 10 μ in diameter. The porosity is evenly distributed.

Fig. 6.08a shows the plot of α against T.

A regression analysis was applied to the results as follows:

for $T < 1673^{o}K$

$$1/k = (7.16 \pm 0.22) + (2.11 \pm 0.02) \times 10^{-2} T \quad (w/cm^{o}K)^{-1} \qquad (6.07)$$

for $500 < T < 2100^{o}K$

$$k = 1/(7.16 + 2.11 \times 10^{-2} T) + 0.73 \times 10^{-13} T^{3} \quad w/cm^{o}K \qquad (6.08)$$

with $1\sigma = 0.61 \times 10^{-3}$ w/cm^{o}K

These equations are plotted in fig. 6.08b, with the broken line representing equation 6.07, and the solid lines representing k and $1/k$ given by equation 6.08.

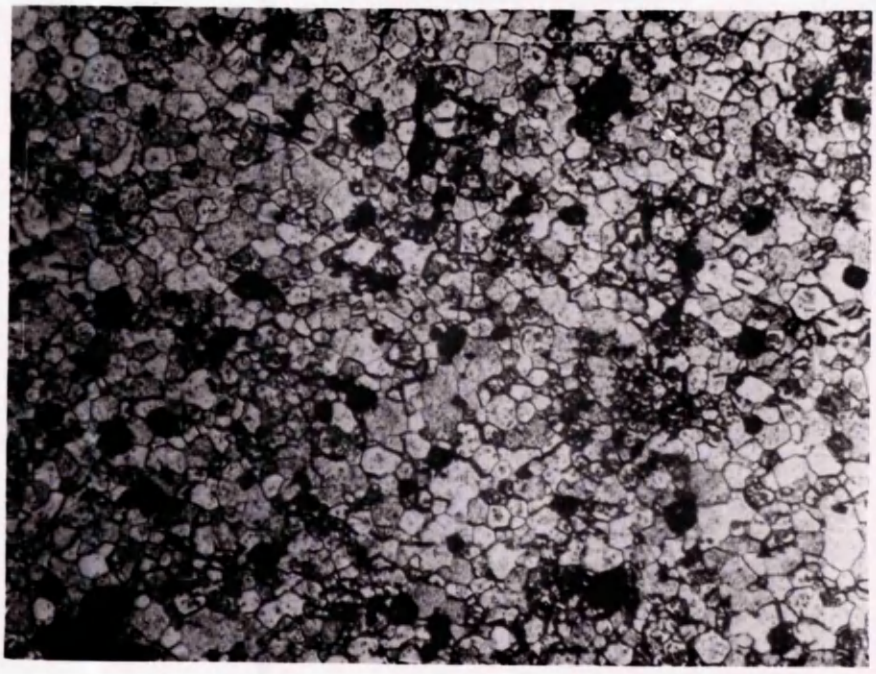

x 300.

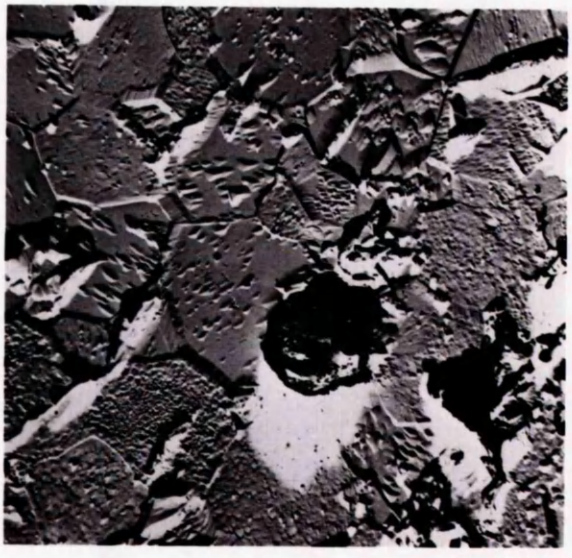

x 1000.

FIG. 6-07. 93[2].

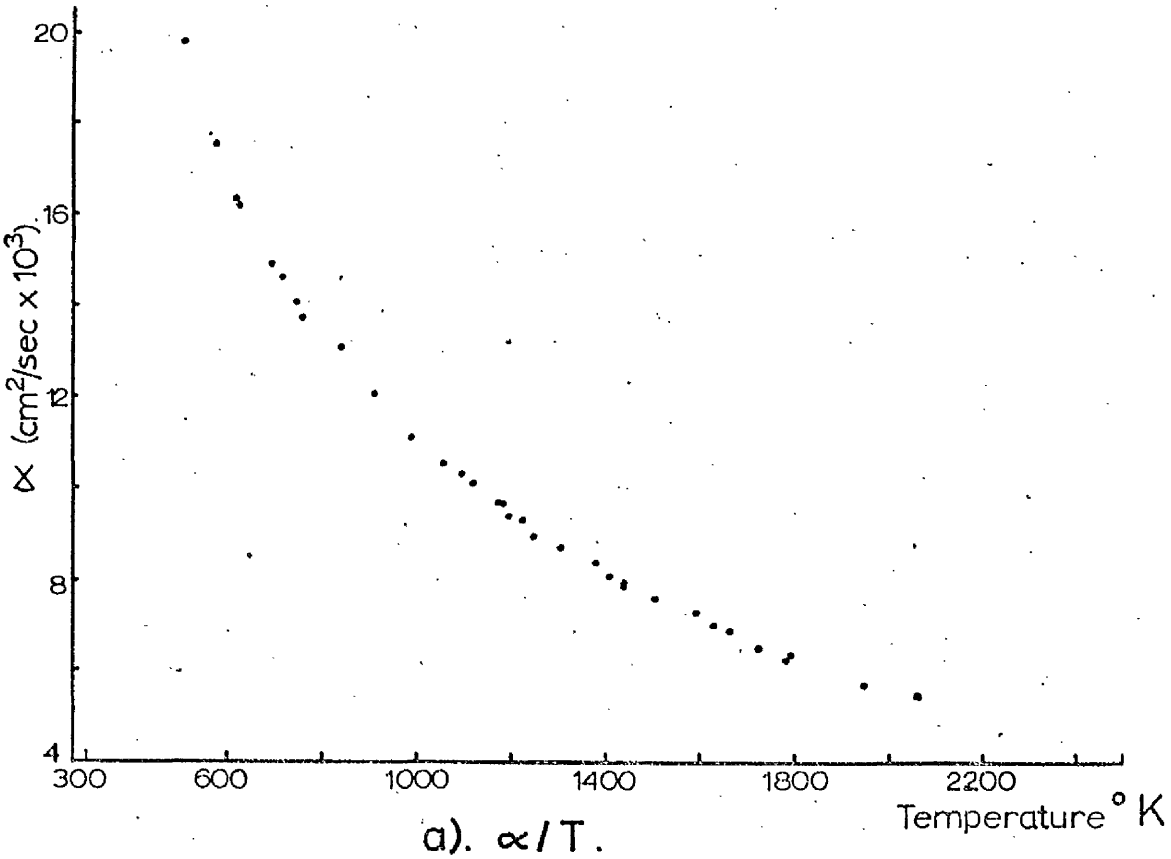

a). α / T.

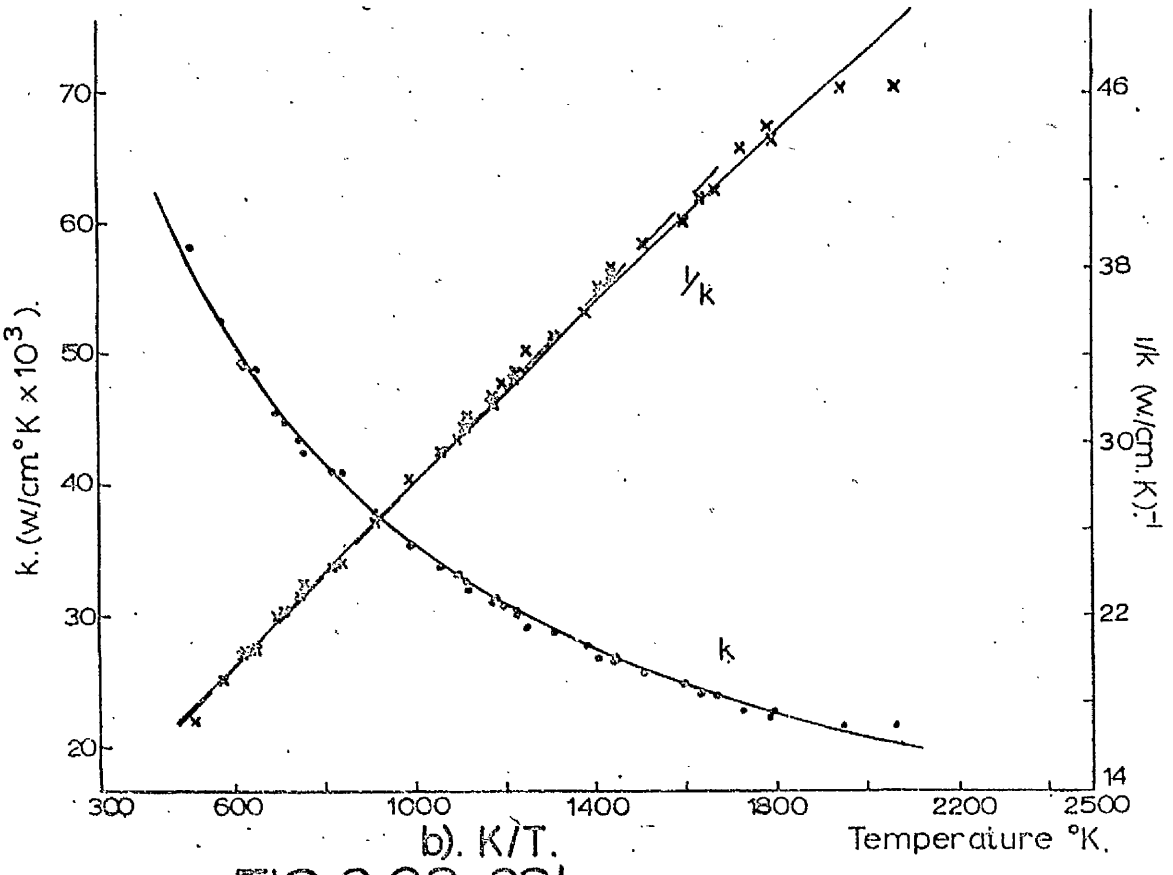

b). K/T.

FIG.6·08. 93'

d) 91^{II}

Density = 10.02 g/cm^3

$^{o}/_{u}$ ratio before = 2.001

" " after = < 2.001

Grain size before = 8 μ

" " after = —

Total impurity level = 285 ppm (90 ppm of copper)

There was no specimen for post test grain size or density measurements, therefore no porosity assessments could be made.

Fig. 6.09a shows the plot of α against T, and fig. 6.09b shows the plots of both k and $^{1}/_{k}$ against T. The broken line in fig. 6.09b represents the equation

$$^{1}/_{k} = (7.69 \pm 0.54) + (2.10 \pm 0.05) \times 10^{-2} T \quad (w/cm^{o}K)^{-1} \qquad (6.09)$$

for $T < 1673^{o}K$.

The solid lines represent the full equation for k and $^{1}/_{k}$ between 500 - 2500^{o}K given by

$$k = {}^{1}/(7.76 + 2.12 \times 10^{-2} T) + 3.53 \times 10^{-13} T^{3} \quad w/cm^{o}K \qquad (6.10)$$

with $1\sigma = 1.26 \times 10^{-3}$ w/cm^{o}K.

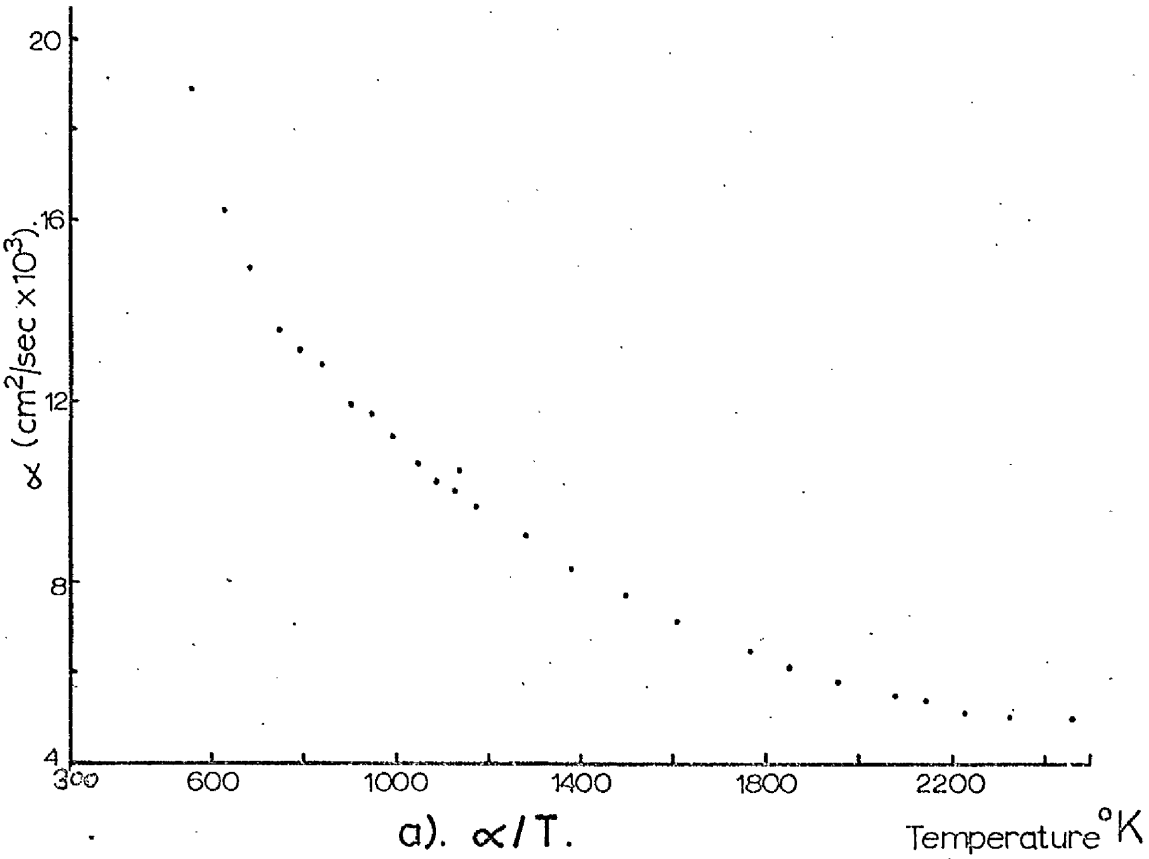

a). ∝/T.

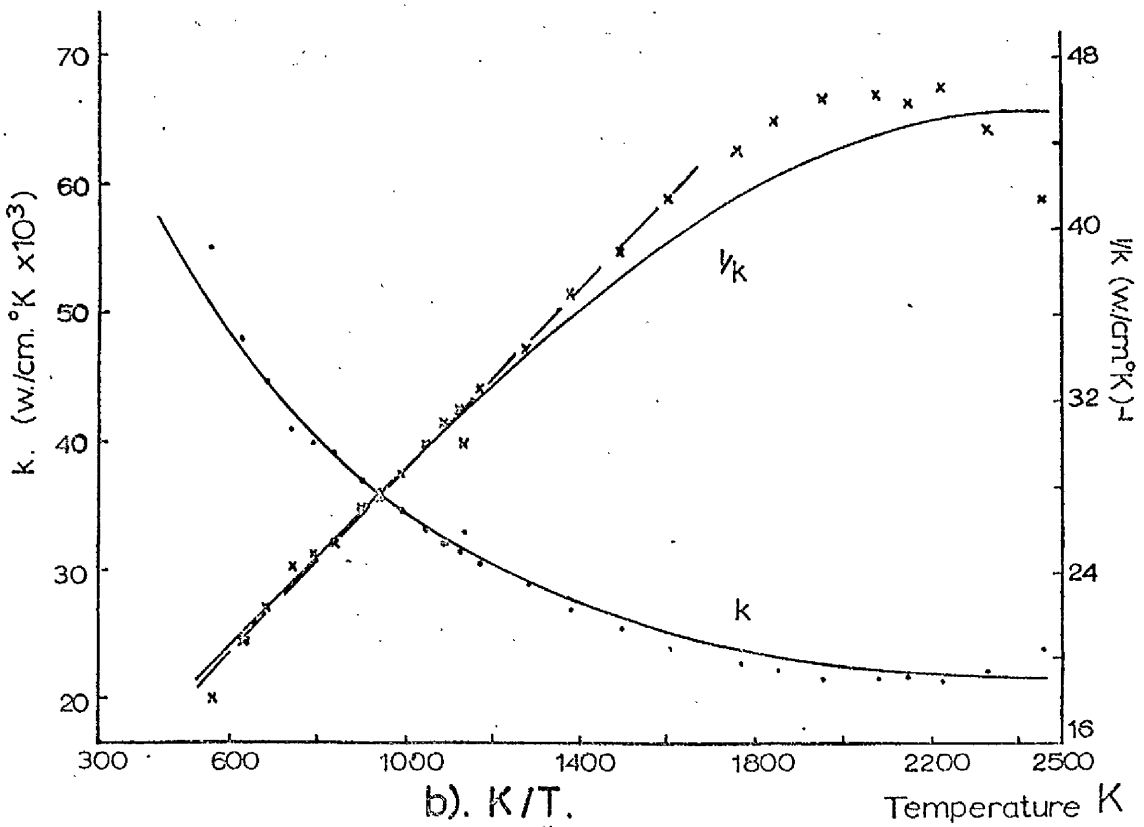

b). K/T.

FIG. 6·09. 91".

e) 91^{I}

Density = 9.97 g/cm^3

O/u ratio before = 2.001

" " after = < 2.001

Grain size before = 6 μ

" " after = 10 μ

Total impurity level = 322ppm (155 ppm of copper).

The micrographs in fig. 6.10 show that the pores are spherical and of the order of 20μ in diameter.

Fig. 6.11a shows the plot of α against T .

Fig. 6.11b shows the plot of both k and $1/k$ against T where the broken line represents the equation.

$$1/k = (7.02 \pm 0.18) + (2.16 \pm 0.02) \times 10^{-2} T \quad (w/cm^{o}K)^{-1} \qquad (6.11)$$

for $T < 1673^{o}K$.

The solid lines represent the full equation for k and $1/k$ between 500 - 2400^{o}K given by

$$k = 1/(7.06 + 2.17 \times 10^{-2} T) + 1.93 \times 10^{-13} T^{3} \quad w/cm^{o}K \qquad (6.12)$$

with $1\sigma = 0.62 \times 10^{-3}$ w/cm^{o}K.

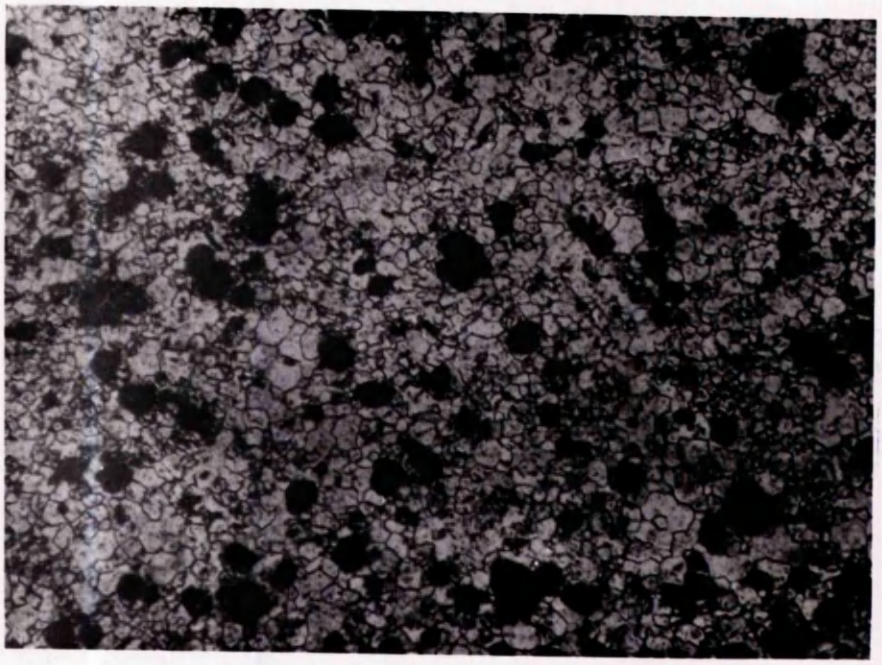

x 300.

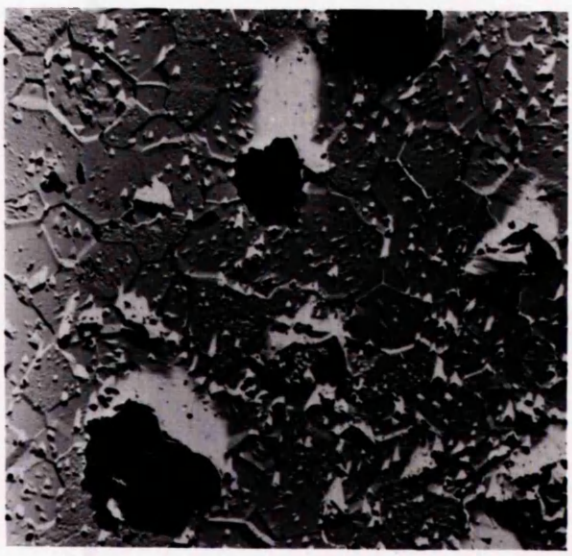

x 1000.

FIG. 6.10. 91 I.

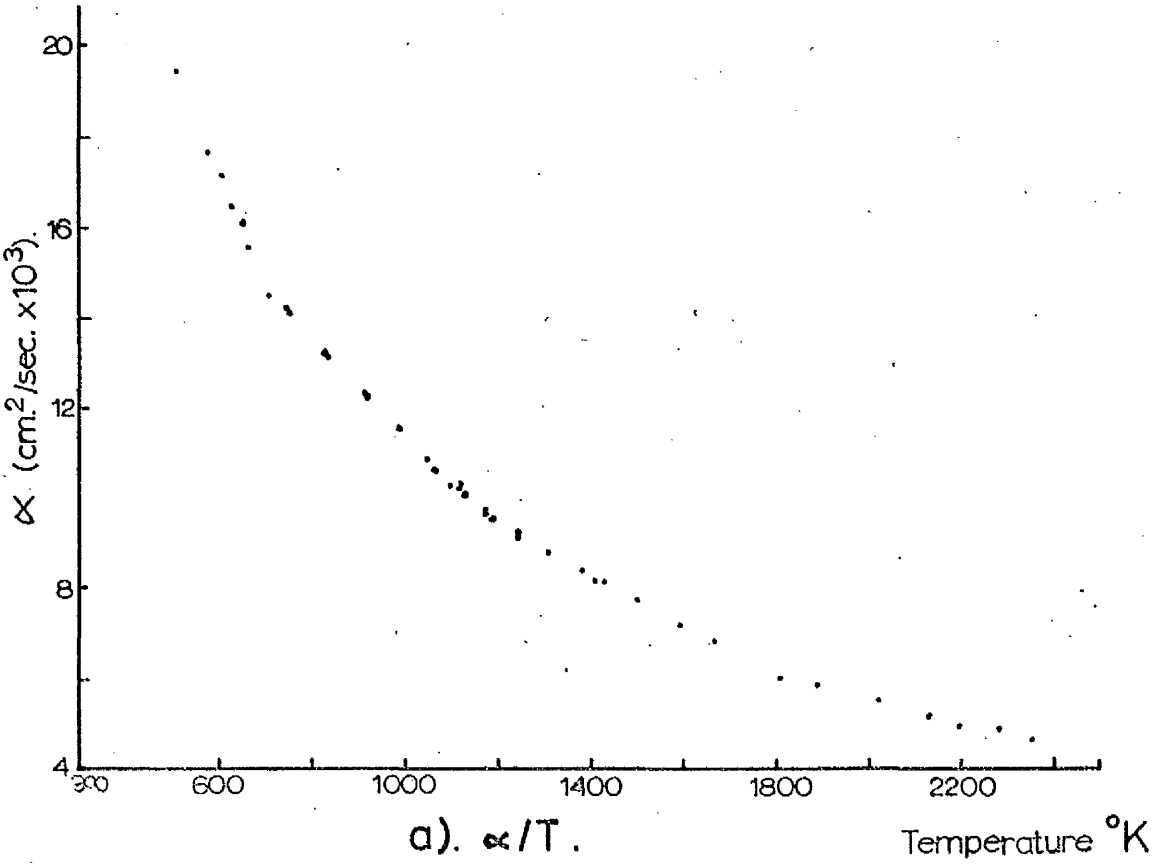
20
16
12
8
4
α (cm.²/sec. x10³).
300
600
1000
1400
1800
2200
a). α/T.
Temperature °K

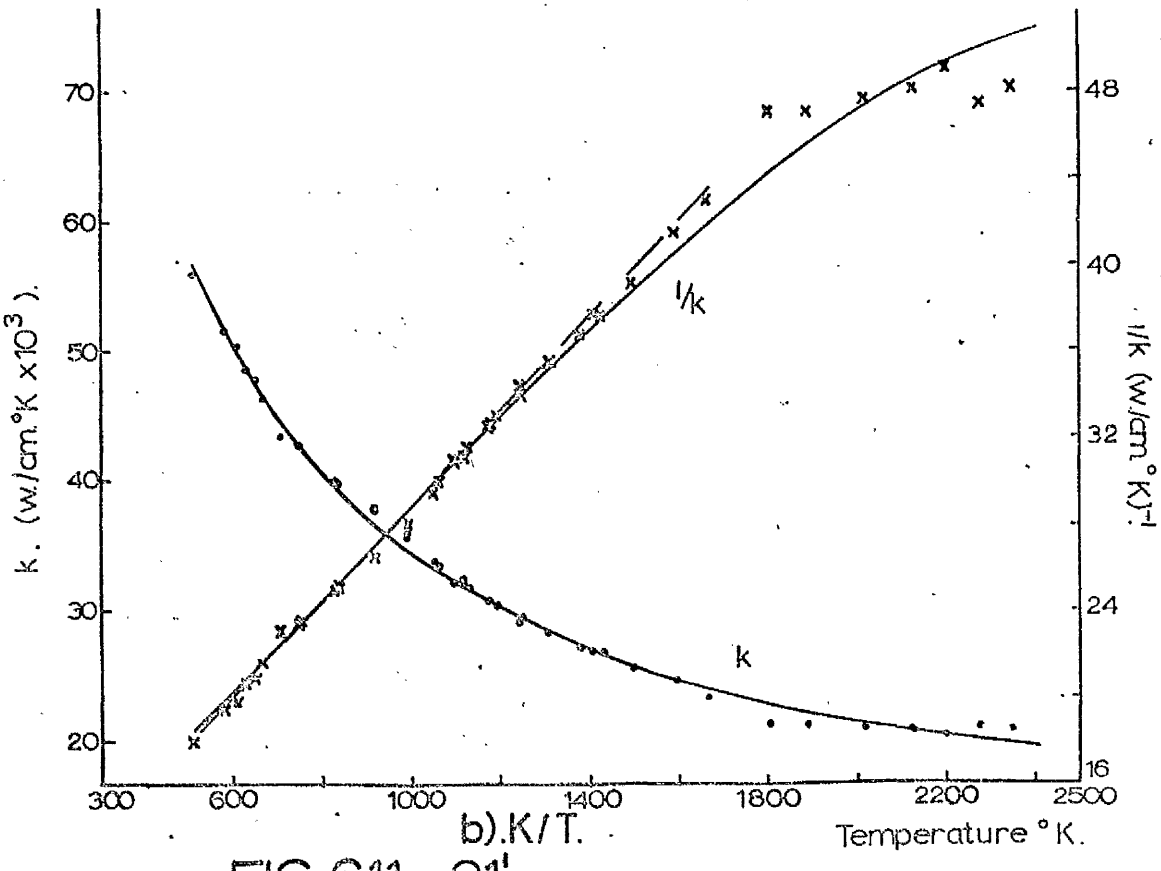
70
60
50
40
30
20
k. (w./cm.°K x10³).
48
40
32
24
16
1/k (w/cm.°K)⁻¹
1/k
k
300
600
1000
1400
1800
2200
2500
b).K/T.
Temperature °K.

FIG.6·11. 91'.

f) 9694

Density = 10.35 g/cm^3

$^{O}/_{u}$ ratio before = 2.001

" " after = < 2.001

Grain size before = 17 μ

" " after = 17 μ

Total impurity level = 177 ppm

This material was originally 96 which had had its pore volume fraction increased and its porosity redistributed to lie mostly at triple points and on grain boundaries. The micrographs in fig. 6.12 show this redistribution, and the pores are spherical with diameters 5 - 10μ.

Fig. 6.13a shows the plot of α against T .

Fig. 6.13b shows the plots of both k and $^{1}/_{k}$ against T. The broken line represents the equation for T < 1673^{O}K given as

$$^{1}/_{k} = (6.66 \pm 0.37) + (1.97 \pm 0.03) \times 10^{-2} T \quad (w/cm^{O}K)^{-1} \qquad (6.13)$$

The solid line in fig. 6.13b represents the full equation for $^{1}/_{k}$ and k between 500 - 2300^{O}K given by:

$$k = {}^{1}/(6.71 + 1.98 \times 10^{-2} T) + 2.01 \times 10^{-13} T^{3} \quad w/cm^{O}K \qquad (6.14)$$

with $1\sigma = 1.00 \times 10^{-3}$ w/cm^{O}K.

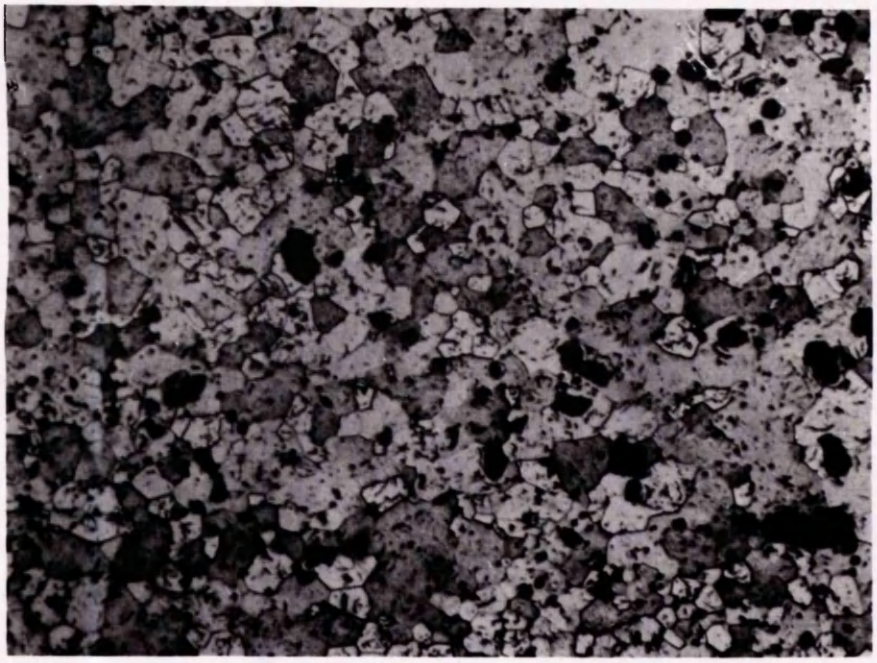

x 300.

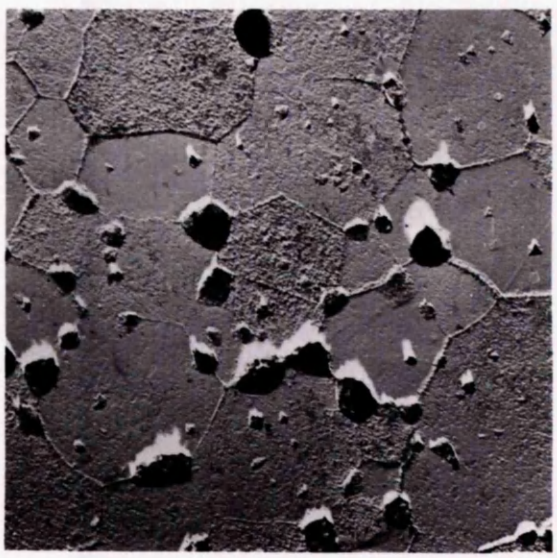

x1500.

FIG. 6·12. 9694.

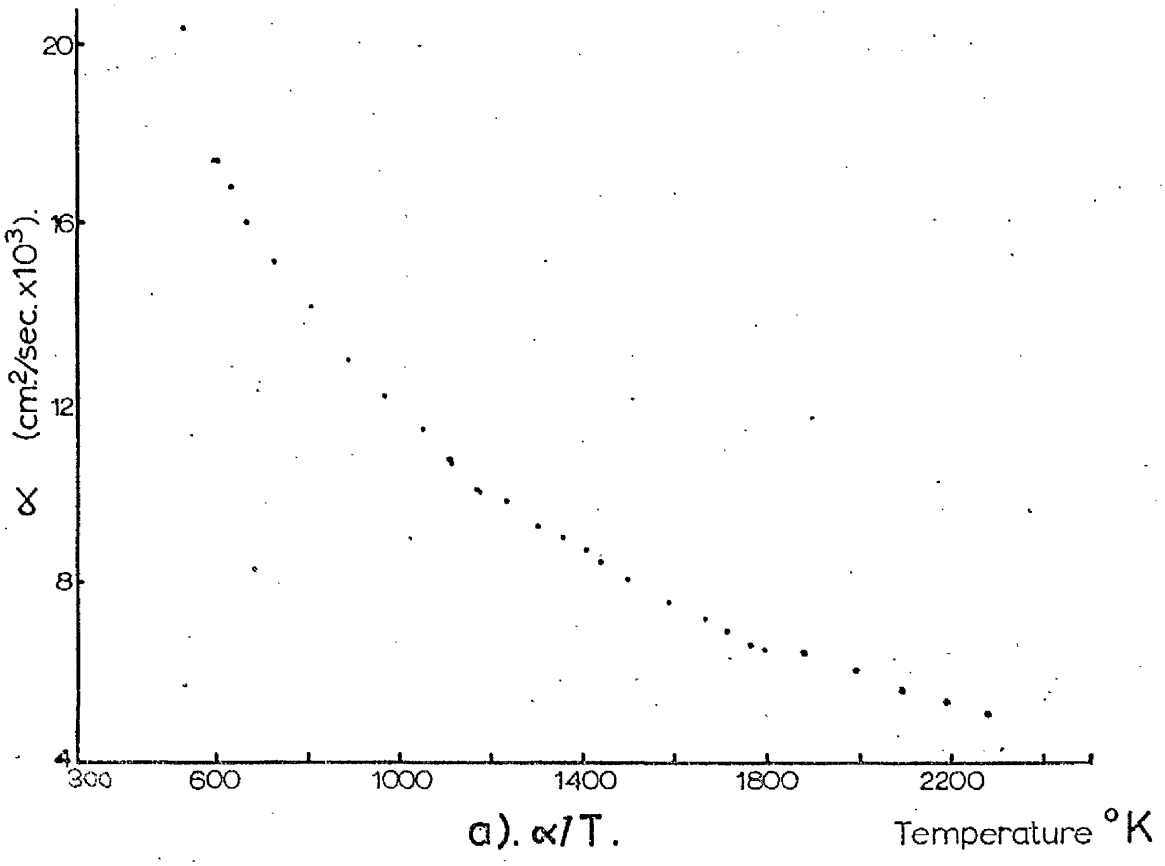
20
16
12
8
4
α (cm²/sec. x10³).
300
600
1000
1400
1800
2200
a). α/T.
Temperature °K

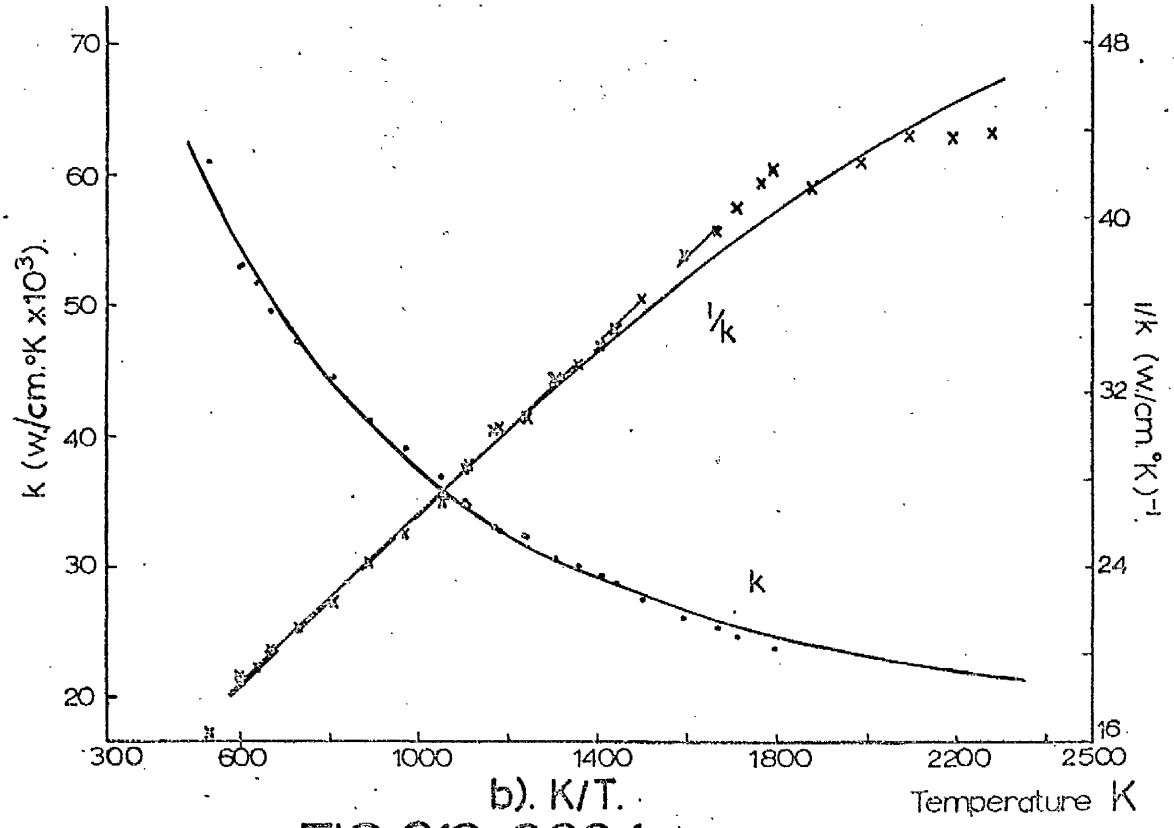
70
60
50
40
30
20
k (w/cm.°K x10³).
48
40
32
24
16
1/k (w/cm.°K)⁻¹.
1/k
k
300
600
1000
1400
1800
2200
2500
b). K/T.
Temperature K

FIG.6·13. 9694.

g) 9691

Density = 10.10 g/cm^3

O/u ratio before = 2.001

" " after = < 2.001

Grain size before = 30 μ

" " after = 30 μ

Total impurity level = 177 ppm

This material was originally 96 which had had its porosity increased and redistributed mostly at triple points and on grain boundaries. The porosity was mostly spherical and less than 20 μ in diameter as is shown in the micrographs in fig. 6.14.

Fig. 6.15a shows the plot of α against T.

Fig. 6.15b shows the plot of k and $^1/_k$ against T, where the broken line represents the equation for T < 1673^{o}K given as:

$$^1/_k = (7.39 \pm 0.27) + (1.93 \pm 0.02) \times 10^{-2} T \quad (w/cm^oK)^{-1} \qquad (6.15)$$

The solid line represents the full equation for k and $^1/_k$ between 500 - 2300^{o}K given by

$$k = {}^1/(7.41 + 1.93 \times 10^{-2} T) + 1.44 \times 10^{-13} T^3 \quad w/cm^oK \qquad (6.16)$$

with $1\sigma = 0.98 \times 10^{-3}$ w/cm^{o}K.

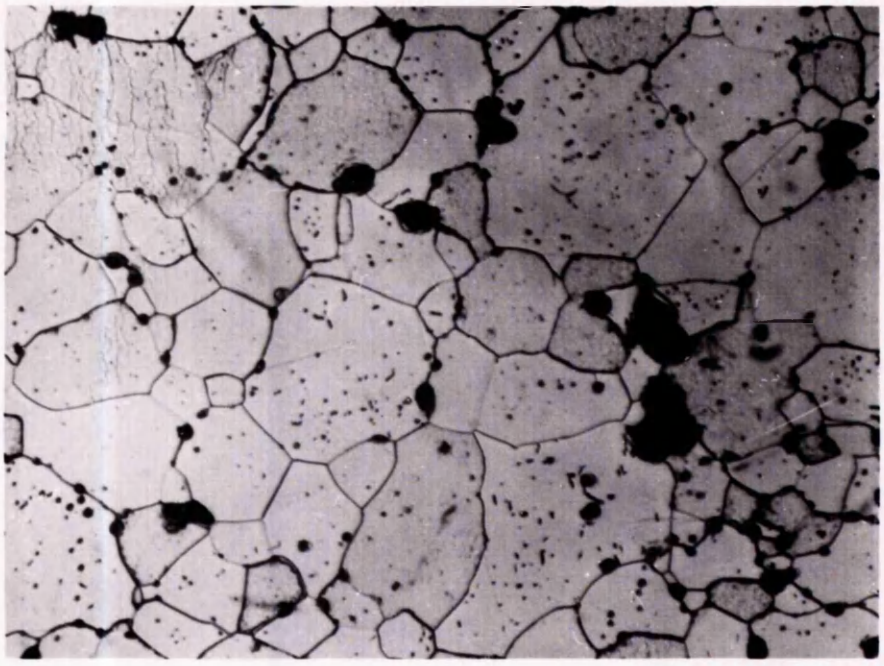

x 300.

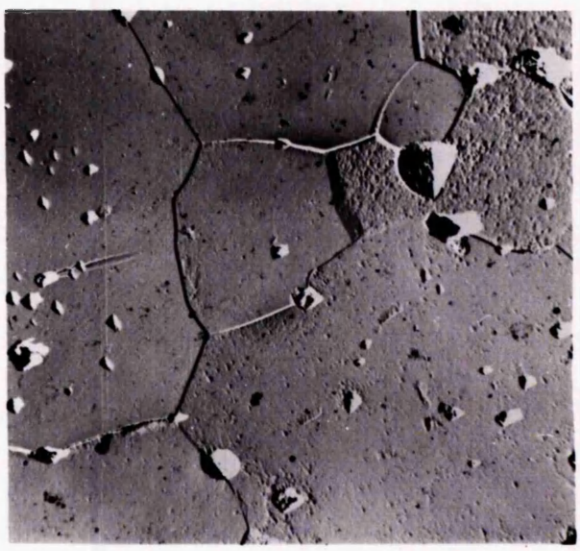

x 1000.

FIG. 614. 9691.

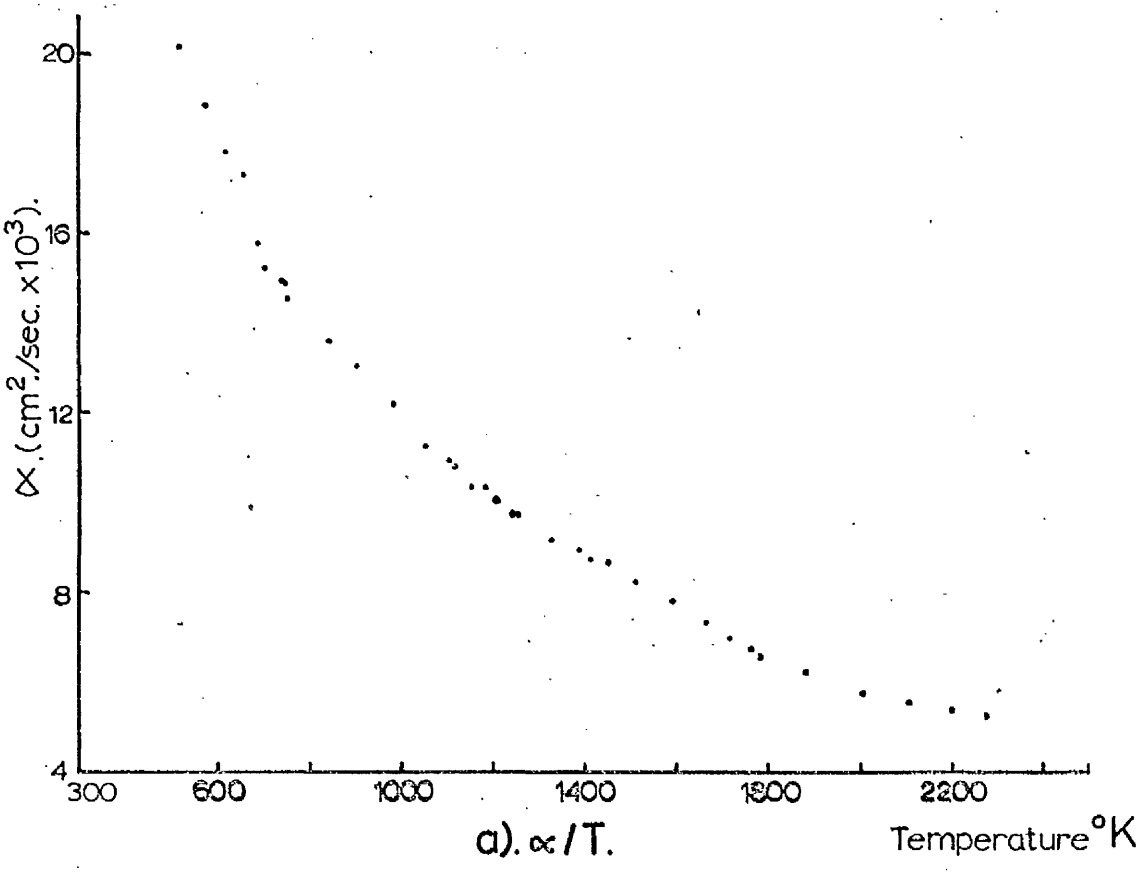
20
16
12
8
4
α. (cm².sec. x10³).
300
600
1000
1400
1800
2200
a). α / T.
Temperature °K

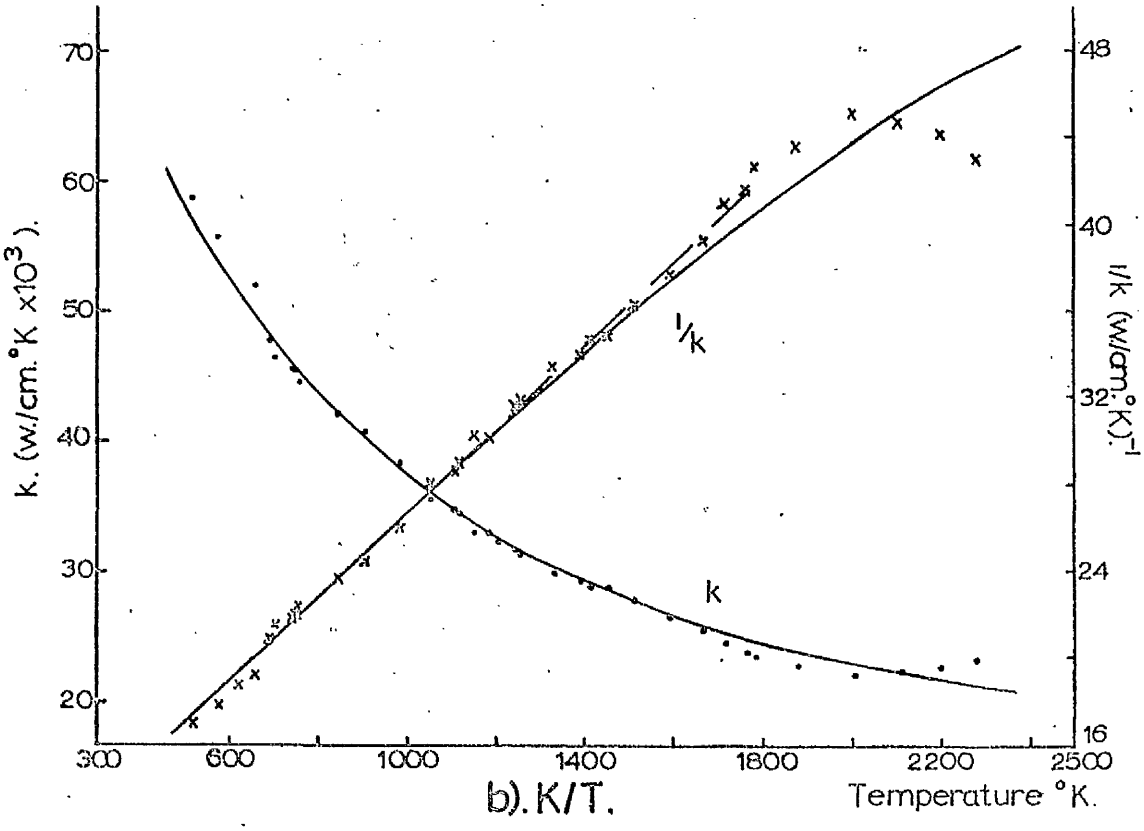
70
60
50
40
30
20
k. (w./cm.°K x10³).
48
40
32
24
16
1/k (w/cm.°K)⁻¹
1/k
k
300
600
1000
1400
1800
2200
2500
b). K/T.
Temperature °K.

FIG.6·15. 9691.

6. 3 Effect of Non-Stoichiometry

The results are presented in the following order:

a) 96 $^{O}/_{U} = 2.006$

b) " $^{O}/_{U} = 2.030$

c) " $^{O}/_{U} = 2.060$

d) 93^{I} $^{O}/_{U} = 2.006$

e) " $^{O}/_{U} = 2.030$

f) " $^{O}/_{U} = 2.060$

Each section contains a history of the material, micrographs and two graphs as in the preceeding section 6.2. All of the specimens lost nearly all of their excess oxygen during testing as can be seen from the post test analysis. This was confirmed by selective measurements taken on the 2.060 specimens during cooling.

a) 96 $^{o}/_{u} = 2.006$

The $^{o}/_{u}$ ratio altered from 2.006 to < 2.001 during testing. The micrograph in fig. 6.16 shows that some of the porosity is irregular in shape ($\sim 30\,\mu$ in diameter), but most of the pores are spherical and $\sim 5\mu$ in diameter on grain boundaries and at triple points.

Fig. 6.17a shows the plot of α against T; and fig. 6.17b shows k and $^{1}/_{k}$ against T. The broken line in fig. 6.17b represents the equation for $T < 1573^{o}K$ given by

$$^{1}/_{k} = (8.80 \pm 0.40) + (1.99 \pm 0.04) \times 10^{-2}\, T \quad (w/cm^{o}K)^{-1} \qquad (6.17)$$

The solid lines in fig. 6.17b represent the full equation for k and $^{1}/_{k}$ between 500 - $2350^{o}K$ given by:

$$k = {}^{1}/(8.90 + 2.01 \times 10^{-2}\, T) + 4.77 \times 10^{-13}\, T^{3} \quad w/cm^{o}K \qquad (6.18)$$

with $1\sigma = 0.97 \times 10^{-3}$ $w/cm^{o}K$

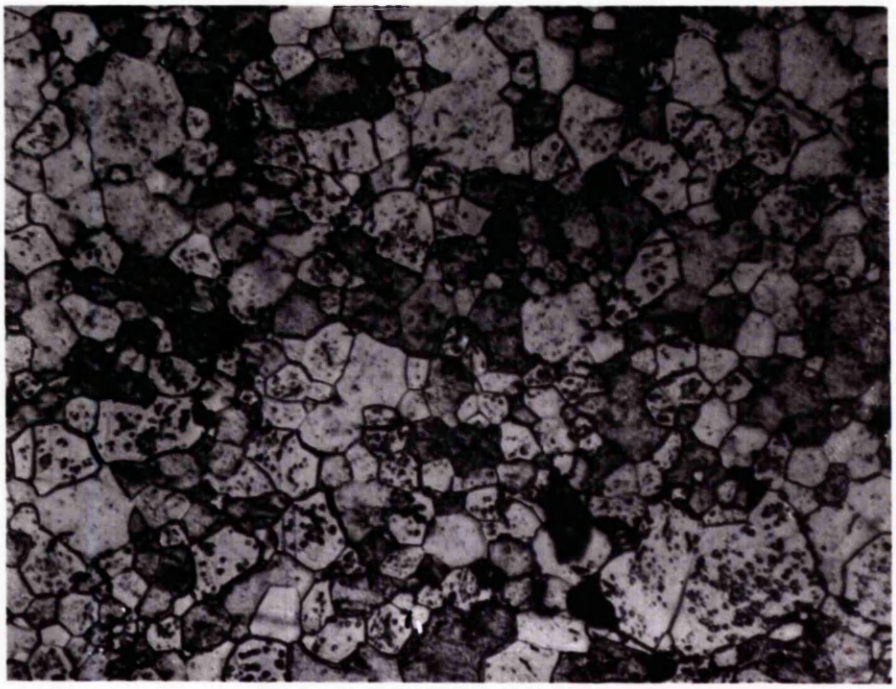

x300

FIG. 6·16. 96($\%_{U}$=2·006).

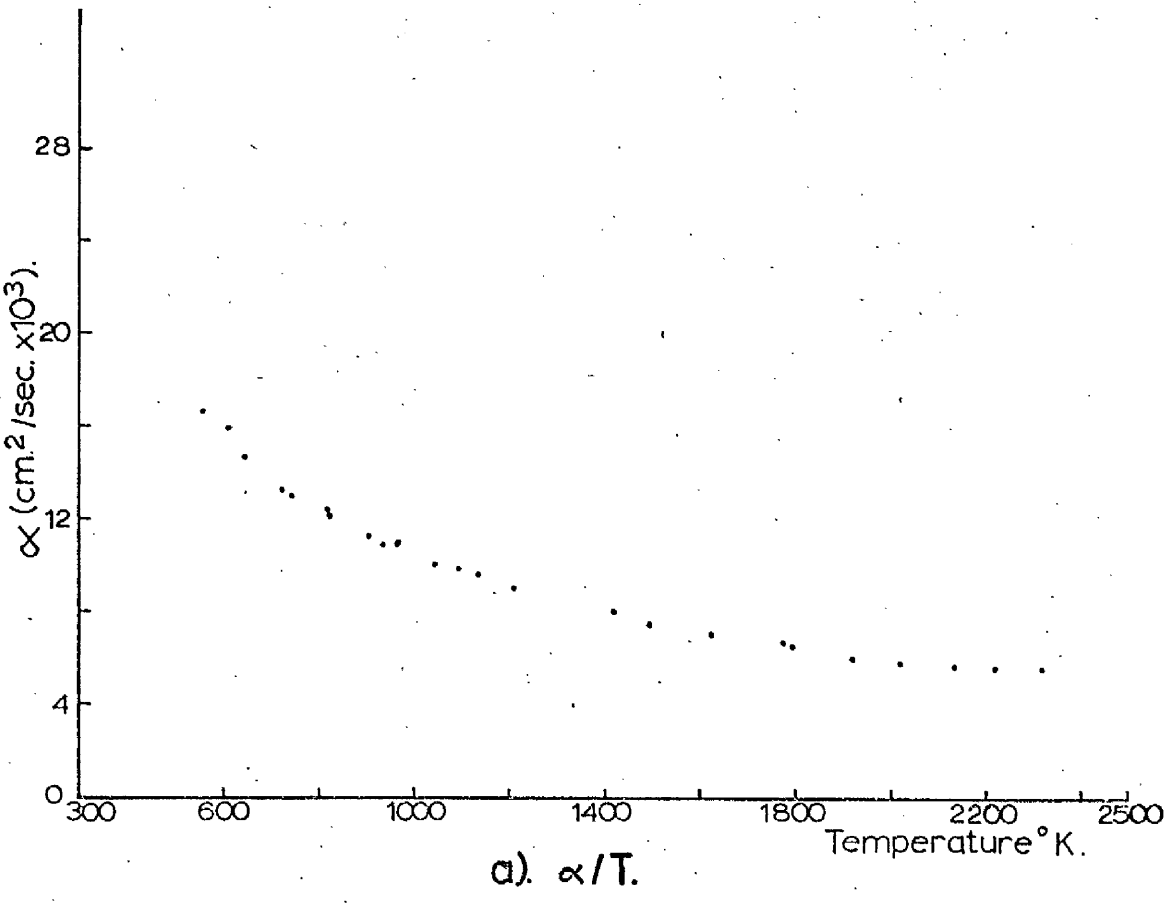

a). α / T.

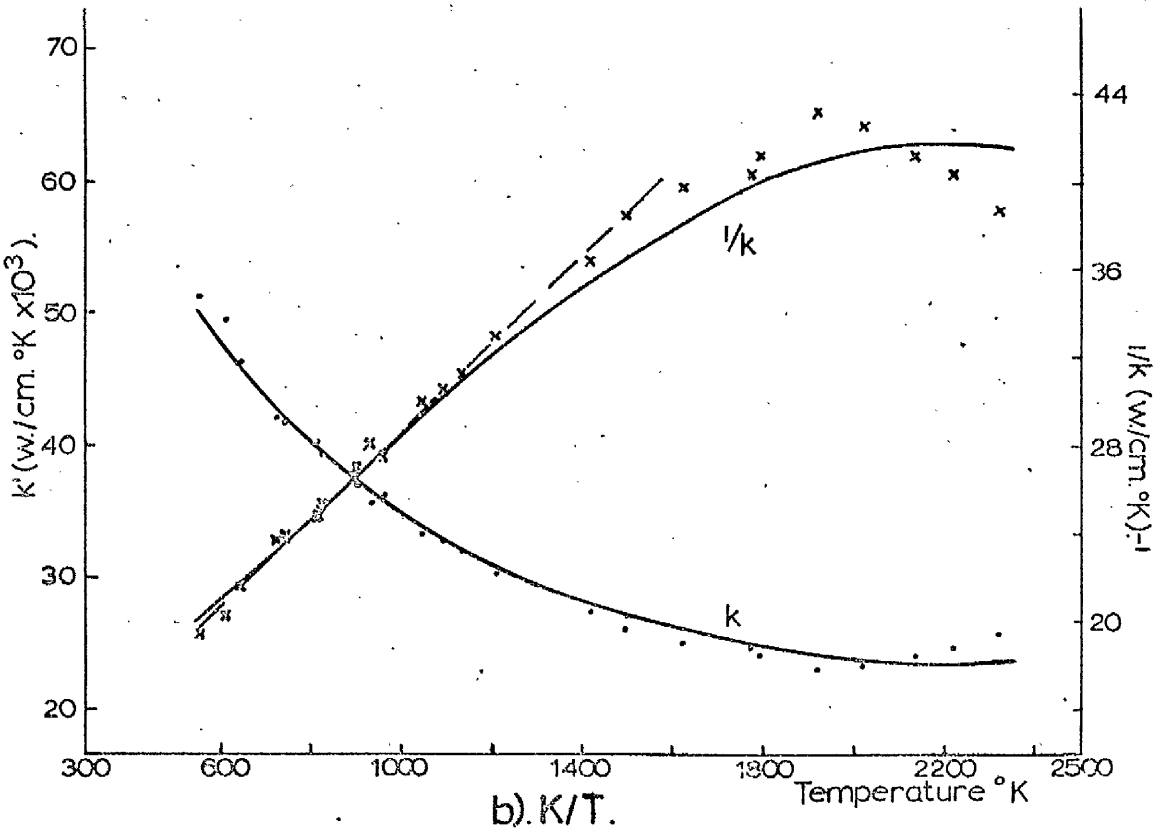

b). K / T.

FIG. 6·17. 96 2·006.

b) 96 $^{o}/_{u} = 2.030$

The $^{o}/_{u}$ ratio altered from 2.030 to < 2.002 during testing. There was no specimen for post test density or grain size determinations, and consequently the values for the original 96 material were used where necessary.

Fig. 6.18a shows the plot of α against T, and fig. 6.18b shows those of k and $^{1}/_{k}$ against T. It can be seen that a definite change in slope occurs between 700 - 750°K, which is more noticeable in the plot of $^{1}/_{k}$ against T. This is due to a phase change which is discussed in the next chapter.

In fig. 6.18b the broken line represents the equation

$$^{1}/_{k} = (13.50 \pm 2.46) + (1.83 \pm 0.24) \times 10^{-2} T \quad (w/cm^{o}K)^{-1} \qquad (6.19)$$

for $753^{o}K < T < 1373^{o}K$

The solid line represents the full equation for k and $^{1}/_{k}$ between 753 - 2403°K given by:

$$k = {}^{1}/(13.84 + 1.88 \times 10^{-2} T) + 6.13 \times 10^{-13} T^{3} \quad w/cm^{o}K \qquad (6.20)$$

with $1\ \sigma' = 1.34 \times 10^{-3}$ $w/cm^{o}K$.

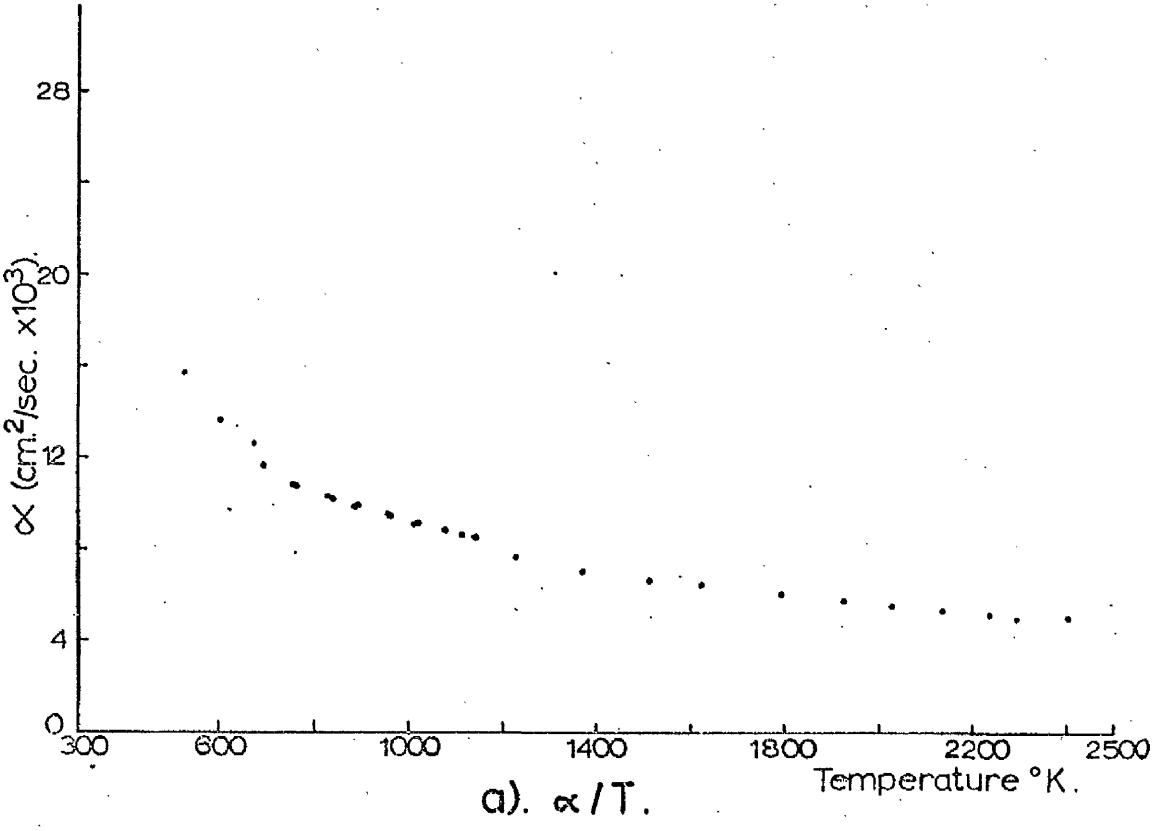

a). α / T.

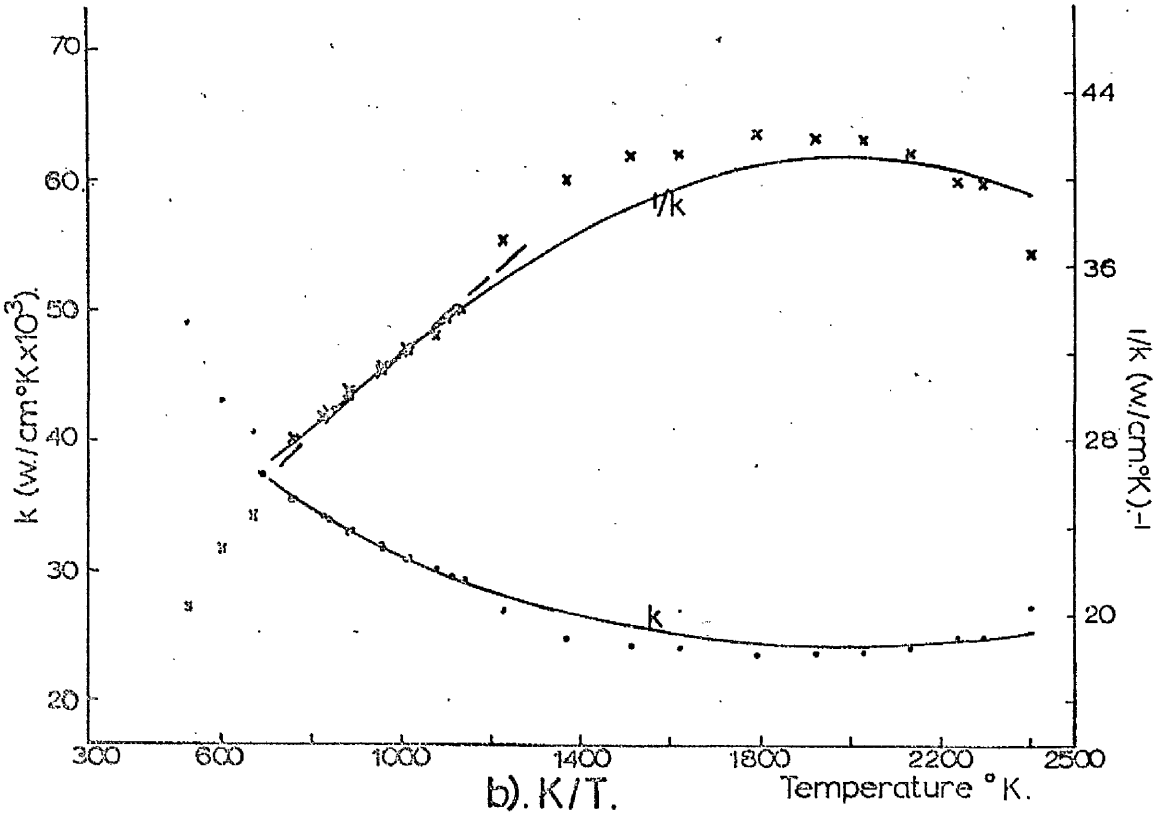

b). K/T.

FIG. 6·18. 96 2·030.

c) 96 $^{O}/_{u}$ = 2.060

The $^{O}/_{u}$ ratio had altered from 2.060 to < 2.002 during testing. The micrograph in fig. 6.19 shows that the porosity is mostly spherical (diameter of $< 5\mu$) lying at triple points and on grain boundaries. There are a few large spherical pores of $\sim 20\mu$ in diameter.

Fig. 6.20a shows the plot of α against T, and it includes the values obtained on the cooling cycle. These values show an increase in the thermal diffusivity at lower temperatures, the values approach those given in the preceding section 6.20a for stoichiometric 96. This increase can, therefore, be associated with a reduction in the $^{O}/_{u}$ ratio, and further proof is found in the post test stoichiometric analysis.

Fig. 6.20b shows the plots of k (dots) and $^{1}/_{k}$ (crosses) against T. Both curves show a gradient change between 700 - 800^{O}K, and this is due to a phase change which will be discussed in chapter 7. Since the shape of the curves is so irregular, it was impossible to apply a regression analysis to any section of the results with any certainty. Instead a best-fit curve was drawn for use in the discussion chapter, where a curve comparing the 'k' values for the non-stoichiometric specimens was required.

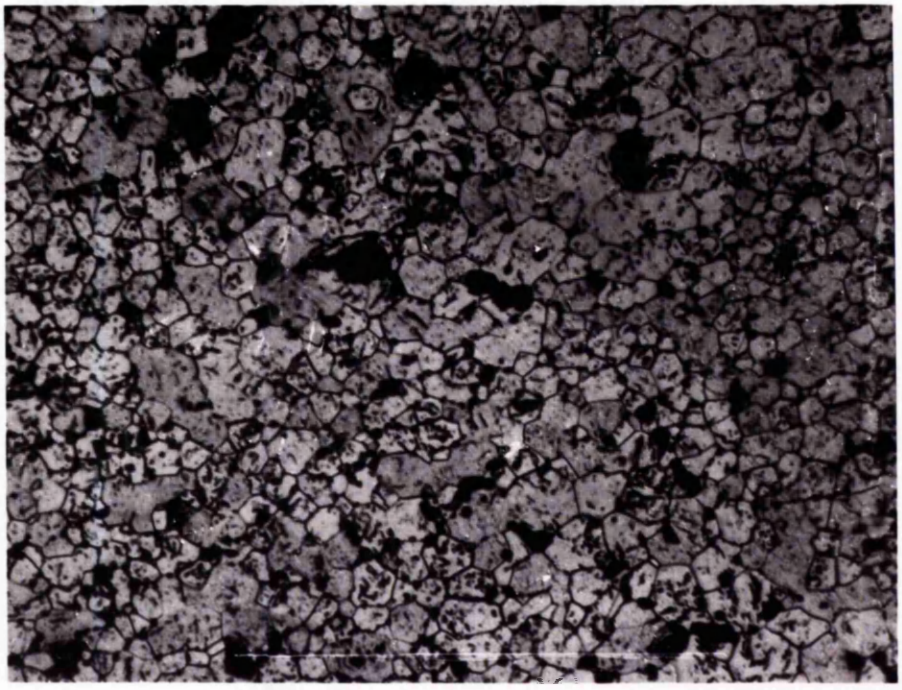

x300

FIG. 619. 96.($^{0}/_{u}$=2·060).

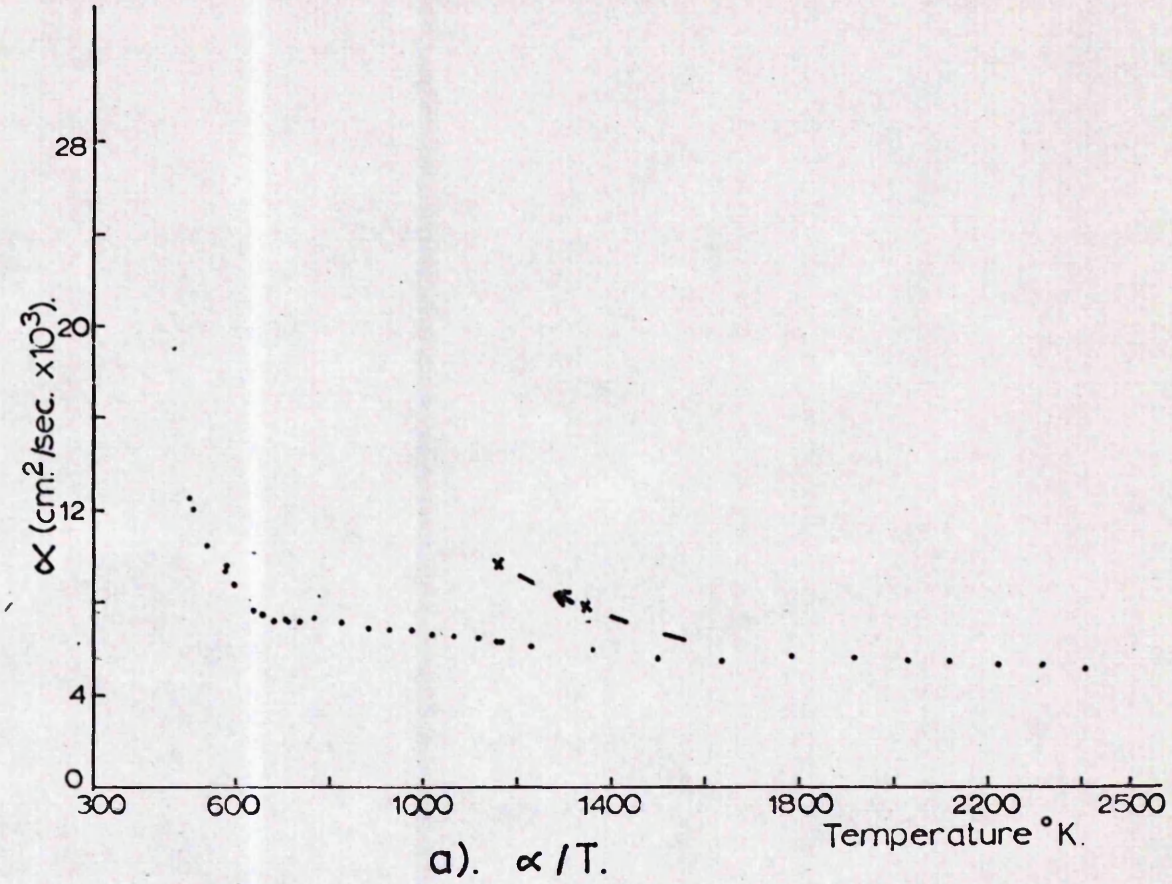

a). α / T.

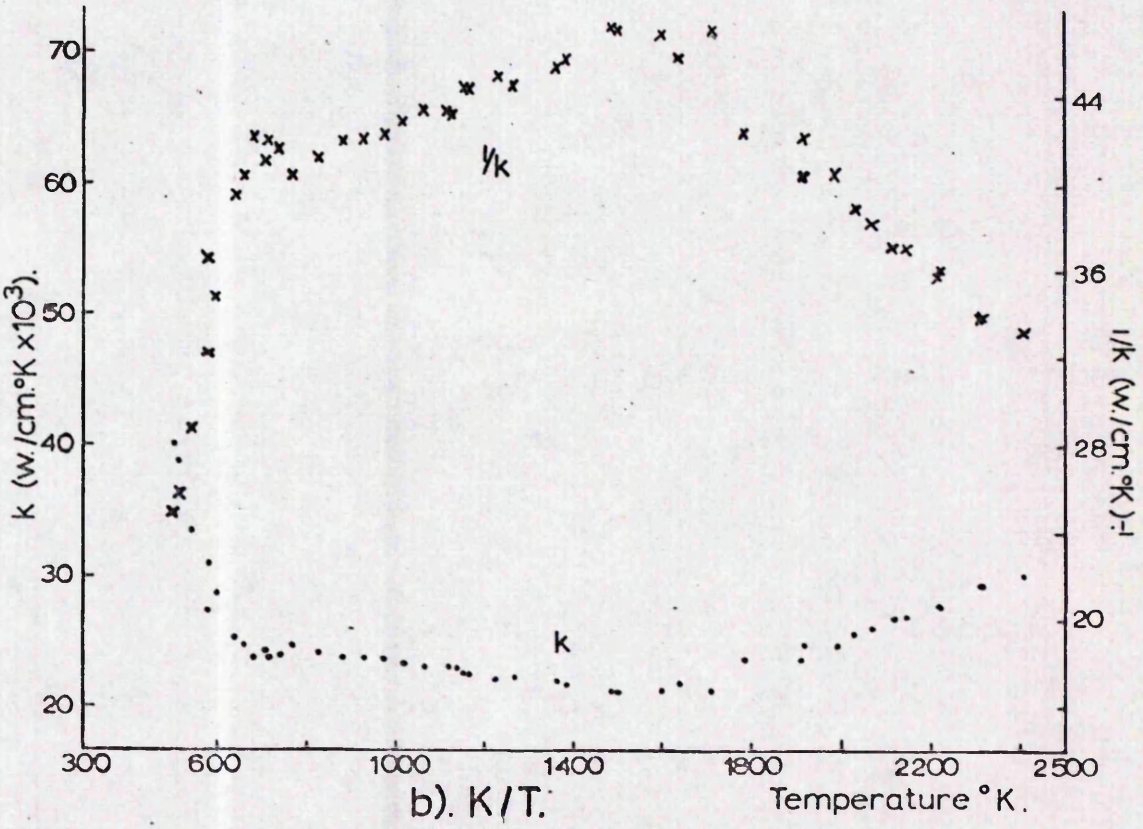

b). K/T.

FIG.6·20. 96 2·060.

d) 93^{I} $^{o}/_{u} = 2.006$

The $^{o}/_{u}$ ratio had altered from 2.006 to < 2.001 during testing. From the micrograph in fig. 6.21 it can be seen that the porosity is spherical ($\sim 20\mu$ in diameter) and lying mostly at triple points and on grain boundaries.

Fig. 6.22a shows a plot of α against T, and fig. 6.22b shows the plots of both k and $^{1}/_{k}$ against T. The broken line represents the equation for $T < 1573^{o}K$

$$^{1}/_{k} = (11.19 \pm 0.39) + (2.04 \pm 0.38) \times 10^{-2} T \quad (w/cm^{o}K)^{-1} \qquad (6.21)$$

The solid line represents the full equation for k and $^{1}/_{k}$ between $526 - 2450^{o}K$ given by:

$$k = {}^{1}/(11.35 + 2.07 \times 10^{-2} T) + 4.40 \times 10^{-13} T^{3} \quad w/cm^{o}K \qquad (6.22)$$

with $1\sigma = 0.80 \times 10^{-3}$ $w/cm^{o}K$.

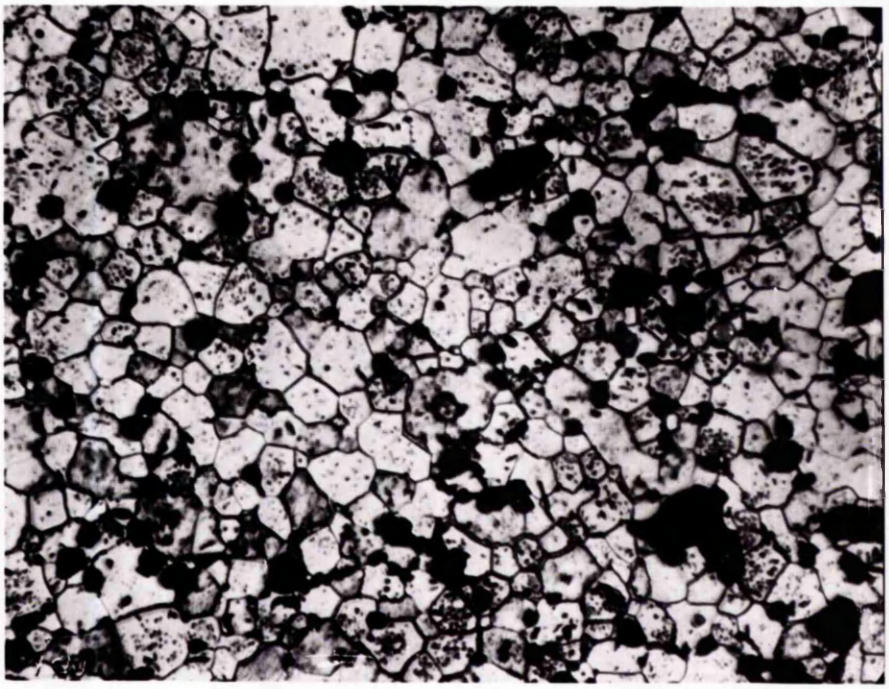

x300

FIG. 6·21. 93^{I}·(%$_{U}$=2·006).

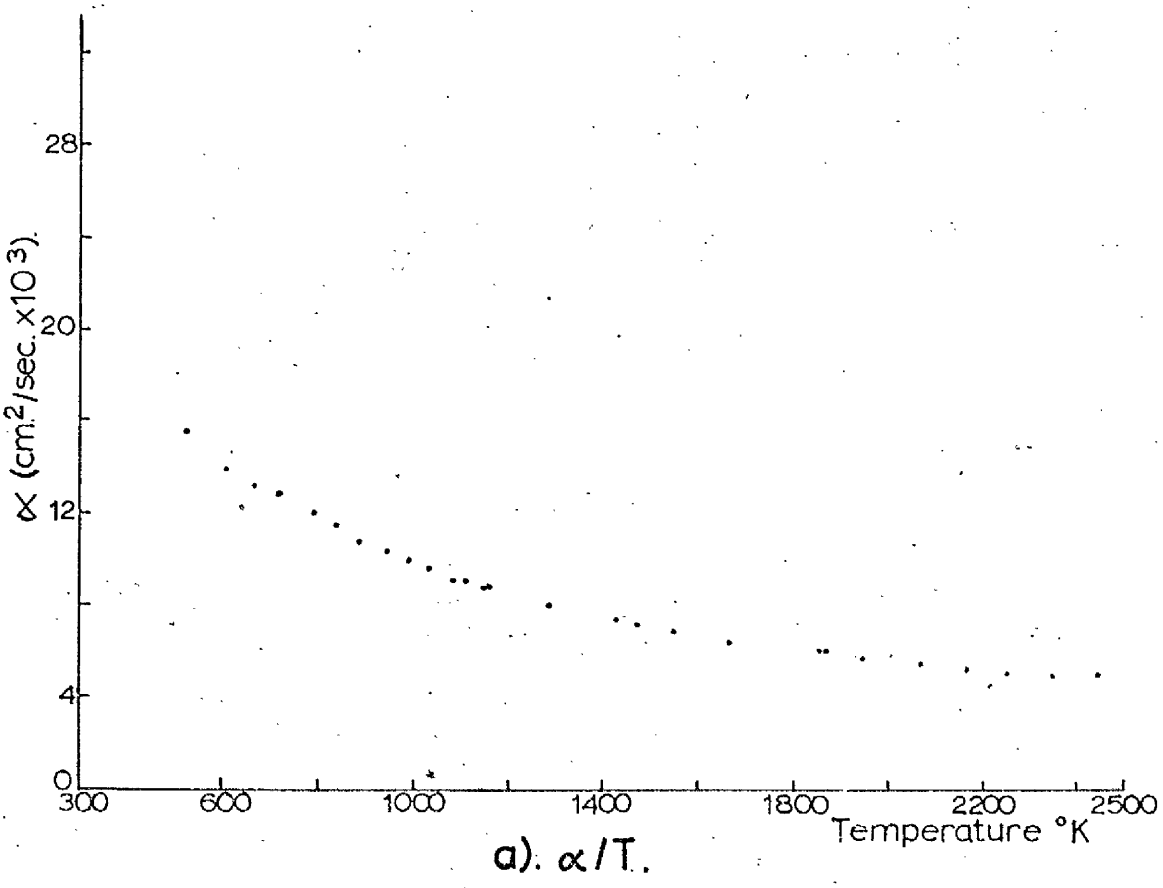

a). α / T.

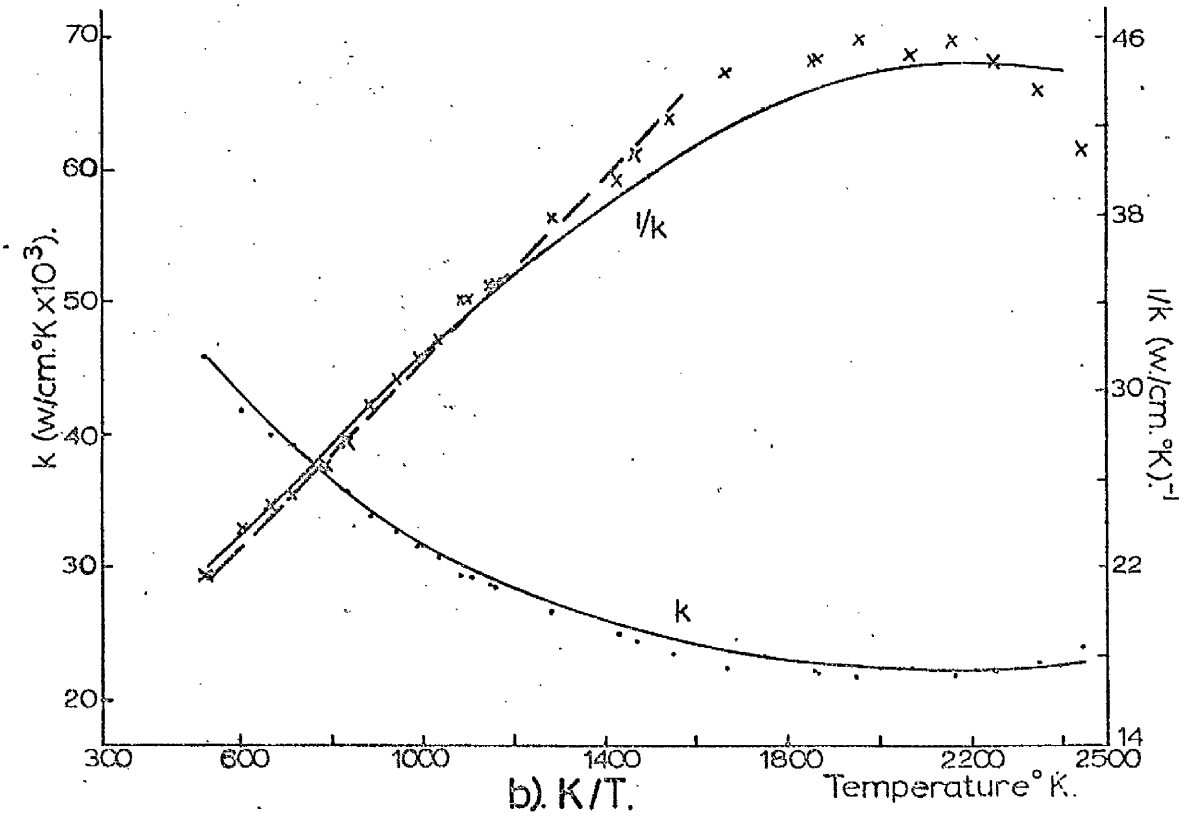

b). K/T.

FIG.6·22. 93' 2006.

e) 93^{I} $^{O}/_{U}$ = 2.030

The $^{O}/_{U}$ ratio had altered from 2.030 to < 2.001 during testing. From the micrograph in fig. 6.23 it can be seen that the porosity is large and spherical.

Fig. 6.24a shows the plot of α against T, and fig. 6.24b shows the plots of k and $^{1}/_{k}$ against T. The plot of $^{1}/_{k}$ against T shows a slight change in the curve around 700°K, and this will be discussed later.

The broken line in fig. 6.24b represents the equation

$$^{1}/_{k} = 12.98 + 2.02 \times 10^{-2} T \qquad (w/cm^{o}K)^{-1} \qquad (6.23)$$

for 753 - 1373°K.

The solid lines represent the full equation for k and $^{1}/_{k}$ between 753 - 2423°K given by

$$k = {}^{1}/\ 12.98 + 2.02 \times 10^{-2} T + 8.70 \times 10^{-13} T^{3} \quad w/cm^{o}K \qquad (6.24)$$

These equations (6.23 and 6.24) were obtained using a best-fit curve since there was insufficient time to perform a regression analysis on the recalculated values of 'α' and 'k'.

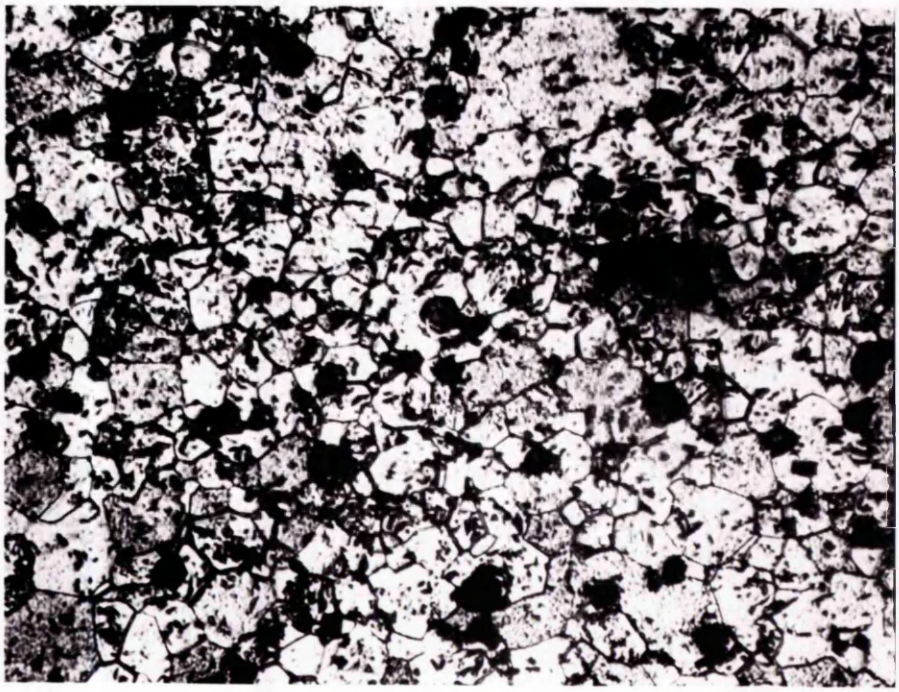

×300

FIG. 6·23. 93% (σ_U=2030).

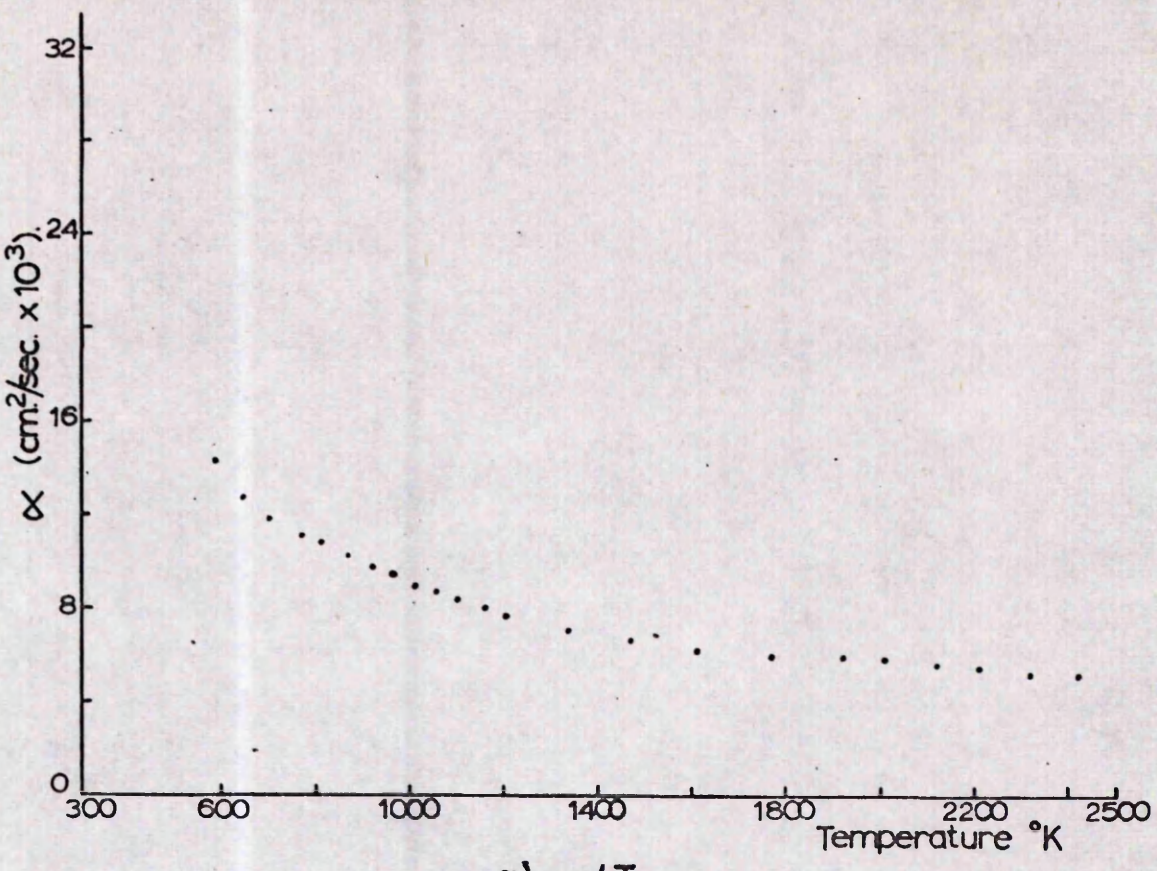

a). α / T.

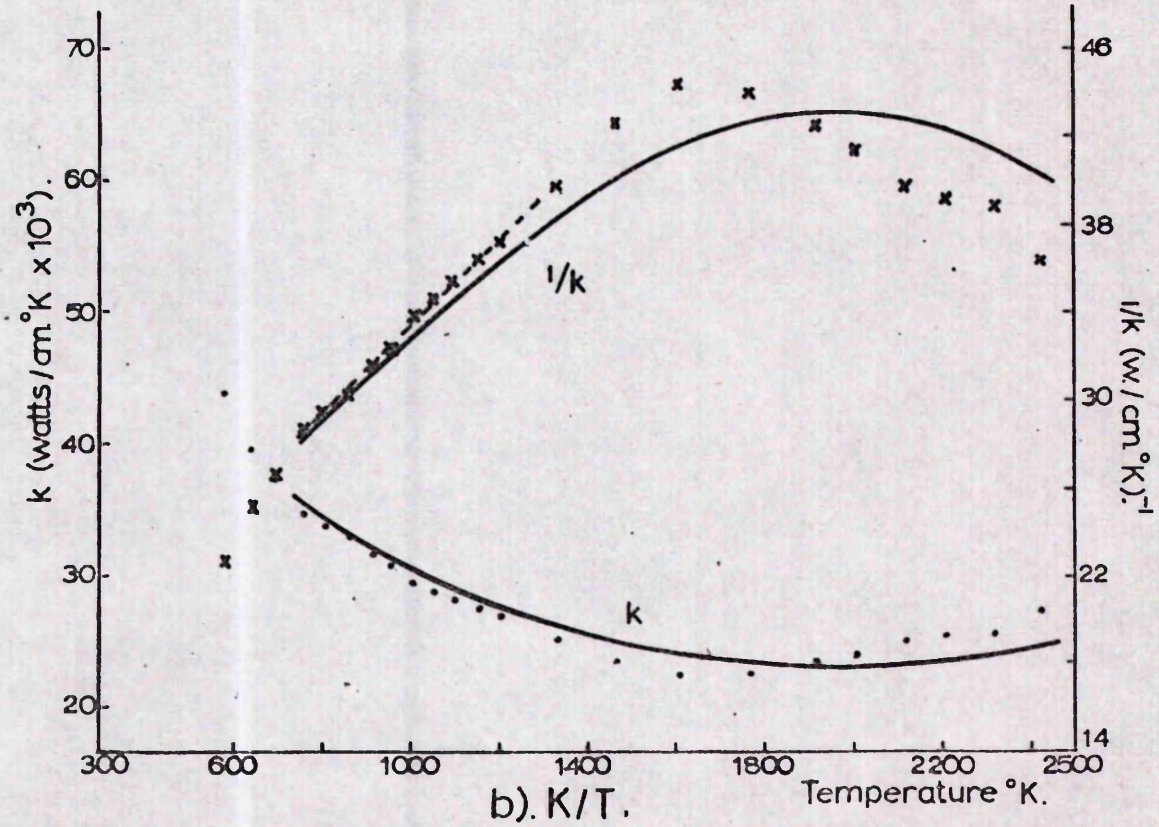

b). K / T.

FIG. 6·24. 93' 2·030.

f) 93^{I} $^{O}/_{u} = 2.060$

The $^{O}/_{u}$ ratio had altered from 2.060 to < 2.001 during testing. From the micrograph in fig. 6.25 it can be seen that the porosity is large and spherical with diameters of the order of 20μ. It lies mostly on grain boundaries and at triple points.

Fig. 6.26a shows the plot of α against T and includes values taken during the cooling cycle. These values show an enhanced diffusivity at lower temperatures, approaching the values for stoichiometric 93^{I} . This enhancement can be attributed to a reduction in the $^{O}/_{u}$ ratio.

Fig. 6.26b shows the plots of k and $^{1}/_{k}$ against T, and both curves show a significant change in slope around 725^{O}K. This will be discussed in the next chapter. Since the curves are so irregular, it was impossible to apply a regression analysis to the values, and so a best-fit curve was used in the discussion when a comparison of the 'k' curves was required.

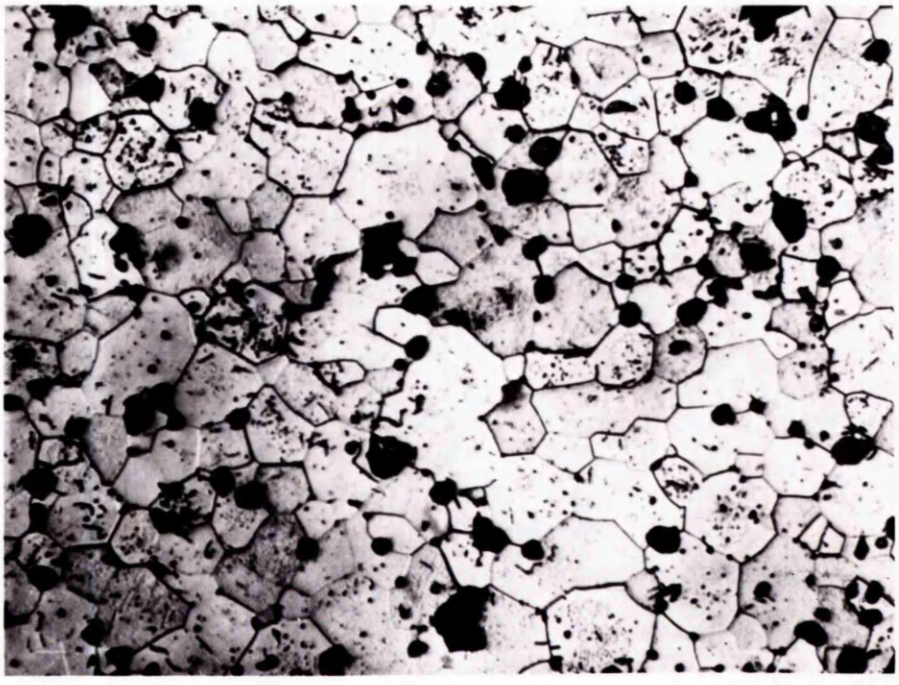

x300

FIG. 6·25. 93% ($^{O}/_{U}$=2·060).

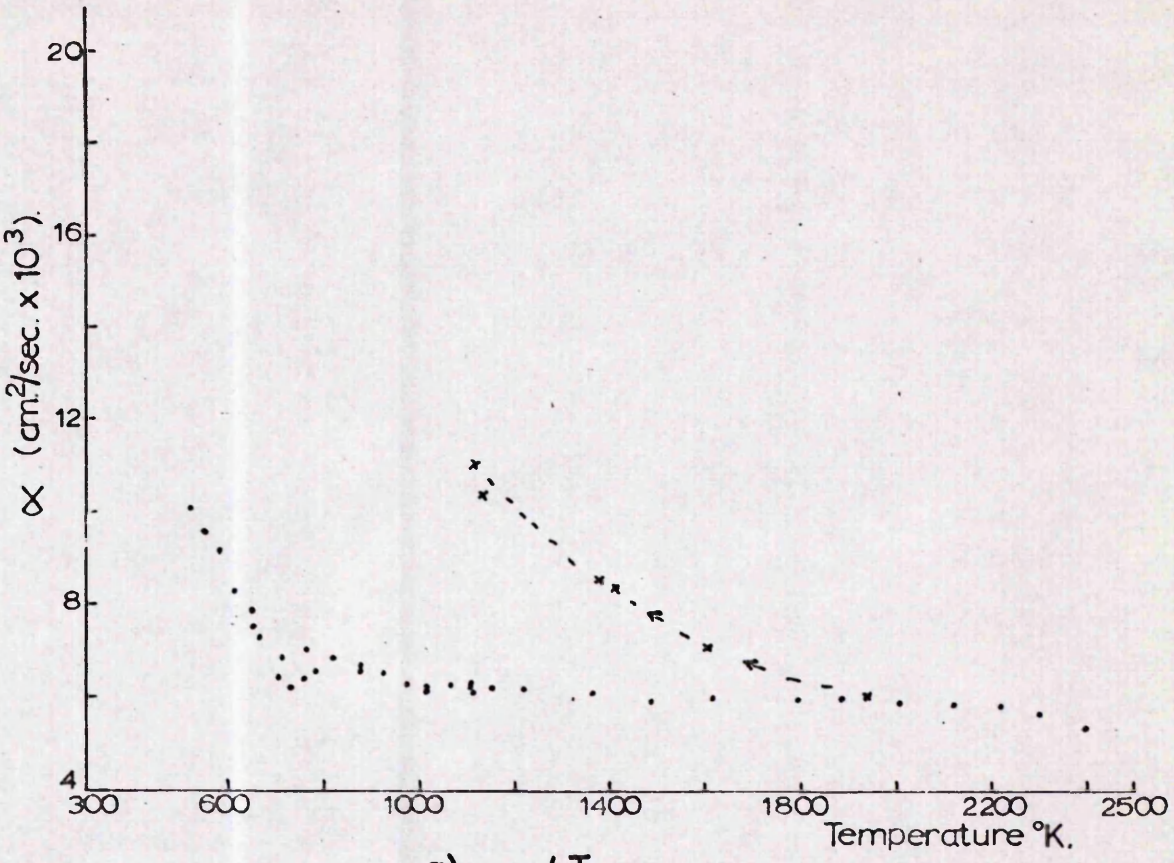

a). α / T.

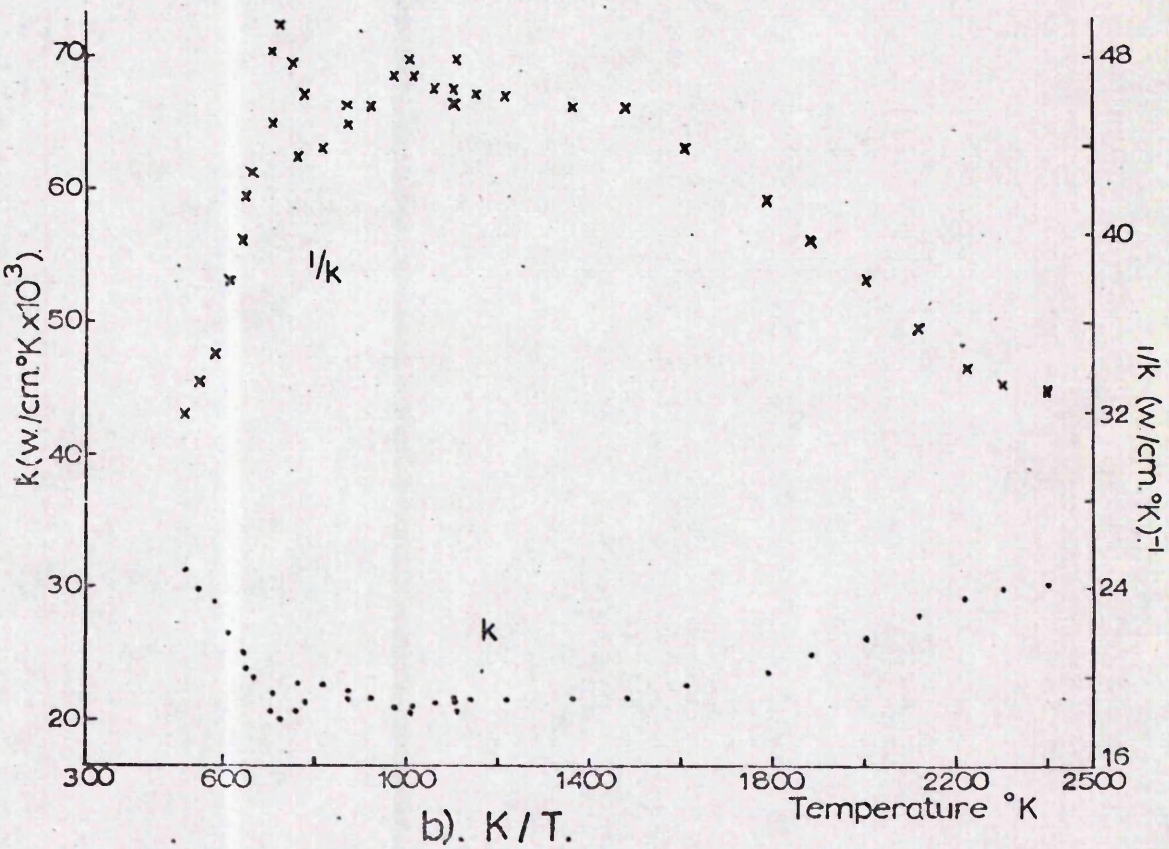

b). K / T.

FIG.6·26. 93' 2·060.

CHAPTER 7

DISCUSSION

1) Effect of Porosity

a) Variation of k with pore distribution

The two batches 9694 and 9691, which were manufactured from 96, gave thermal conductivity values that were higher than those of the specimens with similar densities, i.e. the 93^{I}, 91^{I}, 94^{II} and 91^{II}. In both cases the values of the 9694 and 9691 lay very close to the values of their parent material (96); there being a difference of $\sim 5.5\%$ at $750^{o}K$ and 2% at $2000^{o}K$. This indicates that, since the major portion of the porosity in the 9694 and 9691 lay at triple points and on grain boundaries, such porosity has less thermal resistance than porosity randomly distributed - this being the only difference between the 9694 and 9691 and the other specimens. In fact, when considering only the intergranular porosity, the 9694 and 9691 may have densities very close to that of the original 96 material from which they were manufactured.

It is seen, therefore, that pore distribution has an important effect on the thermal conductivity, with pores on grain boundaries and at triple points having very little effect on the conductivity. For this reason the 9694 and 9691 values have been ignored in the subsequent analysis on the effect of pore volume fraction. It is important to note that in this analysis when using the 'A' and 'B' values for all specimens (except 9694 and 9691) the effect of any differences in distribution has been disregarded, i.e. it has been assumed that the porosity distribution in each specimen is the same.

b) Variation of k with pore volume fraction

All of the data given in the preceding chapter were fitted upto 1673°K to the equation

$$1/k_m = A_m + B_m T \qquad (7.01)$$

Assuming a relationship of the form

$$k_m = k_{95}(1 - \beta p) \qquad (7.02)$$

where $p = \frac{(\text{density of 95\% T.D.} - \text{density of specimen})}{\text{density of 95\% T.D.}}$ (7.03)

it can be seen that

$$k_m = \frac{(1 - \beta p)}{A_{95} + B_{95} T} \equiv \frac{1}{A_m + B_m T} \qquad (7.04)$$

i.e. $$A_m \equiv A_{95}/(1 - \beta p) \qquad (7.05a)$$

$$B_m \equiv B_{95}/(1 - \beta p) \qquad (7.05b)$$

It would be expected that the value of 'A_m' should reflect contributions to the thermal resistivity from such features as point defects, grain boundaries, impurities as well as porosity. Since there is very little variation except in the pore volume fraction and only slightly in the impurity levels of the specimens, it would be expected that the 'A' values should reflect the differences in porosity, and thus the equation for 'A_m' should be significant. The values of 'B' should reflect the contribution to the resistivity solely due to Umklapp processes (see Chapter 1. A), and thus the values of 'B' should be unique.

Before this analysis could be pursued, it was necessary to assume that all the pores within each specimen behave in a similar manner with regard to any effect they may have on

the thermal conductivity. For this reason the values obtained on the 9694 and 9691 specimens were excluded from the analysis and from any comparisons made later with other published data. Similarly the single crystal values were not included in this analysis since neither their stoichiometry nor their impurity concentration had been determined. Also the single crystal values would not contain a contribution to the resistivity from grain boundaries, and this would exclude the use of these values from any direct comparison with the values of the other specimens.

To test the equations in 7.05a and b, plots of 'A' and 'B' against pore volume fraction were made, using the data given in table 7 I. These plots are given in figs. 7.01a and 7.01b. By least squares analysis, straight line fits were obtained as follows:

$$A_m = 6.16 + 30.54p \qquad (w/cm^{\circ}K)^{-1} \qquad (7.06a)$$

$$B_m = 0.0208 + 0.0140p \qquad (w/cm)^{-1} \qquad (7.06b)$$

These equations reduce to

$$A_m = 6.16\ (1 + 4.96p) \qquad (7.07a)$$

$$B_m = 0.0208\ (1 + 0.67p) \qquad (7.07b)$$

where $A_{95} = 6.16\ (w/cm^{\circ}K)^{-1}$, $B_{95} = 0.0208\ (w/cm)^{-1}$

These equations 7.07a and 7.07b can be equated to equations 7.05a and 7.05b respectively, and this yields values of β = 4.96 for 'A' and β = 0.67 for 'B' (neglecting all third order terms in the expansion of $(1 - \beta p)^{-1}$). These values seem to indicate that there is a fault in the above analysis, as one would have expected the values of 'A' and 'B' to give the same

NAME	A $(w/cm^{\circ}K)^{-1}$	B $(w/cm)^{-1}$
96	5.57 ± 0.33	.0202 ± .0003
94^{II}	6.15 ± 0.23	.0215 ± .0002
93^{I}	7.16 ± 0.22	.0211 ± .0002
91^{II}	7.69 ± 0.54	.0210 ± .0005
91^{I}	7.02 ± 0.18	.0216 ± .0002
SX	-1.36 ± 1.20	.0226 ± .0010
95	6.07 Δ	.0208 Δ
100	4.65 Δ	.201 Δ
2.006	8.80 ± 0.40	.0199 ± .0004
96 2.030	13.50 ± 2.46	.0183 ± .0024
2.060	33.50*	———
2.006	11.19 ± 0.39	.0204 ± .0004
93^{I} 2.030	12.98**	.0202**
2.060	40.80*	———

Values taken from $k = (A + BT)^{-1}$ equation

* extrapolated value at $T = 0^{\circ}K$ from single phase region

Δ Calculated values

** Recalculated values ∴ no scatter band

TABLE 7.I

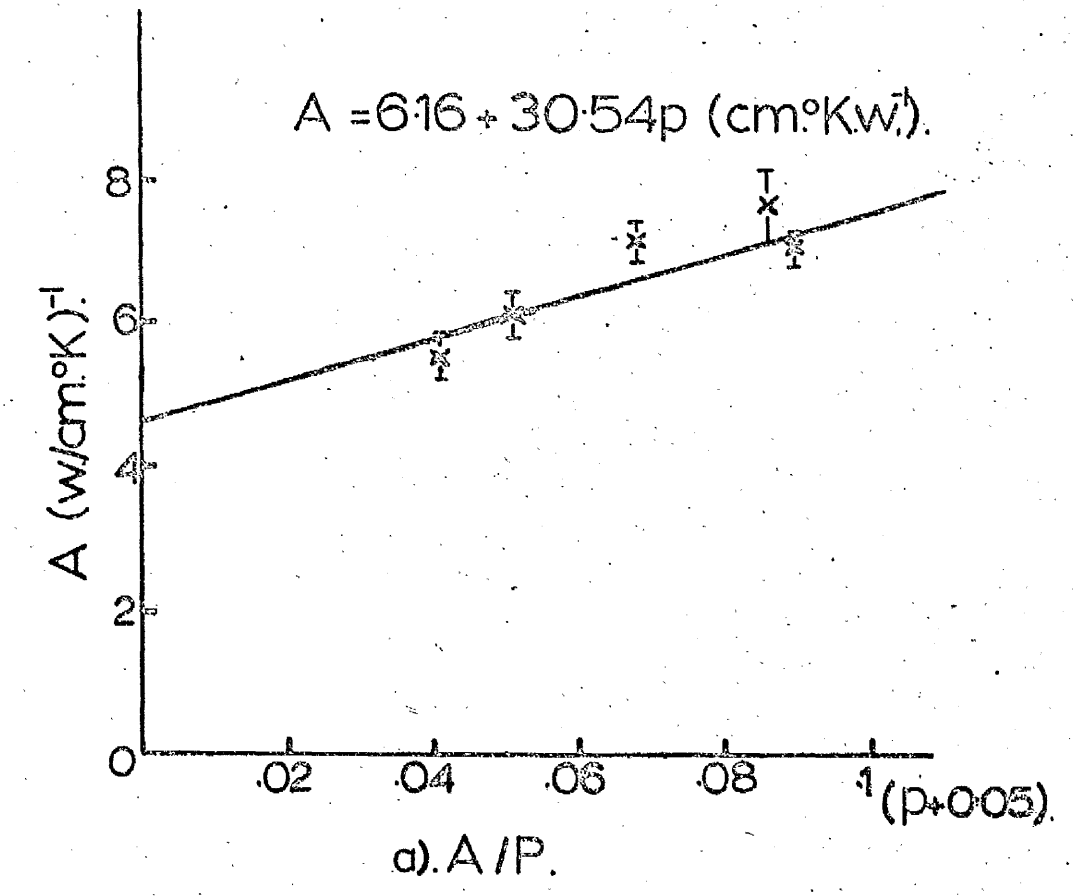

a). A / P.

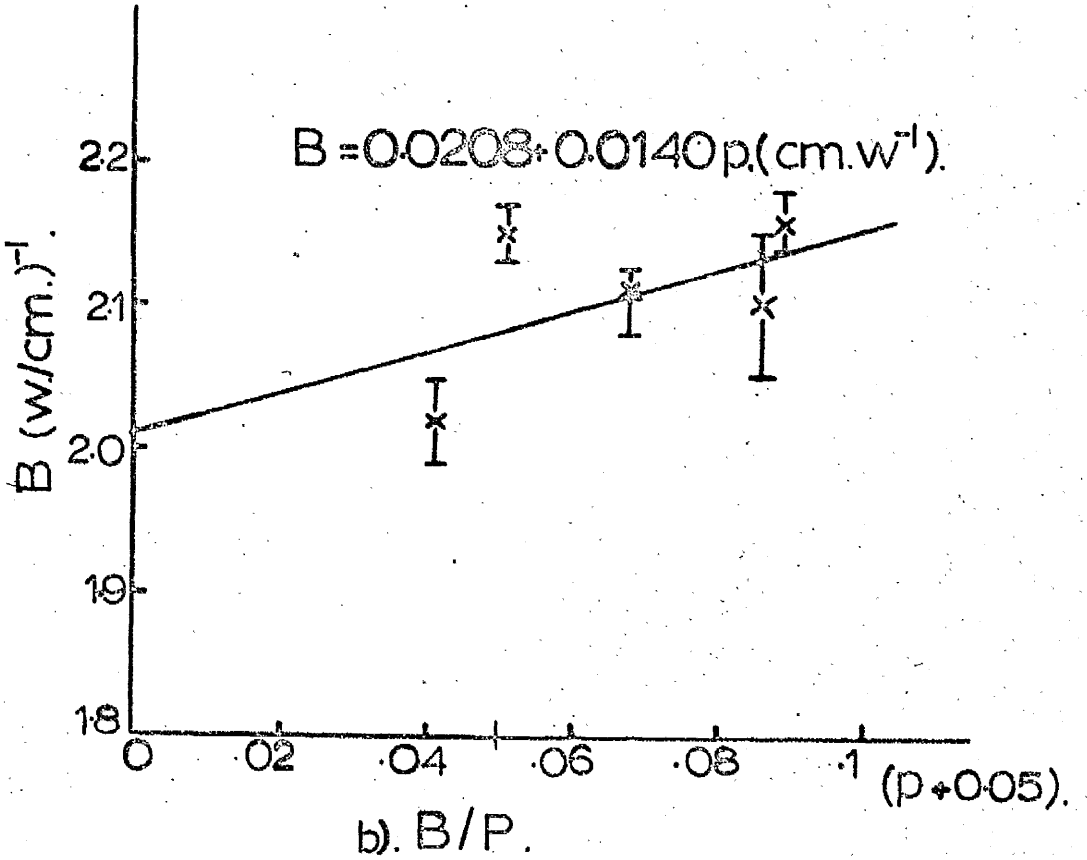

b). B / P.

FIG. 7·01.

value of 'β'. In equation 7.04

$$A_m + B_m T = \frac{A_{95} + B_{95} T}{(1 - \beta p)}$$

'β' may be temperature dependent, and this would mean that 'A' and 'B' would vary in a more complex way with pore volume fraction.

Substituting the values obtained for 'A_m' and 'B_m', equation 7.04 yields

$$k_m = \frac{1}{A_m + B_m T} = \frac{1}{6.16 + 30.54p + T(.0208 + .0140p)}$$

$$= \frac{1}{6.16 + .0208T} \left(1 - p\left(\frac{30.54 + .0140T}{6.16 + .0208T}\right)\right) \qquad (7.08)$$

$$\therefore \beta = \frac{30.54 + .0140T}{6.16 + .0208T} \qquad (7.09)$$

This seems to confirm that β is temperature dependent if the values obtained in equations 7.07a. and b. are correct and if 'A_m' and 'B_m' vary linearly with pore volume fraction.

An attempt was made to determine 'β' using the method employed by Van Craeynest/Stora (60) namely plotting k against pore volume fraction for the selected temperatures of 750°K, 1000°K, 1250°K and 1500°K. Fig. 7.02 shows this plot. Assuming the relationship given in equation 7.02 to hold at for $T < 1673^{\circ}K$

i.e. $k_m = k_{95} (1 - \beta p)$

and using least squares analysis, a 'β' value was calculated for each of the four temperatures stated. The analysis gave a decreasing 'β' with increasing temperature, as shown in fig. 7.03 along with the value obtained by Van Craeynest/Stora (60) Applying a least squares analysis to these values

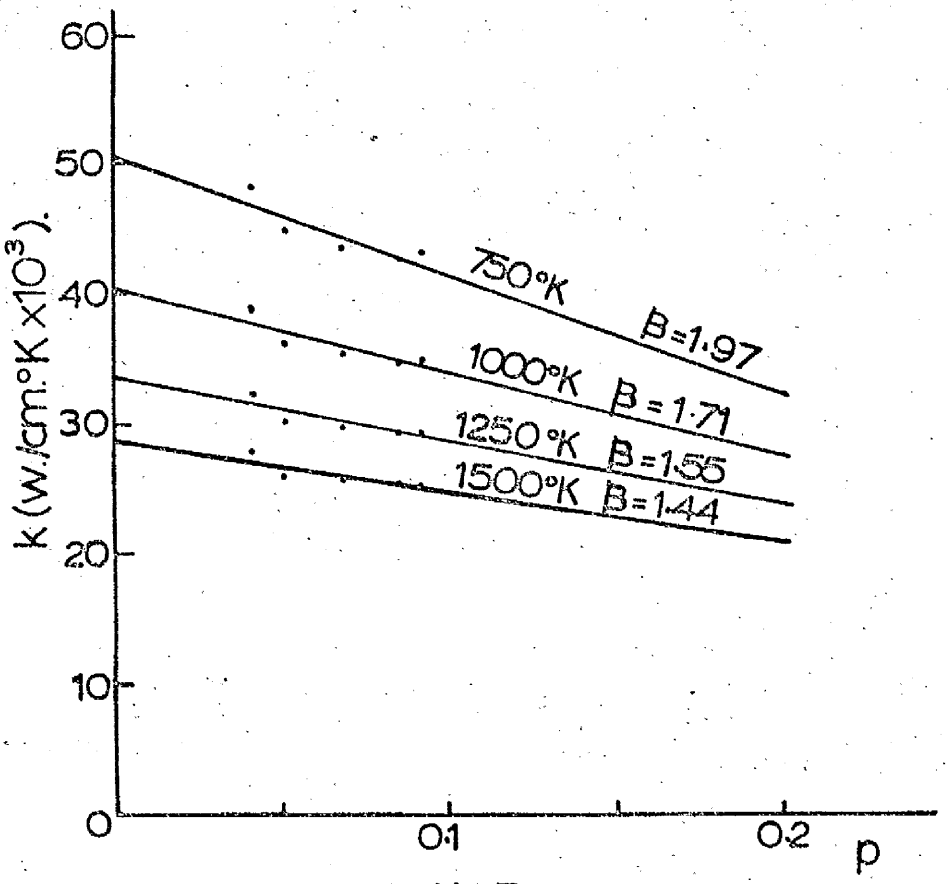

FIG. 7.02. K/P.

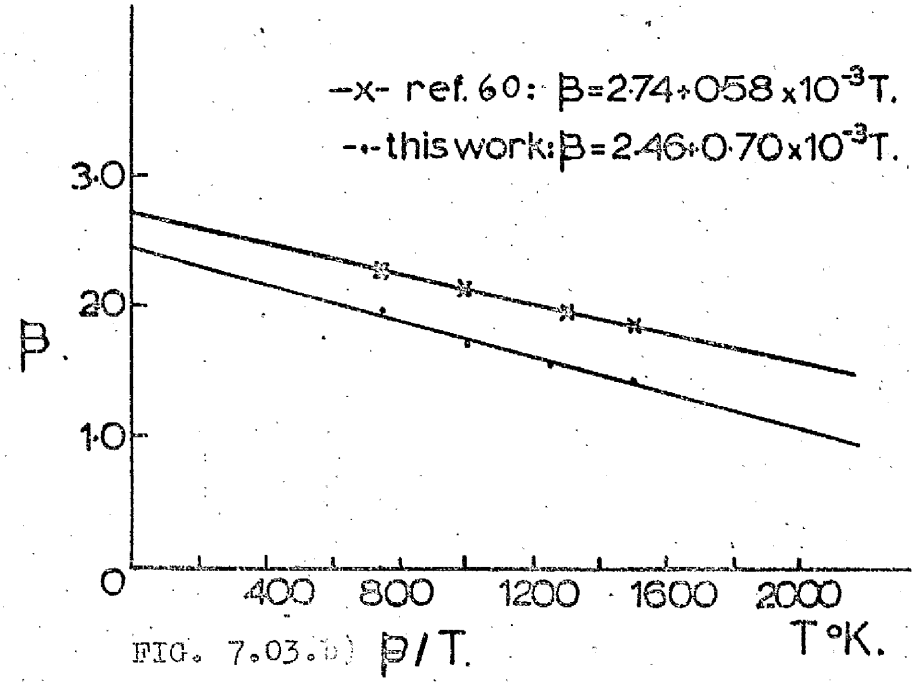

FIG. 7.03. β/T.

gave $\beta = 2.46 - 0.70 \times 10^{-3} T \quad (T^{o}K) \qquad (7.10)$

This value of 'β' is in good agreement with that given by equation 7.09 over the temperature range 700°K to 1800°K, as shown by fig. 7.04, although there is a maximum difference at 1200°K of the order of 6½%. Such a discrepancy could have arisen in the use of least squares analysis.

The only other workers to indicate a temperature dependent 'β' term have been Asamoto et al (61) and Van Craeynest/Stora (60). The latter gave

$$\beta = 2.74 - 0.58 \times 10^{-3} T \quad (T^{o}K) \qquad (7.11)$$

but they gave no reason for this temperature dependency. More recently Marino (62) has studied the possible factors involved and attempted to relate a temperature dependent 'β' to radiation across the pores or to conduction of the gas within the pores. In his analysis he used the expression

$$k_m = \frac{k(1 - p)}{(1 + \alpha p)} \qquad (7.12)$$

He showed that the contribution from radiation across the pores (k^{r}_{pore}) had a maximum value of $\sim 0.5 \times 10^{-3}$ w/cm°K at 3000°K for pores with a diameter (dp) of 200μ. This value decreases with decreasing pore diameter and with decreasing temperature. By applying Marino's analysis to the results in Chapter 7, it would appear that any radiation contribution should be negligible since the pores are spherical and have diameters less than 20μ. For the contribution to the total thermal conductivity from conduction by the gas in the pores, he calculated a maximum of $\sim 7 \times 10^{-3}$ w/cm°K at 3000°K for pores containing helium or hydrogen. This contribution decreases with decreasing temperature, and other gases (krypton and xenon)

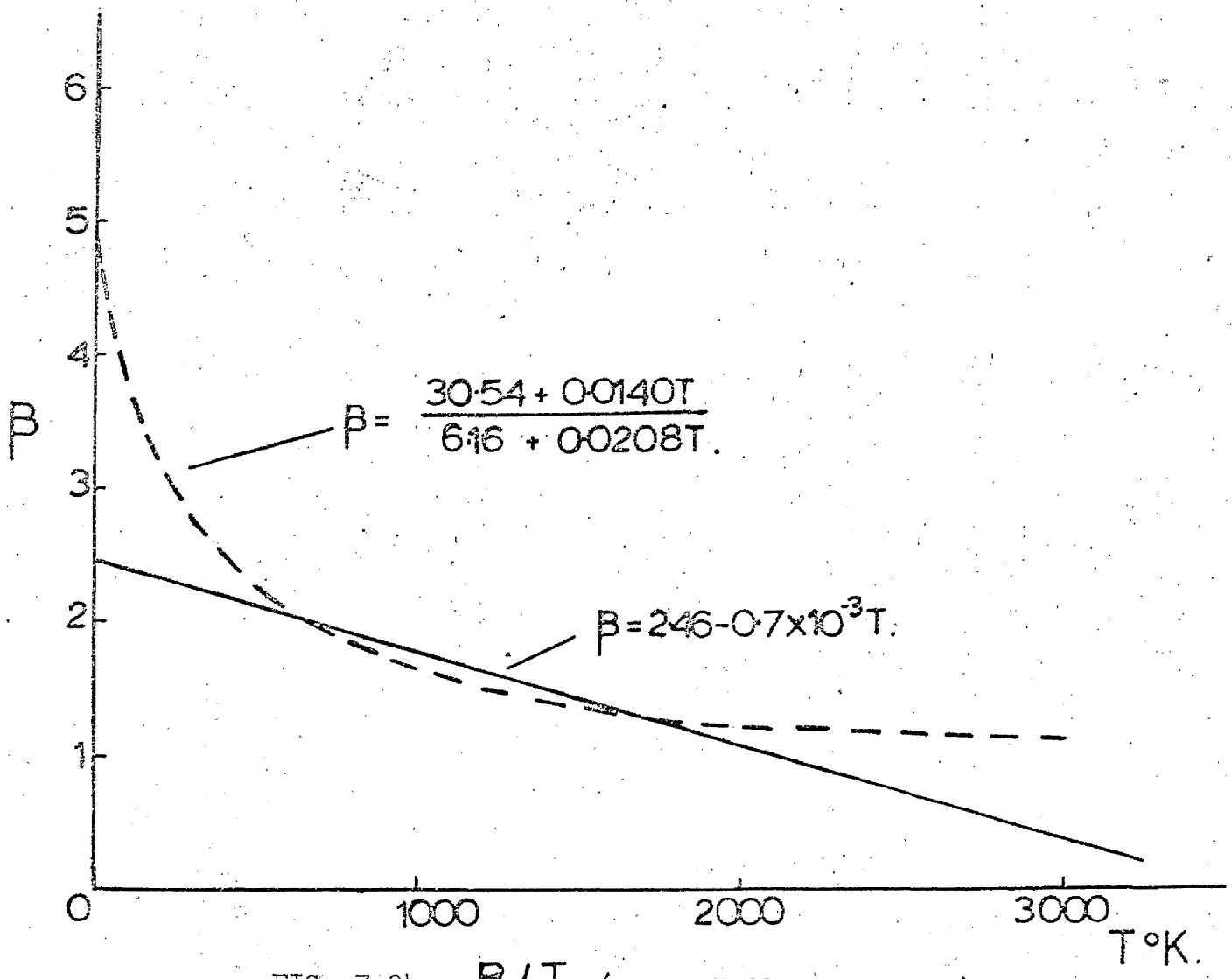

FIG. 7.04. β/T. (eqns. 7.09. and 7.10.)

have values less than 0.5×10^{-3} w/cm°K over all temperatures. When applied to the specimens used here, it would appear that this could account for the temperature dependent 'β' term observed, since the specimens were sintered in hydrogen. However, Ainscough (78) suggested that any hydrogen present would diffuse out rapidly with time. This is born out by Wheeler (106) who thought that, though as much as 1 to 2 μg H_2/gm UO_2 may remain after sintering, on being heated to $\sim$ 500°C in vacuum or inert atmosphere only about 20% would remain in the UO_2. This is due to the high diffusion rate and low solubility of hydrogen in UO_2. The significance of any contribution from hydrogen conduction is further lessened by the fact that the total pore volume and the pore sizes of the specimens under investigation are small. Thus the small volume of hydrogen remaining in the specimen will be contained in small, spherical pores which are well distributed throughout the specimen. It is, therefore, expected that the contribution to the thermal conductivity from conduction across hydrogen-filled pores in UO_2 would be negligible.

In his analysis Marino (62) disregarded any results taken from cracked specimens and any data that showed more than $\pm$ 2% difference between the heating and cooling cycles. In the latter case he assumed microcracking or evaporation of the tungsten coating. However, Bates (43) stated that tungsten coating had no effects on his results. Thus Marino applied very stringent controls over his analysis.

Further to his work, Marino found 'β' to be independent of the pore volume fraction (p), but he made the assertion that any change in 'p' would usually alter the pore shape factor (ε) which could in turn alter 'β' considerably. In this

investigation, the porosity was mostly spherical and less than 20 μ in diameter, although the distribution may have differed slightly between the specimens. It can be assumed, therefore, that 'ε' was constant and equal to unity (for spherical porosity) for all specimens, and thus that 'β' is independent of 'p'.

Since 'β' decreases with temperature, the thermal conductivity values of the different specimens must be converging at high temperatures, where the values need a smaller correction factor to normalise them to say 95% T.D. This is indicated in fig. 7.02 which shows the k values tending to become uniform as temperature increases. This observation may enable some conclusions to be drawn with regard to the temperature dependent 'β' term. In the analysis, 'β' is a factor depending on the geometry of the pores, and is obtained on the assumption that the contribution to the conductivity by heat transfer across the pores is negligible compared to that of the body as a whole. If, therefore, 'β' varies with temperature, either this assumption is wrong or the geometry of the pores alters in some way with temperature. As previously discussed, pore conduction can be effectively ignored, which leads one to the investigation of the effect of temperature on the specimens. If there were to be any densification with temperature, then surely this would be more pronounced for the low density specimens where the concentration of porosity is obviously much higher. This densification would mean the absorption of microporosity by larger pores and the possible migration of pores to grain boundaries. An increase in the conductivity would thus be observed, although the reason for it may not be

observed by metallographic examination. This would account for the convergence of the conductivity data at high temperatures, and consequently account for a temperature dependent 'β' term. However, one must ask oneself if densification is possible over the temperature range under investigation, i.e. 500 - 1600°K. The specimens were held in helium for about 2 hours of which no more than one hour would be spent above 1500°K and only about 20 minutes above 2000°K. It is believed (78) that any densification will occur only at temperatures above 2000°K, since experiments (78) have found that one must hold specimens (90 - 96% T.D.) at 1500°K for at least four weeks to effect a one-percent change in the density. Since 'β' was calculated using the values obtained over the range 500 - 1600°K, one would not expect any densification to have occurred, although one may expect a density increase of upto 1% at temperatures above 2000°K (78). Therefore, it must be assumed that the reason for a temperature dependent 'β' term lies elsewhere.

In a further attempt to explain this dependency, one is led to an analysis of the equations and parameters used to obtain 'β'. If one looks at the relationship derived for given in equation 7.09

$$\beta = \frac{30.54 + 0140T}{6.16 + 0208T}$$

i.e. $$\beta = \frac{AX + BYT}{A + BT} \qquad (7.13)$$

where $$A_m = A(1 + Xp) \qquad (7.14a)$$

and $$B_m = B(1 + Yp) \qquad (7.14b)$$

For 'β' to be independent of T, the values of 'X' and 'Y' should be equal in the above equation 7.13. If one now looks

at the values obtained

$$\text{i.e.} \quad A_m = 6.16(1 + 4.96p)$$

$$B_m = 0.0208(1 + 0.67p)$$

it can be seen that the values of X = 4.96 and Y = 0.67 are not equal.

Whereas there is no reason for the value of 'Y' to increase from 0.67 to about 4.96, the value of 'X' could be reduced, by an indeterminate amount, if one assumes that the low density specimens contain a lot of their porosity in the form of micropores. This microporosity would alter the porosity distribution and would contribute greatly as scattering centres to the thermal resistivity. If this effect increases with decreasing density, it would be reflected in higher 'A' values with increasing pore volume fraction. Thus if it were possible to quantify this effect due to distribution differences, one would be able to obtain the dependence of the 'A' values solely on pore volume fraction and these values of 'A' would be lower than those given by equation 7.07a. Consequently, the value of 'X' would be smaller than 4.96 and it may even be as low as 0.67. In this case 'β' would be equal to 0.67, i.e. very close to unity, and , as discussed in chapter 1.B, there are good theoretical grounds for expecting 'β' to be $\leqslant 1$ for small pore volume fractions and for pores in the form of small spheres. Therefore, since the porosity in the specimens under investigation is small and spherical, a reduction in the value of X from 4.96 to $\leqslant 1$ may provide an explaination for the observed temperature dependence of 'β'.

In order to obtain a 'β' value equal to unity, it would be necessary to have the following types of relationships between

'A' and 'B' and the pore volume fraction

$$A \simeq 6.16 \quad (1 + p) \qquad (7.15a)$$

$$B \simeq 0208 \quad (1 + p) \qquad (7.15b)$$

The values of 'B' would not require alteration by more than a few percent, since there is negligible difference between the calculated curve $B = 0.0208(1 + 0.67p)$ and equation 7.15b. Using equation 7.15a together with the calculated equation 7.07a, it can be seen that the following alterations to the measured 'A' values would be required in order to give a value of unity: A_{96} would have to be increased by 9%; $A_{94}{}^{II}$ would remain unaltered; $A_{93}{}^{I}$ would have to be decreased by $12\frac{1}{2}\%$; $A_{91}{}^{II}$ decreased by 17%; and $A_{91}{}^{I}$ decreased by $8\frac{1}{2}\%$. These percentages are only approximations, and are the values required to fit the measured 'A' values on to the straight line given by the equation 7.15a. However, there are a series of parallel lines giving a 'β' value of unity, and so these percentage alterations may be either high for A_{96} and low for $A_{93}{}^{I}$, $A_{91}{}^{II}$ and $A_{91}{}^{I}$, or vice-versa. The question is then raised regarding the validity for such alterations to the 'A' values.

During the preparation of the initial specimens, it was necessary to sinter and debond the pressed pellets in order to produce solid pellets. These two processes obviously produce a large amount of densification. If some microporosity remained after sintering, one would expect this microporosity to act as scattering centres and to contribute significantly to the thermal resistivity. The effect would be similar to that observed for the pore-redistributed specimens (i.e. 9694 and

9691), only the effect here would be an increase in the distribution rather than a reduction. One would expect more microporosity in the low density specimens, since there is a greater amount of porosity to be removed during sintering and since all of the specimens were sintered for the same time. Therefore, one would expect the 'A' values to increase with increasing pore volume fraction, and for this increase to be related in some undefined way to a size and distribution factor. The drawback to this analysis is the absence of any visual evidence of microporosity, although it could be assumed that such porosity is of the order of hundreds of angstroms.

Therefore, the author believes that the reason for the temperature dependency of 'β' lies in the complex variation of 'A' with porosity, and that in order to relate conductivity to pore volume fraction using

$$k_m = k_{95}(1 - \beta p)$$

one must take into consideration the effect of variations in pore size and distribution between the different pore volume fractions.

c) k_{95}, k_{100}.

The value of $\beta = 2.46 - 0.70 \times 10^{-3} T$ has been used to normalise the results to 95% T.D. For the non-stoichiometric specimens only two densities were used, namely 96 and 93%, thus it was impossible to obtain a 'β' value similar to that above. These results could not, therefore, be normalised to say 95% T.D.. It is of interest to note that Goldsmith/Douglas (30) recently found 'β' to decrease with increasing O/U ratio and to be invariant with temperature. They gave $\beta = 2.8 \pm 0.4$

for $^{O}/_{U} = 2.00$ and $\beta = 1.5 \pm 0.7$ for $^{O}/_{U} = 2.015$, but they could give no reason for this difference even after metallographic examination of pore structure and crystal structure.

Using the above 'β' value, values for the conductivity of 95% T.D. (k_{95}) and 100% T.D. (k_{100}) were obtained upto 1600°K. Fitting the values by least squares analysis to the equation

$$k = (A + BT)^{-1}$$

gave $$^{1}/_{k_{95}} = 6.07 + 2.08 \times 10^{-2}\, T \qquad (w/cm^{o}K)^{-1} \qquad (7.16a)$$

and $$^{1}/_{k_{100}} = 4.65 + 2.01 \times 10^{-2}\, T \qquad (w/cm^{o}K)^{-1} \qquad (7.16b)$$

The values for k_{95} have been compared against the results of other workers given in the I.A.E.A. report (38) which used $\beta = 2.5$ to normalise them to 95% T.D. (see fig. 7.05). The values from equation 7.13 are seen to be higher than most especially Nishijima et al (35). They fit well with those of Stora et al (107) to within 3%, and to within ~ 8% with the results of Vogt et al (54), Godfrey et al (41) and Daniel et al (56). Actual values when compared with the calculated k_{95} (from equation 7.16a) show that the values in this thesis are higher than the others. (see fig. 7.06).

In any detailed comparison it must of course be remembered that when using conductivity data the choice of specific heat data is very important (see chapter 4), and the value of 'β' chosen to normalise the values to 95% T.D. is a crucial factor. A more accurate comparison is obtained by comparing the diffusivity values of previous workers with the values obtained for α_{95} by reconverting k_{95} using Ainscough's C_p data. Fig. 7.07 shows that α_{95} is still higher than most other workers by at least 12% for the region 1250°K to 1600°K.

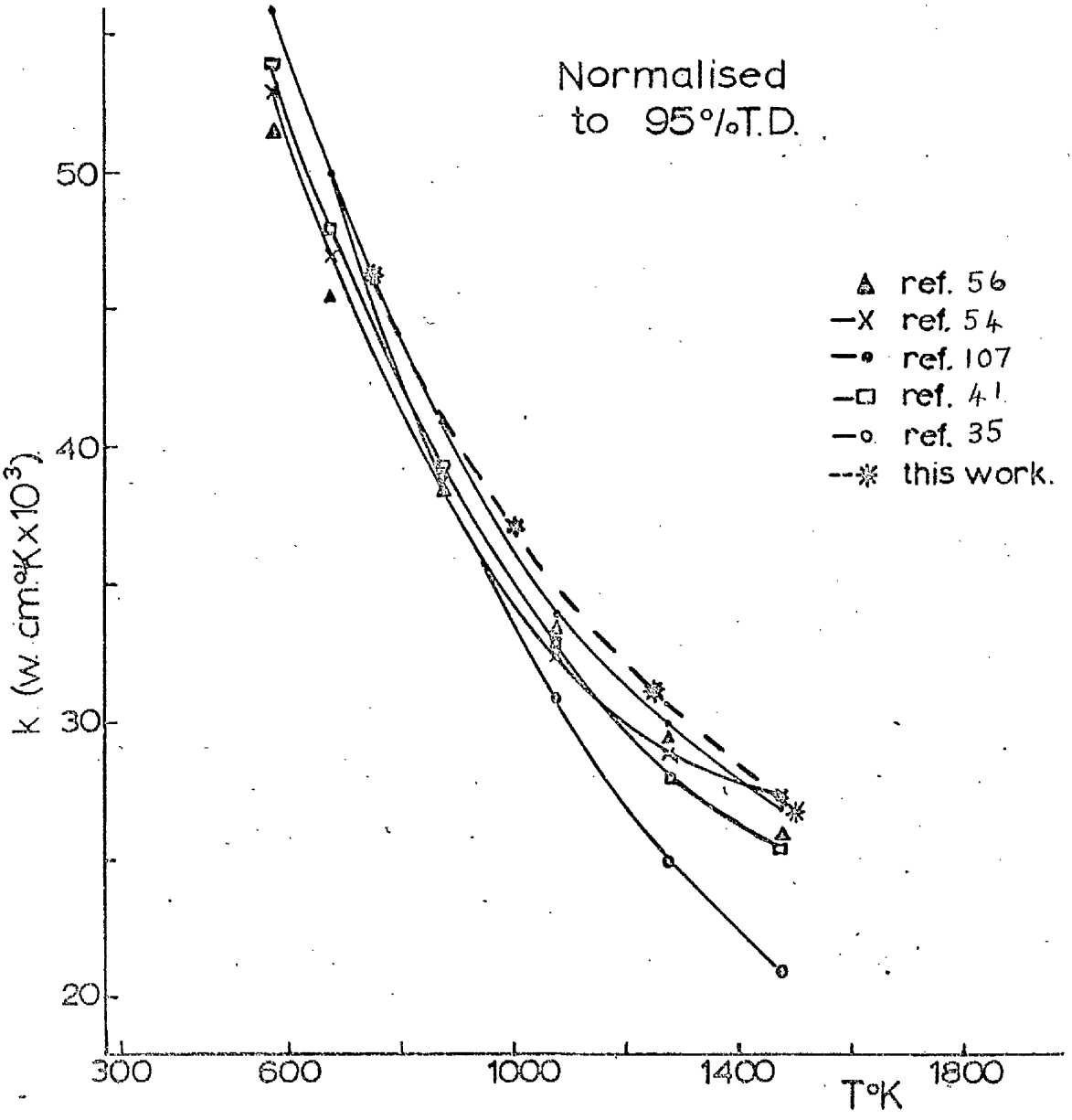

FIG. 7.05. K Data for UO_2
(normalised to 95%T.D (38)).

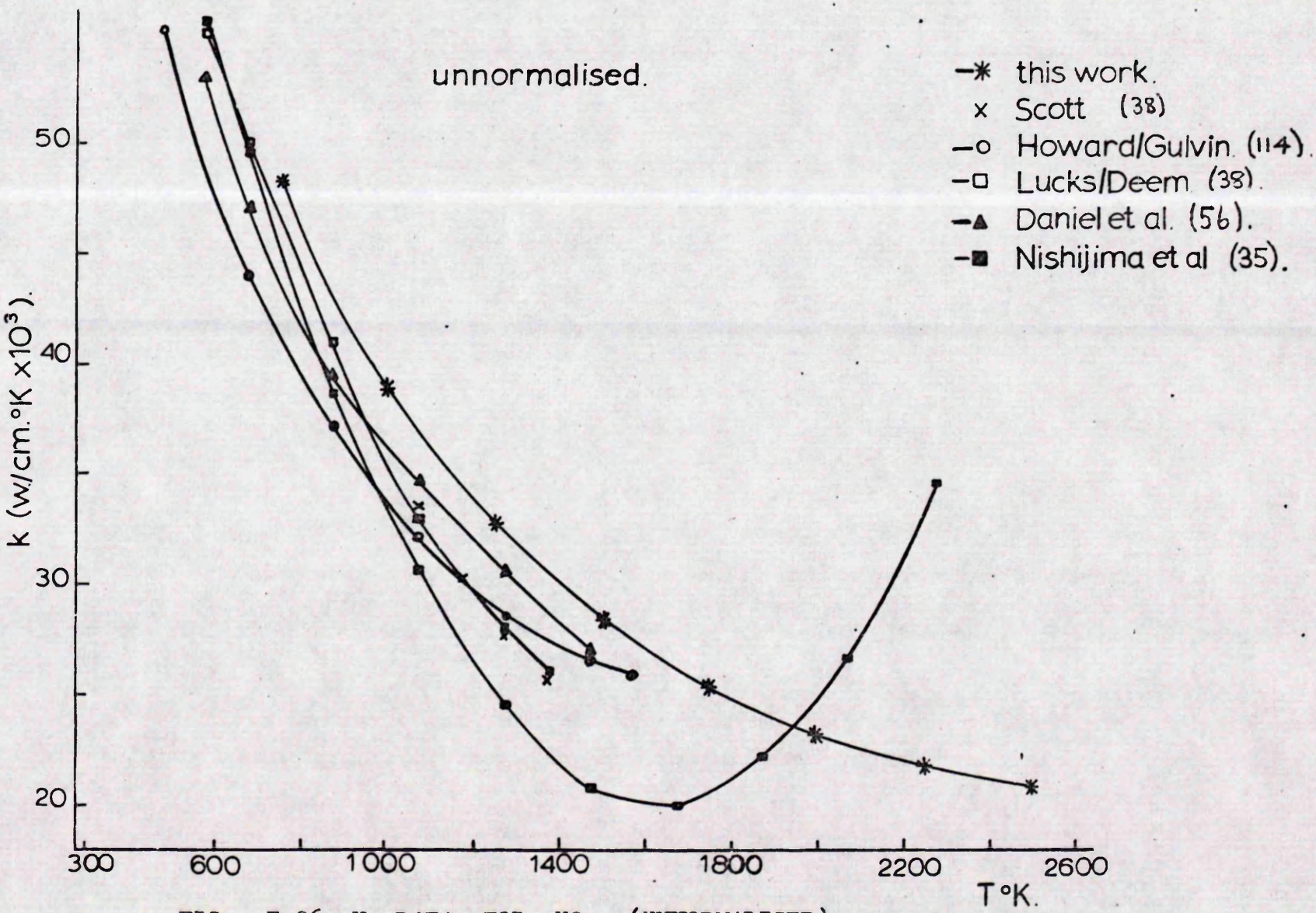

FIG. 7.06. K DATA FOR UO_2 (UNNORMALISED).

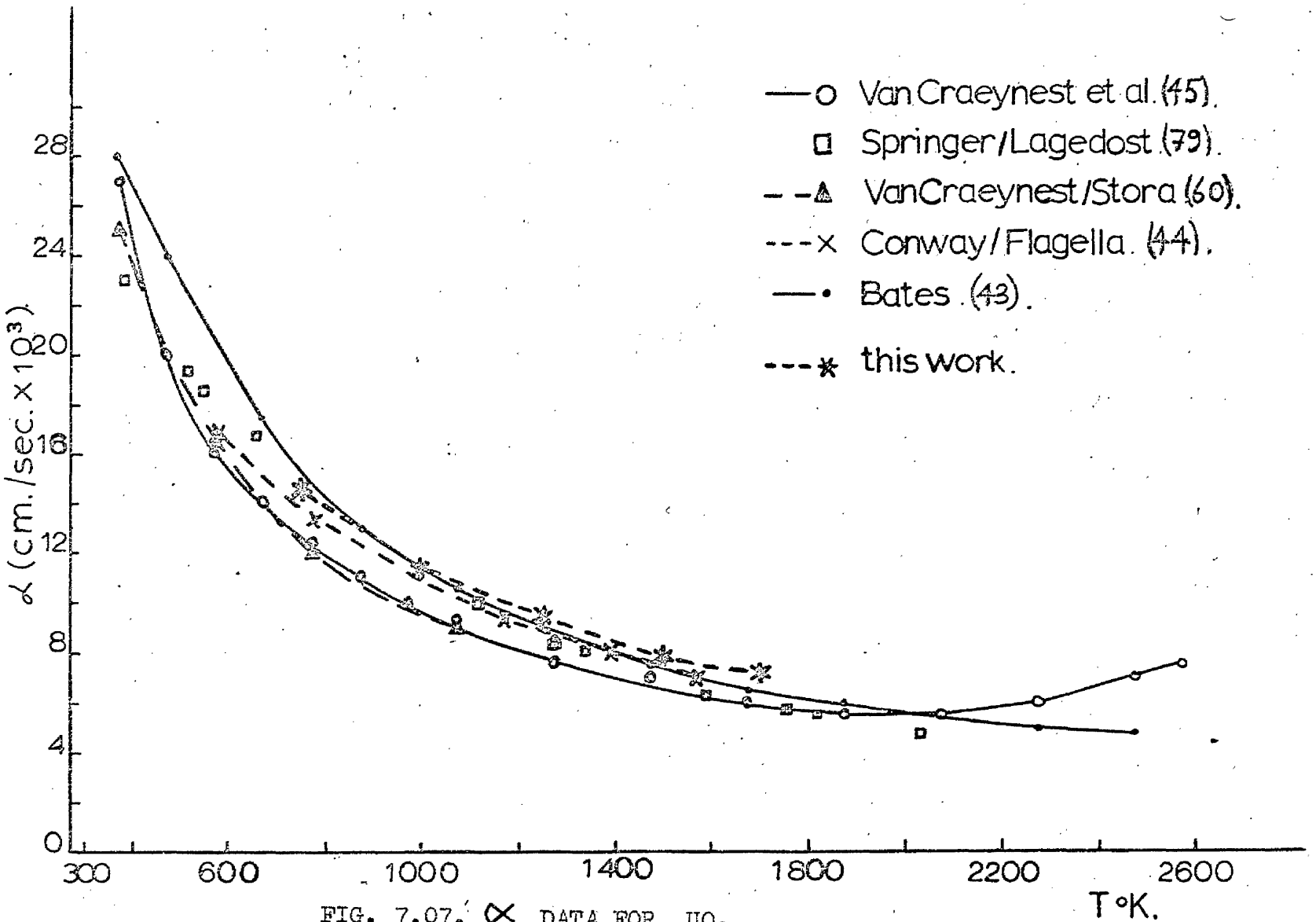

FIG. 7.07. α DATA FOR UO_2.

d) Comparison of $'A'_{100}$ and $'B'_{100}$ with the Single Crystal Values

The values for $'A'_{100}$ and $'B'_{100}$ would be expected to be similar to the values of 'A' and 'B' given for the single crystal table 7.I. One would expect the 'A' value of the single crystal to be small if not equal to zero since the only contribution to the resistivity should be from impurities. The value of 'A' is negative, a factor which has been observed by other workers (Taylor (108) for beryllia, Stuckes (109) for germanium) and which has been indicated as a possibility for insulators by Godfrey et al (41) and Fulkerson et al (110).

The 'B' value should be the same as for $'B'_{100}$, but this is not so as can be seen from table 7.I. The reason for the higher 'B' value of the single crystal is not clear, but it is thought to reflect the uncertainty in the experimental data of the single crystal, i.e. during measurement, difficulties were encountered in aligning the optics so that the laser hit the very small single crystal and also so that the detector focussed on the rear face. The latter proved time consuming rather than difficult since it entailed opening up the vacuum/pressure vessel each time any misalignment was observed.

A value for the Debye temperature (Θ_D) can be obtained using the equation given by Godfrey et al (41)

$$\text{i.e. } R_u \simeq \frac{T}{k_o \cdot \Theta_D} - \frac{1}{k_o \cdot b} \equiv (BT - A') \qquad (7.17)$$

where R_u is the thermal resistivity due to U-process only, k_o is the conductivity extrapolated to zero (Θ_D), and 'b' is an empirical constant.

By comparison with equation 7.01

$$1/k_{total} = R_{total} = R_u + A \qquad (7.18)$$

i.e. $$R_{total} = (BT - A') + A \qquad (7.19)$$

where $B = \frac{1}{k_{\Theta_D}\,\Theta_D}$ from equation 7.17 (7.20)

Using $B = .0226\ (w/cm)^{-1}$ for the single crystal, a value of $\Theta_D = 212^oK$ was obtained using Leibfried/Schlomann's (7) equation (see equation 7.24).

Now from equation 7.17

$$A' = \frac{1}{k_{\Theta_D} \cdot b} = \frac{B\Theta_D}{b} \qquad (7.21)$$

$\therefore$ Using a maximum 'b' of 2 (ref. Ziman (6))

then $A' = 2.40\ (w/cm^oK)^{-1}$

But $(-A' + A) = -1.36\ (w/cm^oK)^{-1}$

$$\therefore\ A = 1.04\ (w/cm^oK)^{-1} \qquad (7.22)$$

i.e. the thermal resistance due to porosity and impurities, including any deviation from stoichiometry, for the single crystal is $1.04\ (w/cm^oK)^{-1}$. The difference between this value and that calculated for 100% T.D. should be the resistivity due to grain boundaries and/or impurities, i.e. $3.61\ (w/cm^oK)^{-1}$

The actual values for the single crystal are much higher than those for the polycrystalline material, being $\sim$ 30% higher than the 96 specimens at 700^oK; $\sim$10% higher at 1400^oK and $\sim$ 9% at 1800^oK. There is a tendency for the results to level out around 1800 to 1900^oK. This does not agree with the results obtained by Daniel et al (56) who observed large enhancement of the conductivity above 1200^oK. They gave

$$k_m = (0.03203 + \frac{17.9}{T} + 1.2 \times 10^{-15} T^{4.2}) \quad (w/cm^oK) \qquad (7.23)$$

Their values were ~ 25% higher than their polycrystalline values at 700°K and ~ 160% higher at 1400°K.

e) B_{100} , Θ_D , λ_u

It was possible using the value of B_{100} to calculate a Debye temperature for UO_2 . Using the Leibfried/Schlömann (7) equation for three phonon Umklapp processes:

$$B = \frac{\gamma^2}{3.45 \times M . \delta . \Theta_D^3} \qquad (7.24)$$

where γ is Grüneisen's constant which for UO_2 equals 1.64 ,

M is the average mass/atom which for UO_2 equals 1.494×10^{-22} g/atom ,

δ^3 is the average volume/atom which for UO_2 equals 1.37×10^{-23} cm^3/atom ,

Θ_D is the Debye temperature.

This equation reduces to

$$B = \frac{0.2181 \times 10^6}{\Theta_D^3} \quad (cm\,^oK^3/w) \qquad (7.25)$$

Using B_{100} = .0201 $(w/cm)^{-1}$ for the calculated value for 100% T.D., a value of Θ_D = 221°K was obtained. This is in reasonable agreement with other workers: Ainscough/Wheeler (111) obtained 213°K using B = .0227 $(w/cm)^{-1}$, and Godfrey et al (41) gave 216°K using B = .0223 $(w/cm)^{-1}$. The value obtained here lies well within the range of Θ_D values quoted i.e. 160°K to 300°K, although most workers tend to give values around 180°K to 190°K.

Further to the above analysis it was possible to obtain the meanfree path of Umklapp processes (l_u) using the relationships:

$$1/k = R = A + BT = \frac{3}{C_v v}\left(\frac{1}{l}\right) \qquad (7.26)$$

which yields $BT = \frac{3}{C_v v}\left(1/l_u\right)$ (7.27)

Thus $l_u = \frac{3}{C_v \, v \, BT}$ (7.28)

Ainscough/Wheeler (111) give

$$\lambda_u = l_u V \qquad (7.29)$$

where λ_u is the wavelength of the Umclapp process, and V is the molar volume = 24.6 cm^3/mole at 300°K.

$$\therefore \lambda_u = \frac{3V}{C_v \, v \, BT} \qquad (7.30)$$

Using the values of Godfrey et al (41) of C_v = 81.6 w.sec/mole °K and v = 4 x 10^5 cm/sec., with B_{100} = .0201 $(w/cm)^{-1}$ for B_{100}

then $\lambda_u = \frac{11.25 \times 10^{-5}}{T}$ cm°K (7.31)

i.e. at 1000°K $\lambda_u = 11.25 \times 10^{-8}$ cm. (7.32)

at 2000°K $\lambda_u = 5.63 \times 10^{-8}$ cm. (7.33)

Ainscough/Wheeler (111) gave 9.3 x 10^{-8}cm at 1000°K and 4.4 x 10^{-8}cm at 2000°K for UO_2 .

From Ainscough's curve fig. 4.02 chapter 4.b. an average C_p value of 0.30 w.sec./g.°K was taken for the range 800°K to 1800°K. Then using

$$C_v = C_p - \frac{V\alpha^2 T}{\chi} \qquad (7.34)$$

where α is the linear expansion coefficient = 10.5 x 10^{-6} $°K^{-1}$ and χ is the isothermal compressibility = 0.62 x 10^{-5} cm^3/w.sec.,

a value of C_v = 76.7 w.sec./mole °K was obtained.

Since this value was within 6% of Godfrey et al's quoted value of 81.6 w.sec./mole °K, the latter was used for convenience and to facilitate quick comparisons with other authors who had

used these values.

f) Variation of k with T at high temperatures

An inspection of the results shows that whereas the equation $k = (A + BT)^{-1}$ seems to fit the results very well upto 1673°K, the full equation

$$k = (A + BT)^{-1} + CT^3 \qquad (7.35)$$

does not fit the results at very high temperatures. This equation assumes that any divergence from linearity in the plot of $^1/k$ against T is due to a radiation contribution (i.e. the CT^3 term). Since this did not fit at $T \geq 1700^oK$, it indicated that the original premise that conduction was solely by phonons and photons was wrong, and that another conduction mechanism must be operating at high temperatures. An attempt was made to calculate a more realistic fit to the observed data at $T > 1400^oK$ by observing the deviation (Δk) of the actual values from those calculated using $(A + BT)^{-1}$

i.e. $$\Delta k = k_m - (A + BT)^{-1} \qquad (7.36)$$

Two relationships were applied to these Δk values as follows:

i $$\Delta k = A_1 T^a \qquad (7.37a)$$

ii $$\Delta k = C_1 e^{n/T} \qquad (7.37b)$$

An examination of these equations gave the following empirical results:

i $\Delta k = A_1 T^a$ $\quad 4.8 \leq a \leq 10$

These values are much higher than the expected value of 3 for a radiation contribution, though Bates (34) suggested a T^{3+x}

term where X = 0.5 to 2.0 for his single crystal. Even so these values are higher than one may expect theoretically.

ii $\Delta k = e^{n/T}$ $n = -(1.8 \pm 0.5) \times 10^4$ (^oK)

There seems to be good theoretical grounds for expecting an exponential temperature dependence at high temperatures (see chapter 1.4).

The Δk values have been plotted in fig. 7.08 together with the values given by a CT^3 term and by a $C_1 e^{n/T}$ term. It can be seen that a CT^3 term is inadequate whereas the exponential term describes the results very well. It is felt, therefore, that equation 7.37b should be used to describe all of the high temperature thermal conductivity data.

In an attempt to define the heat transfer mechanism operating at high temperatures, a value for an electronic contribution (k_{el}) was calculated using the electrical conductivity equation of Bates et al (112)

i.e. $$\sigma = 3.569 \times 10^3 \exp.\left(\frac{-1.15}{kT}\right) \qquad (7.38)$$

together with equation 1.27

i.e. $$k_{el} = 2\left(\frac{k}{e}\right)^2 T\left(\sigma + \frac{2\sigma_n\sigma_p}{\sigma}\left(\frac{E_g}{2kT} + 2\right)^2\right)$$

with $E_g = 2.30$ eV (ref. 113) and $\sigma_p = \sigma_n$.

These calculated values of k_{el} have been plotted in fig. 7.08 and as can be seen they are about X2½ higher than the actual Δk values. This difference can be accounted for if instead of using $\sigma_n = \sigma_p$, one uses either $\sigma_n = 4\sigma_p$ or $\sigma_p = 4\sigma_n$. For this one must assume that there is an equal number of electrons (n_e) and holes (n_p), and that the mobilities (μ_e and

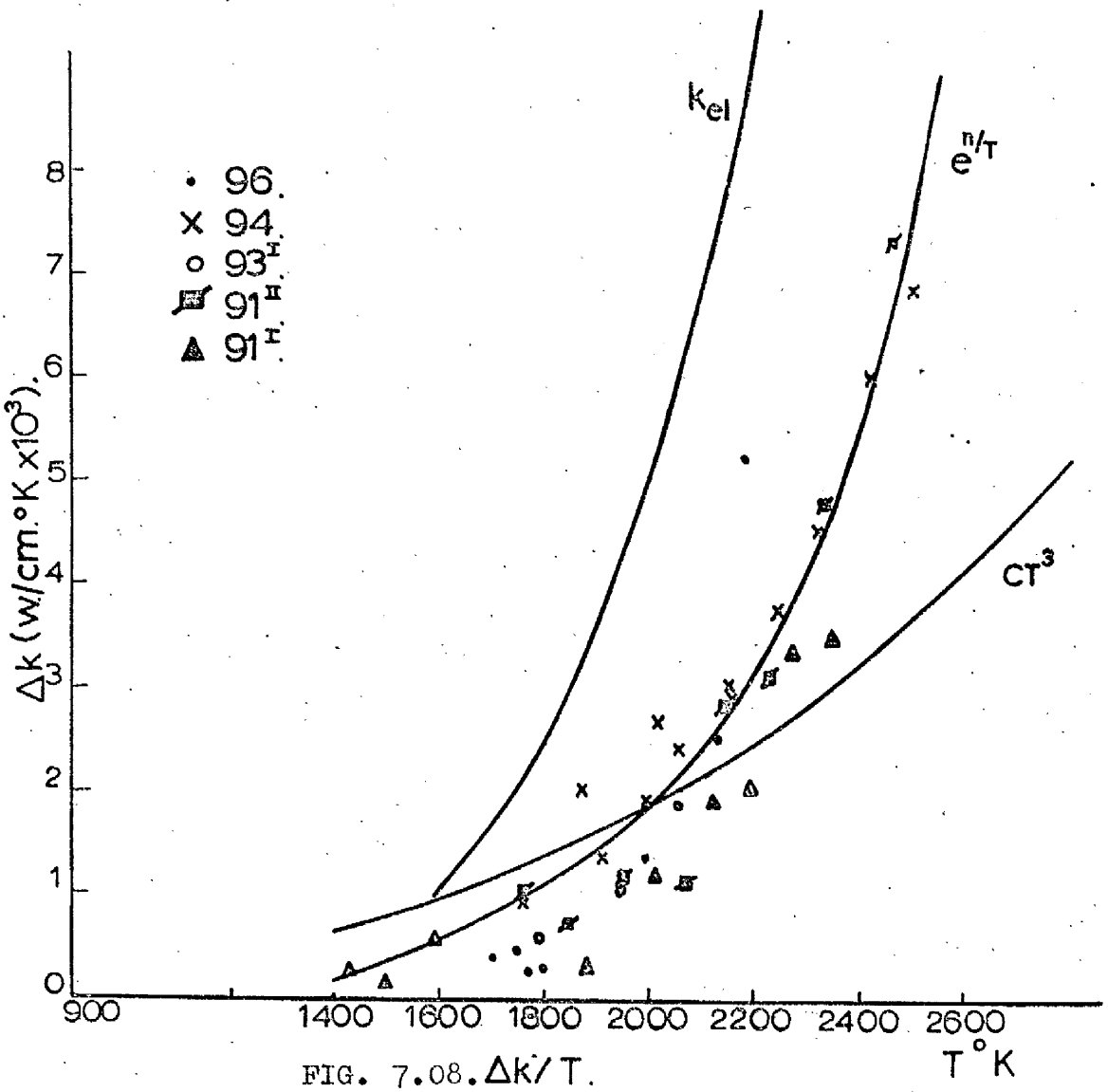

FIG. 7.08. $\Delta k / T$.

μ_p) differ by a factor of 4.

i.e. $n_e = n_p$

and $\mu_e = 4\mu_p$ or $\mu_p = 4\mu_e$

where $\sigma = e(n_e \mu_e + n_p \mu_p)$ (7.39)

Thus the deviation observed in the thermal conductivity data at high temperatures can be attributed to an electronic conductivity contribution, the activation energy of which is given by $n = E/k$ (7.40)

i.e. $E = 1.55$ eV (7.41)

Christensen (13) obtained $E \simeq 0.79$ eV theoretically for 800 - 2000°C, and Godfrey et al (41) gave $E = 0.45$ eV for 900 - 1100°C. Both values are much lower than the value observed here.

As discussed in an earlier chapter (1.4), several authors refer to any electronic contribution in an intrinsic semiconductor as an excitation conduction (k_{ex}). Using equation 1.01

i.e. $k_{total} = k_p + k_{el} + k_r + k_{ex}$

and the relationships

$$k_p \propto 1/T \quad (7.42)$$

$$k_{el} = 2(k/e)^2 T.\sigma, \quad (7.43)$$

$$k_r = \frac{16}{3} \frac{\sigma_s . n^2 . T^3}{\alpha}, \quad (7.44)$$

$$k_{ex} \propto e^{-E/kT} \quad (7.45)$$

(σ_s = Stefan Boltzmann's constant)

one can obtain a value for k_{ex}. Since k_{el} is negligible (at 2000°K $k_{el} \sim 10^{-5}$ w/cm.°K), then this gives

$$k_{total} - (k_p + k_r) = k_{ex} \qquad (7.46)$$

$$\text{i.e.} \quad \Delta k - k_r = k_{ex} \qquad (7.47)$$

The values of Δk lie between 0.03×10^{-3} and 6.00×10^{-3} w/cm.^{o}K over the temperature range 1600 - 2400^{o}K. The values of k_r depend on the values of 'α' and 'n' used, and consequently published values of k_r differ quite markedly. Those of Mogard et al (36) and Bates (34) are much larger than the Δk values, and cannot, therefore, be used in this analysis. However, the values quoted by Christensen (13), being much lower above 1400^{o}K, did enable k_{ex} to be obtained for 2000 - 2400^{o}K. A plot of ln k_{ex} against $^{1}/T$ should give the activation energy, and an approximate value of E = 0.35 eV was obtained. Bates (34) using this analysis and his k_r values obtained a value of E of 0.83 eV for single crystal UO_2 . Similarly, Whitmore (22) gave values of E $<$ 1 eV for TiO_2 , CaF_2 and Al_2O_3, and he postulated that the excitation conduction was by excitons.

The above analysis is only a guide, and more work is required, especially to obtain more exact k_r values from more accurately defined 'α' and 'n' values. Even so, it does indicate that another heat transfer mechanism is operating at high temperatures which yields an electronic contribution.

To complete this investigation into the cause for this exponential divergency, it is necessary to mention whether it could be related to oxygen loss at high temperatures, for as will be shown in the next section (7.2) any decrease in the $^{o}/u$ ratio increases the conductivity considerably. If the specimens had lost oxygen then they would have gone hypostoichiometric - a fact that could not be detected by the $^{o}/u$ analysis but should be detected in subsequent low temperature measurements. The I.A.E.A. panel (104) report that there has been some

confusion over the behaviour of UO_2 above 1800°C. For the reaction

$$<UO_2> = <UO_{2-x}> + \tfrac{1}{2}x\ (O_2)$$

there must be a low partial pressure of oxygen, and the vaporisation of UO_2 must not be predominant. It was felt by Rothwell (113) that this reaction may occur below 1800°C but that the metallic uranium inclusions would be too fine to be detected - he had difficulty detecting those inclusions above 1800°C since they were less than 2μ. He suggested that for low partial pressures of oxygen above the UO_2 and at $T > 1800$°C the UO_2 would lose oxygen and become hypostoichiometric. On cooling it would revert to stoichiometric oxide with metallic uranium - nucleated at grain boundaries or by impurities. The conditions under test in this thesis would suggest that vaporisation of UO_2 was the predominant process (113), and that if metallic uranium was detected then it could just be due to the presence of carbon either from the surroundings (carbon susceptor) or from the remains of any binder used prior to sintering. An examination of the specimens did not reveal any uranium inclusions, although in a couple of specimens there were a few bright orange inclusions $\sim 2\mu$. These were too small to be accurately analysed using the electron probe, whose beam $\sim 1\mu$.

Therefore, in the absence of any observed free uranium metal and of any evidence of higher conductivities on subsequent measurement at low temperatures, this exponential divergence from the linear $k \propto 1/T$ at high temperatures must be due to some additional heat transfer mechanism which is some electronic mechanism involving excited electrons and holes. Further work involving the use of a computer analysis would be required,

before one could draw any definite conclusions as to the most accurate curve form or the actual mechanism operating. A more detailed analysis of the exciton and ambipolar mechanisms within polycrystalline uranium dioxide including activation energies and temperature dependencies would also be of use.

2) Effect of Non-Stoichiometry

a) Variation of k with $^{O}/_{u}$ ratio

Comparison graphs were drawn showing the effect of $^{O}/_{u}$ ratio on the conductivities of 96 and 93^{I} specimens. Both curves are given in fig. 7.09a and fig. 7.09b. These curves tend to converge and actually cross over with the 96 showing cross over at $\sim 1800^{\circ}K$ and the 93^{I} at $\sim 1600^{\circ}K$. This is discussed in the next section (b).

Any alteration in the oxygen content has a large effect on the conductivity, and this fact has been well documented (ref. 1). A plot of conductivity against oxygen/uranium ratio is given in fig. 7.10 from which comparisons with other workers have been made. Godfrey et al (41) show a 5% decrease in conductivity at $673^{\circ}K$ for a change in $^{O}/_{u}$ ratio of 2.006 to 2.012, whereas Goldsmith/Douglas (59) gave a 7% reduction for the same change. Fig. 7.10 shows that for this range at $750^{\circ}K$ a reduction of 7% and 10% occur in conductivity values of the 96 and the 93^{I} respectively. For the change $^{O}/_{u} = 2.00$ to 2.060 at $750^{\circ}K$ there is 100% reduction for both 96 and 93^{I} compared to $\sim$ 60% observed by Goldsmith/Douglas, and at $1000^{\circ}K$ a reduction of $\sim$ 66% compared to $\sim$ 54% for Goldsmith/Douglas. The latter show k to be independent of temperature for an $^{O}/_{u}$ 2.13, similarly Howard/Gulvin (114) found this to be so for $^{O}/_{u} = 2.18$ and $^{O}/_{u} = 2.13$. No such conclusions are possible from fig. 7.10.

b) Variation of k with T

The results show a similar tendency to those of the specimens discussed in section 1, i.e. a decreasing conduct-

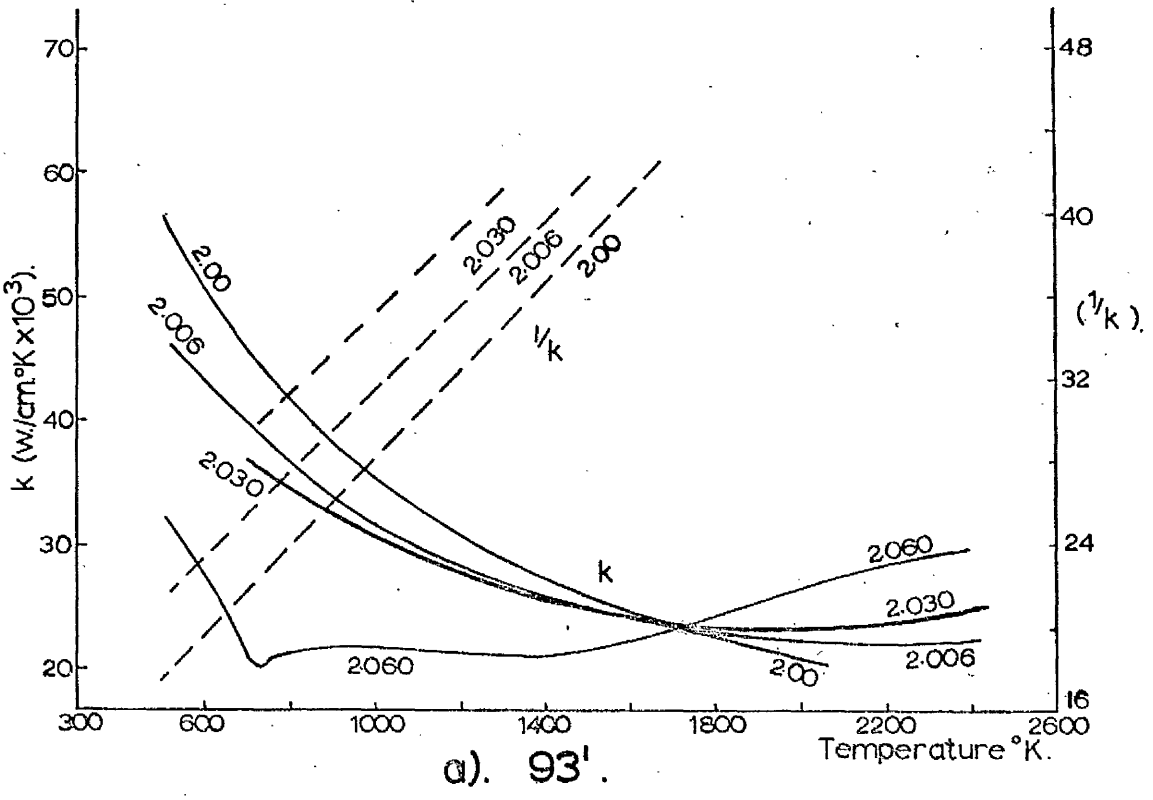

a). 93'.

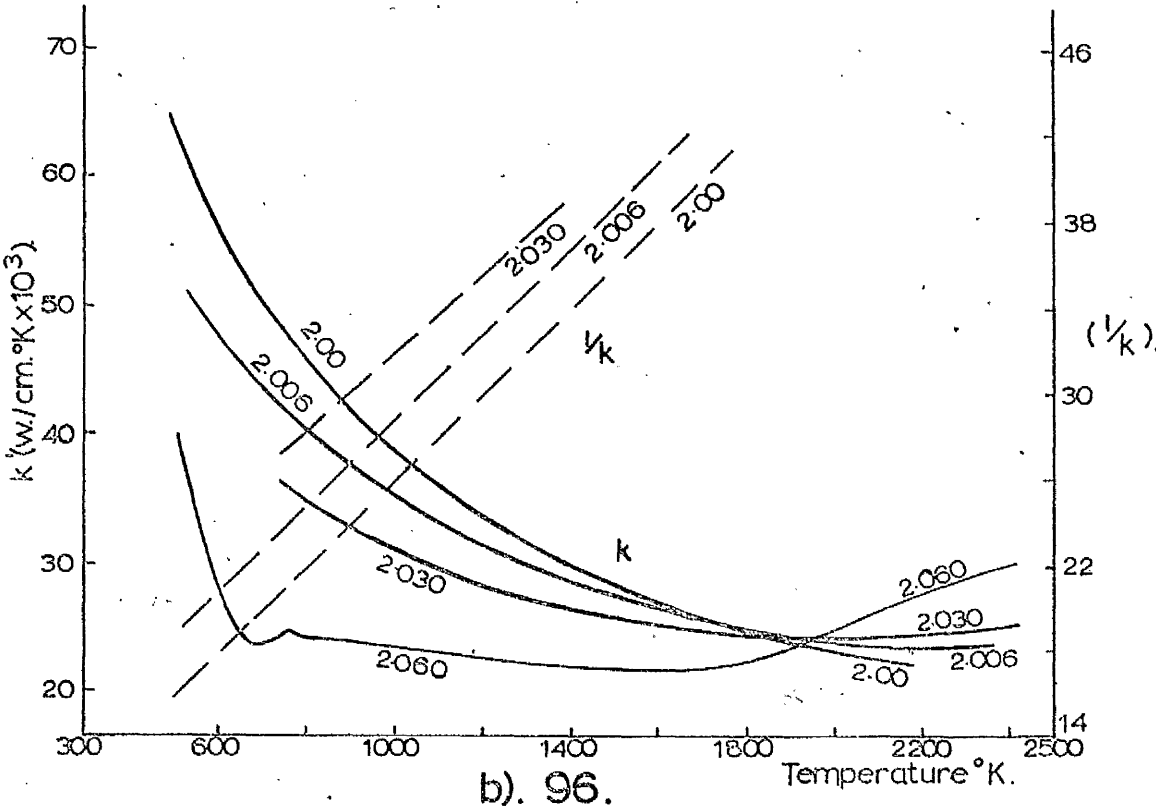

b). 96.

FIG. 7·09. Variation of K with $^{O}/_{u}$ Ratio.

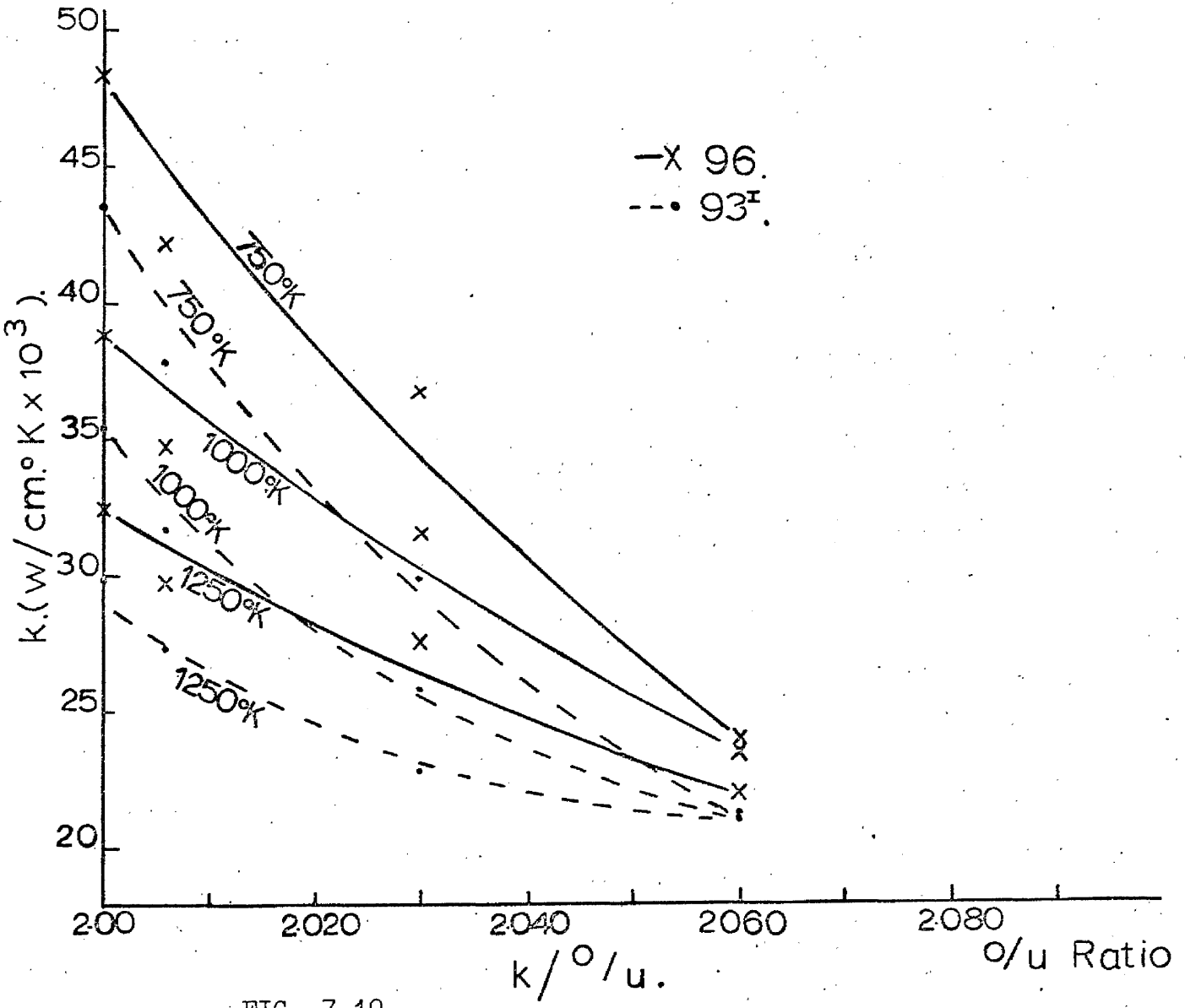
50
45
40
35
30
25
20
k.(w/cm.°K x 10³).
—X 96.
--• 93ᴵ.
750°K
750°K
1000°K
1000°K
1250°K
1250°K
200
2020
2040
2060
2080
k/°/u.
°/u Ratio

FIG. 7.10.

ivity with increasing temperature. Both the k and $^{1}/_{k}$ curves for 96 and 93[I] with $^{O}/_{u}$ ratios of 2.030 and 2.060 show changes in slope between 700 - 800°K, and when one examines the phase diagram (shown in fig. 7.11) for UO_2 , it can be seen that there is a phase change equivalent to the reaction

$$UO_{2+x} + U_4O_{9-y} \longrightarrow UO_{2+x}$$

is occurring.

For an $^{O}/_{u}$ ratio of 2.030 this phase change occurs at about 700°K, and for $^{O}/_{u}$ = 2.060 at about 750°K. It can be taken

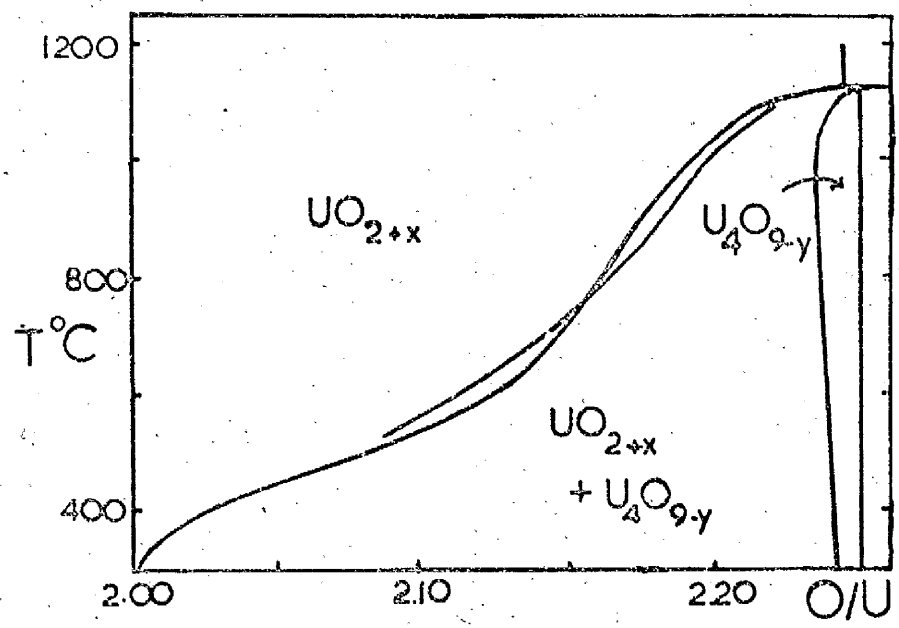

FIG. 7.11. Phase Diagram (after I.A.E.A. (104)).

that the values of conductivity obtained below 700°K are values obtained from a two phase material; i.e. a material with a UO_2 matrix containing interstial oxygen which is randomnly distributed in some areas (UO_{2+x}) and ordered in other areas (U_4O_{9-y}). The continued addition of oxygen in the UO_2 matrix upto $^{O}/_{u}$ = 2.25 leads to long range ordering. For a fuller analysis of

the k values in this region more results at temperatures below 700°K would be required.

The results for the temperature ranges quoted fit the equation $k = (A + BT)^{-1}$ quite well. However, above the linearity region, the non-stoichiometric specimens almost certainly lose oxygen, and probably they lose all of their excess oxygen. Evidence of this loss of oxygen is found in the post-test stoichiometric analysis, and also in the tendency for the cooling cycle for 96 2.060 and 93^{I} 2.060 to approach the values for 96 and 93^{I} respectively.

At high temperatures the curves in fig. 7.09a and fig. 7.09b show convergency and cross over: the 96 show cross over at $\sim$ 1800°K; the 93^{I} at $\sim$ 1600°K. Thus at high temperatures the non-stoichiometric specimens show k values above those of the original stoichiometric material with k 2.060 > k 2.030 > k 2.006 > k 200. It is difficult to obtain an exact explanation for this, although the answer may lie in the use of the wrong C_p data, i.e. too high a C_p value may be being used when in fact the oxygen content of the specimen at a certain temperature demands the use of lower C_p data. Furthermore there is the uncertainty in the calculated C_p data used for the different $^{o}/_{u}$ ratios. These two factors may be conspiring to give too high k values for the non-stoichiometric specimens. Evidence for this may be found in the fact that whereas the k values cross over; the 'α' values tend to merge at high temperatures. The position is further complicated if a photon or an electronic contribution is just becoming significant as the $^{o}/_{u}$ ratio begins to decrease. Evidence of such a contribution

may be found in the fact that, though the same C_p data was used for $^{O}/_{u}$ ratios of 2.00 and 2.006, k 2.06 $\geq$ k 2.00 at high temperatures.

To enable one to suggest the actual mechanism(s) occurring at high temperatures, one would need to observe the rate of loss of oxygen with temperature. A possible method for continuous measurement of the oxygen content has been used by Bates (43), who used a solid electrolyte oxygen meter to continually measure the water and oxygen content of his argon atmosphere. He also determined the impurities with his argon spectrographically. This has the draw back that it would require a flowing - gas system, whereas the apparatus used in this investigation involved a closed system.

It is felt that the tendency for the conductivity curves to converge at high temperatures is due to the loss of oxygen and that an electronic contribution may also just becoming significant at high temperatures.

c) A, $\bar{\sigma}_{O^=}$, $\bar{\sigma}_{i}$.

When one examines the relationship between the 'A' values for the non-stoichiometric specimens and their $^{O}/_{u}$ ratio, it should be possible to calculate a phonon scattering cross section for the excess oxygen ions ($\bar{\sigma}_{O^=}$). Several authors have obtained a value for $\bar{\sigma}_{O^=}$ including Goldsmith/Douglas (59) and Godfrey et al (41). Before this can be done, it is necessary to obtain 'A' values for the 2.060 specimens, which were not given a regression analysis as stated in chapter 6.3. In extrapolating the $^{1}/_{k}$ results from above 700°K to room temperature the following values were obtained

'A' for 96 2.060 = 33.50 $(w/cm^{o}K)^{-1}$ (7.48a)

'A' for 93^{I} 2.060 = 40.80 $(w/cm^{o}K)^{-1}$ (7.48b)

and these have been quoted in table 7.I. It must be remembered that these extrapolated values will correspond to 'A' values for a single phase material (UO_{2+x}). These values were used along with a least squares analysis to obtain the relationships between 'A' and excess oxygen content given by

$$A_{96} = 4.64 + 446x \quad (w/cm^{o}K)^{-1} \quad (7.49a)$$

$$A_{93^{I}} = 5.41 + 526x \quad (w/cm^{o}K)^{-1} \quad (7.49b)$$

where $x = {}^{o}/_{u} - 2.00$

There is some doubt as to the validity of this analysis since i there is considerable uncertainty in the extrapolated values as the region from which they are extrapolated is seen to be very irregular (figs. 6.20b, 6.26b chapter 6.3), and ii it is uncertain upto what concentration of excess O = ions a linear relationship is applicable, since this analysis assumes that the excess O ions are acting as independent scattering centres even upto a concentration of 3% (i.e. ${}^{o}/_{u} = 2.060$). In fact these excess ions may not be acting independently, thus their scattering power may be reduced as their concentration increases (cf. other solid - solutions where linear relationships apply only upto small concentrations). Thus it may be more accurate to apply a linear relationship only for the range ${}^{o}/_{u} = 2.00$ to ${}^{o}/_{u} = 2.006$.

However, it is felt that this analysis will yield some useful parameters for comparison with Goldsmith/Douglas (59) who gave

$$A_{96} = 1.9 + 351x \qquad (w/cm^{o}K)^{-1} \qquad (7.50)$$

This equation and equations 7.48a and b have been plotted in fig. 7.12.

An increase in 'A' with $^{o}/_{u}$ is to be expected, assuming all other factors to be the same, since the increase in the number of oxygen ions will cause a corresponding increase in the number of phonon - impurity interactions. Godfrey et al (41) gave $A = 5.1\ (w/cm^{o}K)^{-1}$ as the average of their A values for $^{o}/_{u} = 2.01$; Goldsmith/Douglas gave $A = 5.4\ (w/cm^{o}K)^{-1}$ for the same ratio, whereas fig. 7.12 shows $A = 8.8\ (w/cm^{o}K)^{-1}$. The value in this investigation is on the high side therefore, the difference between $'A'_{96}$ and $'A'_{93}$ will be due to the differences in porosity, grain size and impurity content between them. From fig. 7.12 the thermal resistance due to grain size, porosity and all impurities other than excess oxygen ions will be the value of 'A' at $^{o}/_{u} = 2.00$, i.e. zero excess oxygen concentration. These values are $4.64\ (w/cm^{o}K)^{-1}$ for 96 and $5.41\ (w/cm^{o}K)^{-1}$ for 93^{I}. An average phonon scattering cross section can be calculated for the excess oxygen ions ($\bar{\sigma}_{o=}$). Using equation 7.26

$$k = {}^{1}/_{k} = (A + BT)^{-1} = \tfrac{1}{3} C_{v} \bar{v} \bar{l}$$

$$\text{and} \quad {}^{1}/_{l} = \Sigma\ \bar{\sigma}_{I} N_{I} \qquad (7.51)$$

where $\bar{\sigma}_{I}$ is the average phonon scattering cross section due to the I^{th} type impurity, and N_{I} is the concentration of that impurity.

$$\therefore\ A = \frac{3}{C_{v} v} \left(\bar{\sigma}_{o=} N_{o=} + \bar{\sigma}_{i} N_{i} \right) \qquad (7.52)$$

where excess oxygen and other impurities have been separated.

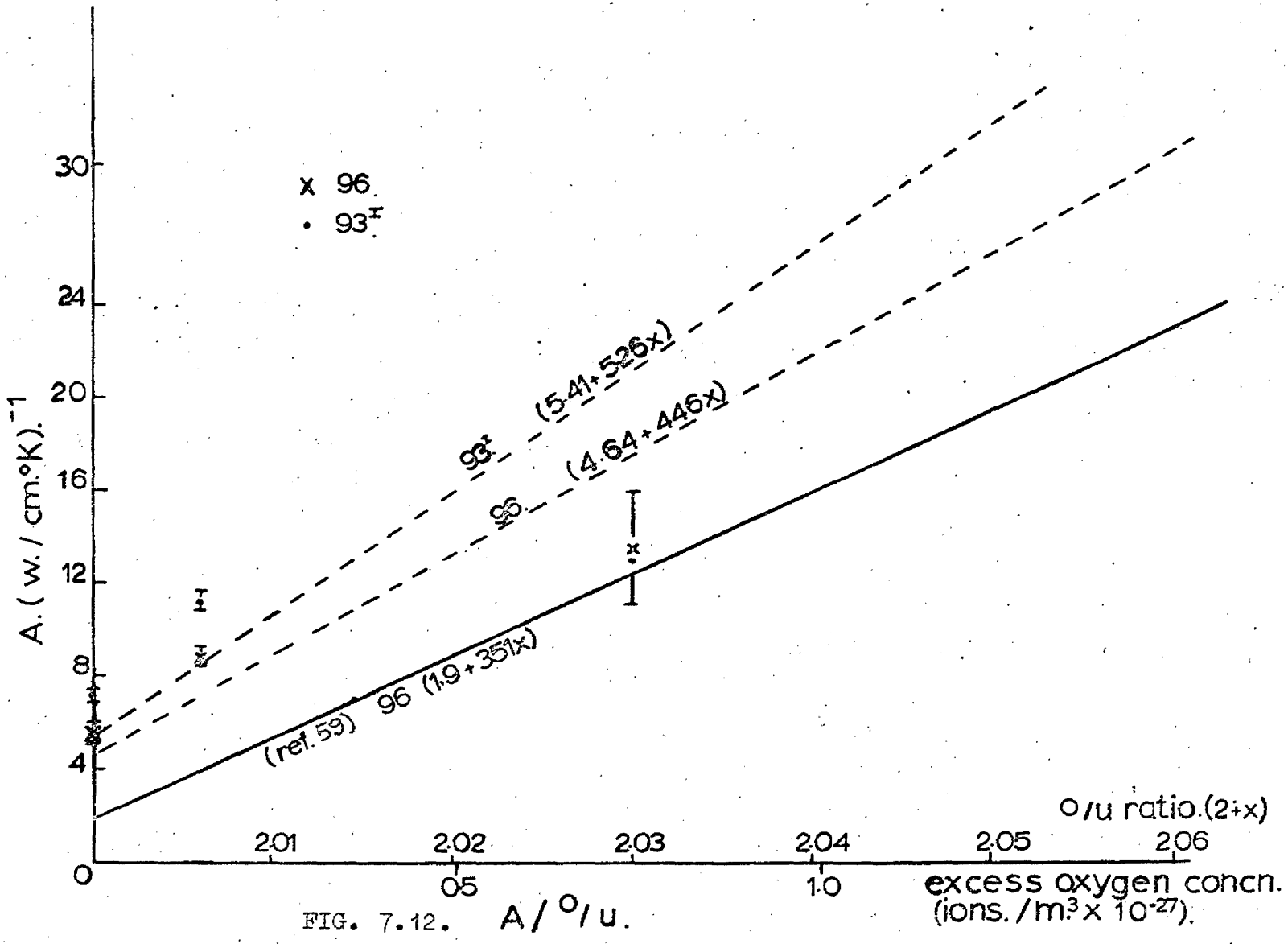
A. (w. / cm.°K).⁻¹
30
24
20
16
12
8
4
0
X 96.
• 93ᵀ
93ᵀ (5.41+.526x)
96 (4.64+.446x)
(ref. 59) 96 (1.9+.351x)
2.01
2.02
2.03
2.04
2.05
2.06
O/u ratio.(2+x)
.05
1.0
A / O/u.
excess oxygen concn.
(ions./m³ x 10⁻²⁷).

FIG. 7.12.

Assuming N_i (impurity concentration) to be constant, and differentiating with respect to $N_{o=}$ equation 7.52 yields:

$$\frac{dA}{dN} = \frac{3}{C_v . v} . \bar{\sigma}_{o=} \qquad (7.53)$$

Using the values quoted by Godfrey et al (41) of $C_v = 81.6$ w. sec/mole ^oK and $v = 4 \times 10^5$ cm/sec., this equation reduces to

$$\frac{dA}{dN} = 2.28 \times 10^{-6} . \bar{\sigma}_{o=} \quad (w/cm^2\ ^oK)^{-1} \qquad (7.54)$$

From fig. 7.12

$$\frac{dA}{dN} = \begin{cases} 17.49 \times 10^{-21} & (w/cm^4\ ^oK)^{-1} \text{ for } 96_I \quad (7.55a) \\ 21.18 \times 10^{-21} & (w/cm^4\ ^oK)^{-1} \text{ for } 93^I \quad (7.55b) \end{cases}$$

Thus $\bar{\sigma}_{o=} = 7.67 \times 10^{-15}$ cm^2 for 96 (7.56a)

$= 9.29 \times 10^{-15}$ cm^2 for 93^I (7.56b)

These can be compared to :

Goldsmith/Douglas (59) $\bar{\sigma}_{o=} = 6.3 \times 10^{-15}$ cm^2

and Godfrey et al (41) $\bar{\sigma}_{o=} = 6.02 \times 10^{-15}$ cm^2

The agreement is, therefore, quite good, and could probably have been improved depending on the extrapolated values for the 2.060 specimens being more accurately obtained, i.e. more k measurements above 700^{o}K.

From equation 7.52 a phonon scattering cross section for impurities ($\bar{\sigma}_i$) can be calculated; i.e. by putting $N_{o=} = 0$ and using $A_{96} = 4.64$ (w/cm^{o}K)$^{-1}$, N_i is 177ppm., which is equivalent to 4.32×10^{18} impurities/cm^3.

$$\therefore \quad \bar{\sigma}_i = 4.64/ (2.28)(4.32)(10^{12}) \qquad (7.57)$$

$$= 4.71 \times 10^{-13} \text{ cm}^2 \text{ for } 96$$

(compared with $\bar{\sigma}_{o=} = 7.67 \times 10^{-15}$ cm^2)

For 93^I, $N_i = 484$ppm $= 1.18 \times 10^{19}$ imps./cm^3, $A_{93^I} = 5.41$ (w/cm^{o}K)$^{-1}$ and $\bar{\sigma}_i = 2.01 \times 10^{-13}$ cm^2.

This last analysis is not strictly defined since no account of scattering by factors such as grain boundaries, porosity or point defects has been considered, i.e. the 'A' values used have been said to be due solely to impurity scattering. However, it is a useful guide in that, although the scattering due to impurities has been overestimated, such scattering is still seen to be less effective than that due to the introduction of excess interstial oxygen ions.

d) Variation of B with $^{O}/_{u}$ ratio

An examination of the 'B' values for the non-stoichiometric specimens (table 7.I), shows them to decrease slightly with increasing $^{O}/_{u}$ ratio. Goldsmith/Douglas (59) observed this effect and predicted B = 0 at $^{O}/_{u} \simeq 2.13$, a fact that makes k independent of temperature for specimens with $^{O}/_{u}$ ratios of this value. No such extrapolations are possible from the data in table 7.I, there being insufficient data points and none above an $^{O}/_{u}$ ratio of 2.030 (see fig. 7.13).

The reason for these 'B' values being lower than those for the specimens of varied densities may be due to the use of different specific heat curves (chapter 4.b),

$$\text{i.e.} \quad BT = \frac{3}{C_v v}\left(\frac{1}{l_u}\right) \tag{7.58}$$

$$\therefore (B)p.(T).(C_v)p.(v)p.(l_u)p. = (B)o/_u.(T).(C_v)o/_u.(v)o/_u.(l_u)o/_u \tag{7.59}$$

where the suffixes '$^{O}/_{u}$' and 'p' represent the non-stoichiometric and varied density specimens respectively. Assuming v and l_u to be constant for all porosity and excess oxygen concentrations

$$\text{then} \quad (C_v)p.(B)p = (C_v)o/_u.(B)o/_u \tag{7.60}$$

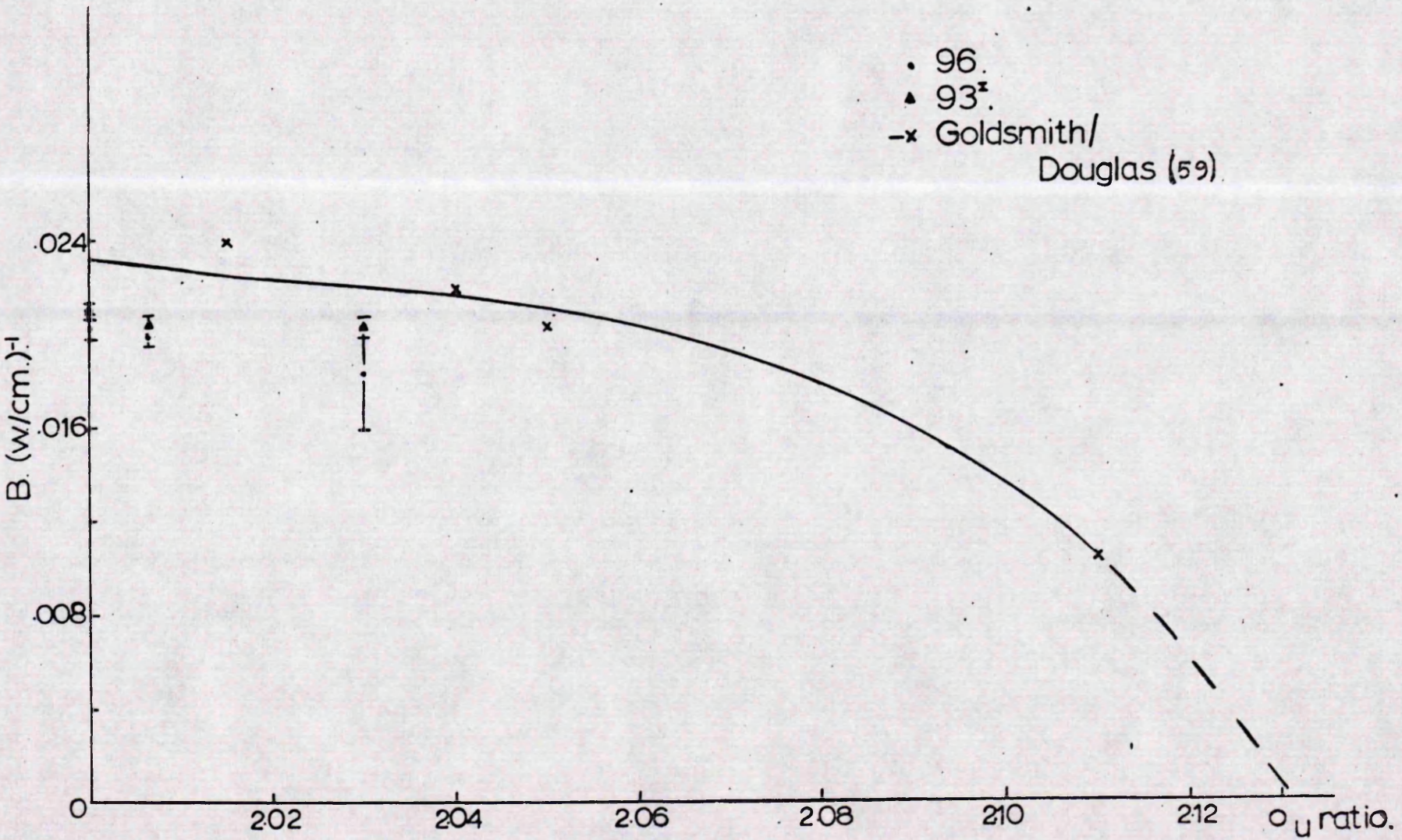
• 96.
▲ 93ˣ.
–x Goldsmith/
Douglas (59)
B. (w./cm.)⁻¹
.024
.016
.008
0
202
204
206
208
210
212
O/U ratio.

FIG. 7.13. B / O/U.

The values used were

$$(C_p)o/_u \geq (C_p)p \tag{7.61}$$

and assuming $C_p \equiv C_v$ (7.62)

thus one would expect $(B)o/_u < (B)p$ (7.63)

Therefore, the difference in the B values may reflect the difference in the specific heat curves used.

CONCLUSIONS

Thermal diffusivity measurements were made between 500 - 2500°K on specimens of varying pore volume fractions, varying oxygen/uranium ratios and for a single crystal, using a laser - flash method that has been well characterised.

The effect of porosity

1) At low temperature conductivity is described by the equation

$$k = (A + BT)^{-1}$$

for $T < 1673^{\circ}K$, where conduction is predominantly by phonons. The values of 'A' and 'B' are related to the pore volume fraction (p) by the following equations

$$A = 6.16 + 30.54p \qquad (w/cm^{\circ}K)^{-1}$$

$$B = 0.0208 + 0.0140p \qquad (w/cm)^{-1}$$

where $p = \dfrac{\text{density 95\% T.D. - density of specimen}}{\text{density of 95\% T.D.}}$

2) Above 1673°K, the k deviates from the linear form given above, and an exponential term is required. Thus the complete equation for 500 - 2500°K is given by

$$k = (A + BT)^{-1} + Ce^{-n/T}$$

where $n = (1.8 \pm 0.5) \times 10^{4} \quad (^{\circ}K)$

This exponential term is related to an electronic conduction process with an activation energy of ~ 1.55 eV.

3) The effect of pore distribution has an important effect on k, i.e. pores on grain boundaries and at triple points have less thermal resistance than intergranular pores.

4) The thermal conductivity decreases with increasing pore volume fraction (p), and k and p are related by

$$k_m = k_{95} (1 - \beta p)$$

where $\beta = 2.46 - 0.70 \times 10^{-3} T \quad (T^oK)$

The temperature dependence of β was attributed to an increase in the concentration of microporosity with increasing pore volume fraction.

5) Values for k_{95} and k_{100} were calculated using the above value as follows :

$$k_{95} = (6.07 + 2.08 \times 10^{-2} T)^{-1} \quad w/cm^oK$$

$$k_{100} = (4.65 + 2.01 \times 10^{-2} T)^{-1} \quad w/cm^oK$$

for $T \leq 1600^oK$. These values agree well with other authors although they are slightly higher.

6) A Debye temperature θ_D of 212^oK was calculated for the single crystal ($B = .0226 (w/cm)^{-1}$), and $\theta_D = 221^oK$ for 100% T.D. material ($B = .0201 (w/cm)^{-1}$). Similarly the wavelength of U - processes was calculated as 11.25 - 5.63 Å for 1000 - 2000^oK.

The effect of non-stoichiometry

7) Enhancement of the thermal conductivity is observed at high temperatures for all non-stoichiometric specimens. This is due to the specimens losing oxygen and thus to the use of C_p values which are too high. It is felt that some electronic contribution may be occurring at the same time as oxygen is being lost.

8) In the equation $k = (A + BT)^{-1}$ the following relationships for 'A' were obtained

$A = 4.64 + 446x$ for the 96 batch

and $A = 5.41 + 526x$ for the 93$^{\text{I}}$ batch

where $x = {}^{O}/_{U}$ ratio $- 2$.

9) Mean phonon scattering cross sections were calculated for excess oxygen ions ($\bar{\sigma}_{O^=}$) and for other impurities ($\bar{\sigma}_i$) as follows

$\bar{\sigma}_{O^=} = 7.67 \times 10^{-15}$ cm^2 for the 96 batch
and 9.29×10^{-15} cm^2 for the 93^I batch

$\bar{\sigma}_i = 4.71 \times 10^{-13}$ cm^2 for 96 (N_i = 177ppm)
and 2.01×10^{-13} cm^2 for 93^I (N_i = 484ppm)

Thus scattering by excess oxygen ions is much larger than scattering by other impurity atoms.

SUGGESTIONS FOR FUTURE WORK

1) A more quantitative analysis is required relating the thermal resistivities of pores on grain boundaries and at triple points to those of intergranular pores.

2) More comprehensive cycling measurements should be made in order that any changes occurring in the specimen at high temperatures may be detected.

3) A wider range of pore volume fractions would enable more detailed analysis of the variation of 'β' with temperature.

4) A method for measuring the specific heat values of test specimens; especially the non-stoichiometric ones would enable more reliable conductivity data to be calculated. Otherwise a direct method for measuring the conductivity of the hyperstoichiometric specimens should preferably be used.

5) More detailed characterisation of the hyperstoichiometric specimens before and after testing would improve the subsequent analyis of the data. To this end more specimens should be prepared for metallographic and polarographic analyses and also for more detailed cycling during testing to be performed.

6) Some method of monitoring the gas content of the system during testing would enable the rate of loss of oxygen by the hyperstoichiometric specimens at high temperatures to be calculated. This would enable a better understanding of the reason for the observed enhancement in their conductivity values.

7) More work is required for UO_2 to calculate such parameters as the absorption coefficient (α) and the refractive index (n) in order that precise k_r values can be obtained. Similarly more high temperature work is required in determining electron

and hole mobilities. This would enable a more exact analysis of the high temperature heat transfer mechanism within UO_2 to be made.

8) On the analysis side, the use of a method that can detect whether the specimens have gone hypostoichiometric would be advantageous.

REFERENCES

1. Hobson I. C. . M. Sc. Thesis (1969)
2. Taylor R. , unpublished.
3. Ainscough J. B. , U.K.A.E.A. Internal Memo PUI/70/P8 (1970)
4. Affortit C./Marcon J. P., Reve Int. Hautes Temp. 7 (3), 236 (1970)
5. Peierls R., Ann. Physik 3, 1055 (1929)
6. Ziman J.M., Scientific American 217, 180 (1967)
7. Leibfried G./Schlomann E., Akad. Wiss. Gottingen, Math. Physik, K1 (2A) 71 (1954)
8. Lawson A. W., J. Phys. Chem. Solids 3, 154 (1957)
9. Dugdale J. S./Macdonald D., Phys. Rev. 98, 1751 (1955)
10. Keyes R. W., ibid 115, 564 (1959)
11. White G. K./Woods S. B., Phil. Mag. 3, 785 (1958)
12. Ziman J. M., "Electrons and Phonons" Oxford (1960)
13. Christensen J. A., WCAP - 2531 (1963)
14. Lee D. W./Kingery W. D., J. Am. Cer. Soc. 43 (11) 594 (1960)
15. Frohlich H./Kittel C., Physica 20, 1086 (1954)
16. Price P. J., Phys. Rev. 95, 596 B2 (1954); Phil. Mag. 46, 1252 (1955)
17. Devyatkova E. D., Soviet Phys. - Solid State 1 (4), 555 (1958)
18. Viskanta R., Nucl. Sci. and Eng. 21, 13 (1965)
19. Pikus G. E., Soviet Phys. Tech. Phys. 1, 32 (1956)
20. Joffe A., Can. J. Physics 34, 1342 (1956)
21. Krumhansl J. A., J. Phys. Chem. Solids 8, 343 (1959)
22. Whitmore D. H., J. Appl. Phys. 31, 1109 (1960)
23. Busch G./Schneider M., Physica 20, 1084 (1954)
24. Kittel C., Intro. to Solid State Phys. 4th ed. Wiley (1971)
25. DeConinck R./Devreese J., Phys. Status Solidi 32, 823 (1969)

26. Aronson S. et al, J. Chem. Phys. 35, 1382 (1961)

27. Nagels P. et al, J. Appl. Phys. 35 (4) 1175 (1964)

28. Devreese J. et al, Phys. Status Solidus 17, 825 (1966)

29. Herring C., J. Phys. Chem. Solids 8, 543 (1959)

30. Kanai Y./Nii R., ibid p.338

31. Willardson R. et al, J. Inorg. Nucl. Chem. 6, 19 (1958)

32. Hasiguti R./Kiyoura R., Proc. 2nd U.N. Conf. Peaceful Uses of Atomic Energy, Geneva, 6, 34 (1958)

33. Hartmann W., Z. Physik 102, 709 (1936)

34. Bates J. L., 2nd Conf. on Thermal Conductivity, Ottawa p.189 (1962)

35. Nishijima T. et al, J. Am. Cer. Soc. 48 (1), 31 (1965)

36. Mogard et al, 3rd Conf. U.N. Peaceful Uses of Atomic Energy, paper 608 (1964)

37. Myers/Gyllander, I.A.E.A. Panel (1963)

38. I.A.E.A. Tech. Rpt. Series No.59, Vienna (1966)

39. DeHalas D. R., Nucleonics 21 (10), 92 (1963)

40. Kubota T. et al, J. Nuc. Sci. and Tech. (Tokyo) 1 (3), 93 (1964)

41. Godfrey T. et al, J. Am. Cer. Soc. 48 (6), 297 (1965)

42. Springer J. et al, BMI - X - 10210 (1967)

43. Bates J. L., BNWL - 1223, p.2.7 (1969)

44. Conway J./Flagella P., GEMP 1013 p.225 (1969)

45. Van Craeynest J. C. et al, CEA - R - 3764 (1969)

46. Stoddard J./Mc Cormick N., Nuc. Sci. Eng. 39, 126 (1970)

47. Eucken A., Forsch, Gebiete Ingenieurw. B3, Forschungsheft No.353 (1932)

48. Russell H. W., J. Am. Cer. Soc. 18 (1), 1 (1935)

49. Maxwell J. C., "A Treatise on Electricity and Magnetism" (N.Y. 1954)

50. Loeb A. L., J. Am. Cer. Soc. 37 (II), 96 (1954)

51. Francl J./Kingery W., ibid p.99

52. Biancheria A., Trans. Am. Nuc. Soc. 9, 15 (1966)

53. M^{c} Ewan J. et al, J. Nuc. Mat. 24, 109 (1967)

54. Vogt J. et al, AB Atomenergi Internal Rpt. RMB - 527 (1964)

55. Serizawa M. et al, Proceedings of 8th Conf. on thermal conductivity, Indiana p.549 (1968)

56. Daniel J. et al, H W - 69945 (1962)

57. Ross A. M., A.E.C.L. Rpt. No.CRFD - 817 (1960)

58. Kjaerheim G./Rolstad E., HPR 80, p.40 (1967)

59. Goldsmith L./Douglas J., TGR Rpt. 2103 (W) (1971)

60. Van Craeynest J. C./Stora J., J. Nuc. Mat. 37 (2) 153 (1970)

61. Asamoto R. et al, G.E.A.P. 5493 (1968)

62. Marino G. P., J. Nuc. Mat. 38, 178 (1971)

63. Gibby R. L., ibid p.163

64. Moore J./M^{c} Elroy D., J. Am. Cer. Soc. 54 (1), 40 (1971)

65. Parker W. et al, J. Appl. Pyhs. 32 (9), 1679 (1961)

66. Weeks C. et al, Proc. 7th Conf. thermal conductivity, Maryland, p.387 (1967)

67. Parker W./Jenkins R., Advanced Energy Conversion 2, 87 (1962)

68. Cowan R. D., J. Appl. Phys. 32, 1363 (1961)

69. Cutler M./Cheney G., ibid 34 (7), 1902 (1963)

70. Cape J./Lehman G., ibid p.1909

71. Watt D. A., Brit. J. Appl. Phys. 17, 231 (1966)

72. Taylor R./Cape J., Appl. Phys. Leters 5 (10), 212 (1964)

73. Jain S./Goel T., Brit. J. Appl. Phys. 2 (1), 573 (1968)

74. Taylor R., ibid 16, 509 (1965)

75. Iacobelli R./Moretti S., Paper to "Colloque Int. Chimie des Hautes Temps." (1965)

76. Ackermann R. J. et al, J. Opt. Soc. Am. 49, 1107 (1959)

77. Guseva L. G., p.5 "Investigation into Electrical Discharge in Gases" by B. Klyarfel'd (1964)

78. Ainscough J. B., private communication

79. Springer J./Lagedrost J., BMI - X - 10231 (1968)

80. Mirkin L.I., "Handbook of X-Ray Analysis of Polycrystalline Materials" (1964)

81. Rough F./Dickerson R., Nucleonics 18 (3), 74 (1960)

82. Krikorian O. H., UCRL - 6132 (1960)

83. Bradshaw W./Mathews C., LMSD - 2466 (1958)

84. Warde J. M., Technical Bulletin 94, Refractories Institute, Pittsburgh.

85. Baker/Baldock, see ref. 104

86. Conway J. et al, Trans. Am. Nuc. Soc. 6, 153 (1963)

87. Burdick M./Parker H., J. Am. Cer. Soc. 39 (5), 181 (1956)

88. M^{c} Ewan J. R., see ref. 112.

89. Murray P./Thackray R., Rpt. No. M/M - 22, 1 - 4

90. Moore G./Kelley K., J. Am. Chem. Soc. 69 (2), 2105 (1947)

91. Conway J./Hein R., J. Nuc. Mat. 15 (1) 149 (1965)

92. Godfrey T. et al, ORNL - TM - 1596 (1966)

93. Popov E. et al, Z. Inorg. Chim. 3, 1734 (1958)

94. Ogard A./Leary J., Rap. L.A. - D.C. 8620 (1965)

95. Hein R./Flagella P., GEMP 578 (1968)

96. Hein R. et al, J. Nuc. Mat. 25, 99 (1968)

97. Affortit C., High Temp. - High Press. 1 (1), 27 (1969)

98. Leibowitz L. et al J. Nuc. Mat. 29 (3), 356 (1969)

99. Engel T. K., ibid 31 (2), 211 (1969)

100. Gronvold F. et al, J. Chem. Thermo. 2, 665 (1970)

101. Hoch M., Revue Int. Hautes Temp. 7 (3), 242 (1970)

102. Fredrickson D./Chasanov M., J. Chem. Thermo. 2, 623 (1970)

103. Shaw D., TRG Memo. 5134 (W) (1970)

104. I.A.E.A. Tech. Rpt. Series No.39, Vienna (1965)

105. Montgomery M. H., USAEC HW 76303. p.2.25 (1963)

106. Wheeler M. J., J. N. Mats. 40, 189 (1971)

107. Stora J. et al, CEA - R - 2586 (1964)

108. Taylor R. E., J. Am. Cer. Soc. 45 (2), 74 (1962)

109. Stuckes A. D., Phil. Mag. 5, 84 (1960)

110. Fulkerson W. et al, Phys. Rev. 167 (3), 765 (1968)

111. Ainscough J./Wheeler M., Brit. J. Appl. Phys. 2 (1) 859 (1968)

112. Bates J. et al, J. Am. Cer. Soc. 50 (12), 652 (1967)

113. Rothwell E., J. Nuc. Mat. 6, 229 (1962)

114. Howard V./Gulvin T., IG - 51 (RD/C) (1961)